

DTIC FILE COPY

2

AD-A200 426

NAVAL POSTGRADUATE SCHOOL Monterey, California



THESIS

SIGNAL ACQUISITION AND PROCESSING FOR
AUTONOMOUS SPACE SHUTTLE CARGO BAY
ACOUSTIC MEASUREMENTS (NASA G-313)

by

David P. Kuebler

June 1988

Thesis Advisor:

Steven L. Garrett

DTIC
ELECTE
NOV 17 1988
S D
CE

Approved for public release; distribution unlimited

88 11 17 027

REPORT DOCUMENTATION PAGE

1a. REPORT SECURITY CLASSIFICATION UNCLASSIFIED			1b. RESTRICTIVE MARKINGS			
2a. SECURITY CLASSIFICATION AUTHORITY			3. DISTRIBUTION / AVAILABILITY OF REPORT Approved for public release; distribution unlimited.			
2b. DECLASSIFICATION / DOWNGRADING SCHEDULE			4. PERFORMING ORGANIZATION REPORT NUMBER(S)			
4. PERFORMING ORGANIZATION REPORT NUMBER(S)			5. MONITORING ORGANIZATION REPORT NUMBER(S)			
6a. NAME OF PERFORMING ORGANIZATION Naval Postgraduate School		6b. OFFICE SYMBOL (If applicable)		7a. NAME OF MONITORING ORGANIZATION Naval Postgraduate School		
6c. ADDRESS (City, State, and ZIP Code) Monterey, California 93943-5000			7b. ADDRESS (City, State, and ZIP Code) Monterey, California 93943-5000			
8a. NAME OF FUNDING / SPONSORING ORGANIZATION Office of Naval Research		8b. OFFICE SYMBOL (If applicable) 1112		9. PROCUREMENT INSTRUMENT IDENTIFICATION NUMBER		
8c. ADDRESS (City, State, and ZIP Code) 800 N. Quincy St. Arlington VA 22217			10. SOURCE OF FUNDING NUMBERS			
			PROGRAM ELEMENT NO.	PROJECT NO.	TASK NO.	WORK UNIT ACCESSION NO.
11. TITLE (Include Security Classification) Signal Acquisition and Processing for Autonomous Space Shuttle Cargo Bay Acoustic Measurements (NASA G-313)						
12. PERSONAL AUTHOR(S) David P. Kuebler						
13a. TYPE OF REPORT Masters thesis		13b. TIME COVERED FROM TO		14. DATE OF REPORT (Year, Month, Day) 1988, June		15. PAGE COUNT 107
16. SUPPLEMENTARY NOTATION "The views expressed in this thesis are those of the author and do not reflect the official policy or position of the Department of Defense or the U. S. Government."						
17. COSATI CODES			18. SUBJECT TERMS (Continue on reverse if necessary and identify by block number)			
FIELD	GROUP	SUB-GROUP	Acoustics, Vibroacoustics, NASA G-313, Signal processing, Resonant Modes			
19. ABSTRACT (Continue on reverse if necessary and identify by block number) A narrowband trigonal acoustic transducer array and digital signal processing software are described in support of Space Shuttle Vibroacoustic experiment (NASA G-313). The three co-planar, vibrationally isolated pressure-sensing microphones, the preamplifiers and the filters are designed to meet dynamic range and anti-aliasing requirements for the digitization and processing of recorded flight data with one Hertz resolution within the 30-780 Hz baseband acoustic spectrum. The experiment is designed to operate in environments up to 160 dB SPL and provides modal recognition and directional information to identify resonances and localize high intensity sound sources within the ambient launch environment of the Space Shuttle Cargo Bay. Also included is a model of the empty Cargo Bay resonances and modal density calculations based on an adiabatic perturbations of a rigid, right circular cylindrical enclosure. (R)						
20. DISTRIBUTION / AVAILABILITY OF ABSTRACT <input checked="" type="checkbox"/> UNCLASSIFIED/UNLIMITED <input type="checkbox"/> SAME AS RPT <input type="checkbox"/> DTIC USERS				21. ABSTRACT SECURITY CLASSIFICATION UNCLASSIFIED		
22a. NAME OF RESPONSIBLE INDIVIDUAL Steven L. Garrett			22b. TELEPHONE (Include Area Code) (408) 646-2540		22c. OFFICE SYMBOL 616y	

Approved for public release; distribution unlimited.

Signal Acquisition and Processing for
Autonomous Space Shuttle Cargo Bay
Acoustic Measurements (NASA G-313)

by

David Paul Kuebler
Lieutenant, United States Navy
B. S., University of Texas, 1982

Submitted in partial fulfillment of the
requirements for the degree of

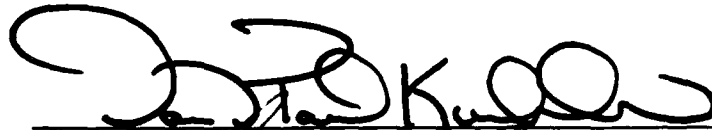
MASTER OF SCIENCE IN ENGINEERING ACOUSTICS

from the

NAVAL POSTGRADUATE SCHOOL

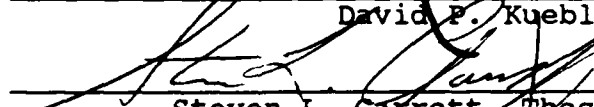
June 1988

Author:



David P. Kuebler

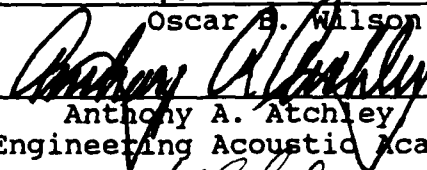
Approved by:



Steven L. Garrett, Thesis Advisor



Oscar B. Wilson, Second Reader



Anthony A. Atchley, Chairman
Engineering Acoustic Academic Committee



Gordon E. Schacher,
Dean of Science and Engineering

ABSTRACT

A narrowband trigonal acoustic transducer array and digital signal processing software are described in support of Space Shuttle Vibroacoustic experiment [NASA G-313]. The three co-planar, vibrationally isolated pressure-sensing microphones, the preamplifiers and the filters are designed to meet dynamic range and anti-aliasing requirements for the digitization and processing of recorded flight data with one Hertz resolution within the 30-780 Hz baseband acoustic spectrum. The experiment is designed to operate in environments up to 160 dB SPL and provides modal recognition and directional information to identify resonances and localize high intensity sound sources within the ambient launch environment of the Space Shuttle Cargo Bay. Also included is a model of the empty Cargo Bay resonances and modal density calculations based on an adiabatic perturbation of a rigid, right circular cylindrical enclosure.



SEARCHED	INDEXED
SERIALIZED	FILED
APR 1978	
FBI - MEMPHIS	
By	
Date	
Dist	
A-1	

THESIS DISCLAIMER

The reader is cautioned that computer programs developed in this research may not have been exercised for all cases of interest. While every effort has been made, within the time available, to ensure that the programs are free of computational and logic errors, they can not be considered validated. Any application of these programs without additional verification is at the risk of the user.

TABLE OF CONTENTS

I.	INTRODUCTION -----	1
	A. STATEMENT AND APPROACH -----	1
	B. HISTORICAL BACKGROUND -----	3
	C. SCOPE -----	7
II.	HARDWARE DESIGN AND TESTING -----	8
	A. MICROPHONE SELECTION -----	8
	B. PREAMPLIFIER AND ANTI-ALIASING FILTER ----- DESIGN	10
	C. MEASUREMENT OF FRONT END CHARACTERISTICS --	11
III.	THEORY AND ANALYSIS -----	17
	A. RECEIVED SIGNAL THEORY -----	17
	1. Introduction -----	17
	2. Development -----	17
	3. Resonance -----	21
	4. Modal Model -----	23
	5. Strong Point Sources in the Far Field--	37
	B. ANALYSIS TO DATE -----	40
IV.	FLIGHT DATA PROCESSING -----	49
	A. DISCUSSION -----	49
	B. ILS -----	49
	C. FRONT END ELEMENT DIFFERENTIAL ANALYSIS ---	50
	D. RESONANCE RECOGNITION -----	54
	E. STRONG SOURCE RECOGNITION -----	55
	F. EXAMPLE PROBLEM -----	56

V. CONCLUSIONS AND RECOMMENDATIONS -----	79
APPENDIX A (Specifications for Model 2510 Endeeco -- Microphone)	80
APPENDIX B (Specifications for Burr-Brown OPA 111 -- Operational Amplifier)	83
APPENDIX C (Specifications for Analog ----- Devices DAS 1153 A/D Converter)	87
LIST OF REFERENCES -----	92
INITIAL DISTRIBUTION LIST -----	94

LIST OF TABLES

- I. Shaker Table Test Results at One g Peak---- 10
- II. Front End Response Data in Calibrator Box.---15
- III. Front End Response Data in Muzzerall ----- 16
Calibration Tube.
- IV. Results of 1/14.7 Scale Model Compared ----- 36
with Cylindrically Symmetric Approximation.

LIST OF FIGURES

2.1	Pre-amplifier and Anti-aliasing Filter -----	12
2.2	Photograph of Front End Assembly -----	13
3.1	Microphone Isolation Cannister -----	18
3.2	GAS CAN Lid Assembly -----	19
3.3	Top View of Space Shuttle Cargo Bay -----	25
3.4	Shuttle Cargo Bay Dimensions -----	26
3.5	Plexiglass Model Experiment Dimensions -----	27
3.6	Photograph of Plexiglass Model -----	28
3.7	Microphone Bias Circuitry for Model -----	29
3.8	Equal Amplitude Contours First Mode of Plexiglass Model and Cylinder -----	31
3.9	Equal Amplitude Contours Second Mode of Plexiglass Model and Cylinder -----	32
3.10	Equal Amplitude Contours Third Mode of Plexiglass Model and Cylinder -----	33
3.11	Equal Amplitude Contours Fourth Mode of Plexiglass Model and Cylinder -----	34
3.12	Equal Amplitude Contours Fifth Mode of Plexiglass Model and Cylinder -----	35
3.13	Arrival Angle of Plane Wave Incident Upon Co-planar Trigonal Array -----	38
3.14	Experimental Apparatus used in 2 Element Array Phase Experiment ---	41
3.15	Time Series Comparison of Received Signal--- By 2 Element Array (0° Offset)	42
3.16	Time Series Comparison of Received Signal -- By 2 Element Array (45° Offset)	43
3.17	Time Series Comparison of Received Signal -- By 2 Element Array (90° Offset)	44

3.18	Time Series Comparison of Received Signal -- By 2 Element Array (135° Offset)	45
3.19	Time Series Comparison of Received Signal -- By 2 Element Array (180° Offset)	46
4.1	Sample Data Channel 1 for Test Case -----	57
4.2	Sample Data Channel 2 for Test Case -----	58
4.3	Record Data Channel 1 for Test Case -----	60
4.4	Record Data Channel 2 for Test Case -----	61
4.5	FFT Comparison of Channels 1 and 2 -----	62
4.6	Maximum Values Output by Batch File PEAKS --	63
4.7	Bin Values Near Maxima Listed by GRABVALUES -	64
4.8	FFT Comparison With Time Series Bin Shift -- Correction for Phase Differential	66
4.9	Bin Values Near Maxima for Phase ----- Corrected Data	67
4.10	Sample Data Channel 1 Near Resonant Mode --- Pressure Minima	68
4.11	Sample Data Channel 2 Near Resonant Mode --- Pressure Minima	69
4.12	FFT Comparison Channels 1 and 2 for Phase -- Corrected Data at Pressure Minima	70
4.13	FFT Bin Values for Phase Corrected Data ---- Near Values Minima	71
4.14	Travelling Wave Sample Data Channel 1 -----	73
4.15	Travelling Wave Sample Data Channel 2 -----	74
4.16	Travelling Wave Record Data Channel 1 -----	75
4.17	Travelling Wave Record Data Channel 2 -----	76
4.18	FFT Comparison Channels 1 and 2 for Phase -- Corrected Travelling Wave Data	77
4.19	FFT Bin Values for Phase Corrected Data for -	78

ACKNOWLEDGMENTS

Sincere appreciation is expressed to: Dr. Steve Garrett, whose enthusiasm is contagious; his henchmen Dr. Dave Gardner and Dr. Tom Hofler, two tenacious scientists of fortune who have the knack of beating the most nebular and chaotic notion into a realizable form; Dr. O. B. Wilson for proofreading this thesis; Dr. Armstead for showing me something I have not seen before; Drs. Ziomek and Moose for making signal analysis understandable and fun; and good friends like Hakan and Dano for making homework bearable and school a better place to be.

Many thanks to all of the folks out at Fort Ord Craft Shop who fired my wigged out ceramic creations, the company that made the crash bars for my motorcycle, and residents of the third floor of the BOQ, who were relieved to find out that I was playing the cello and not torturing cats in room 351. Special thanks to my best friend Holly. We also acknowledge the financial support of the Office of Naval Research.

I. INTRODUCTION

A. STATEMENT AND APPROACH

This thesis is designed to assist in the implementation of the NASA project G-313 acoustic analysis of the Space Transportation System Orbiter Vehicle (Space Shuttle) payload bay specifically by:

1. Designing and testing the microphone, pre-amplifier, and anti-aliasing filter "front end" capable of measuring pressure levels up to 160 dB SPL narrowband at frequencies from 30 to 780 Hz, providing a low noise output not to exceed ± 5 volts peak amplitude compatible with digitization and data storage hardware designed for this project by previous experimenters.

2. Developing an optimal signal processing technique and writing the software to automate the analysis of received flight data to resolve the distribution of acoustic energy, both active and reactive, within a 30 to 780 Hz bandwidth.

3. Making measurements of the response characteristics of the measuring apparatus to be used as inputs to the signal processing software to correct any signal perturbations introduced by the measurement.

The overall project milestones include:

1. Developing a vibrationally isolated directional coplanar array capable of measuring sound fields up to 160 dB SPL.

2. Providing a low noise pre-amplifier and anti-aliasing filter with a ± 5 volt peak dynamic voltage output and roll-off between 780 and 1000 Hz to support a 2000 sample per second digitization rate.

3. Developing non-volatile, durable mass storage capabilities for the digital data.

4. Providing a package capable of servicing and protecting the data throughout the space flight until recovery.

5. Providing an analysis package capable of retrieving and interpreting the formatted flight data that is able to resolve resonant modes and provide directional information to strong singular sources of acoustic energy.

This project's realization has involved the efforts of many fine individuals, and in essence, most of the hardware considerations were complete at the time this thesis began investigating data reduction schemes and putting the final touches on the front end design and testing. The following is a brief history of the motivation and prior contributions to the NASA G-313 vibroacoustic project.

B. HISTORICAL BACKGROUND

In 1985, LT S. E. Palmer, Dr. S. L. Garrett, Dr. O. B. Wilson, and Dr. S. W. Yoon outlined to the AIAA Shuttle Environment Operations Conference in Houston Texas [Ref. 1], a proposal to use a vibrationally isolated trigonal array of pressure microphones, a digital solid state bubble memory recorder, and narrowband digital processing technology autonomously mounted in a NASA Getaway Special Canister, to make improved acoustic measurements of pressure levels and distributions within the cargo bay, enhancing the data base used by STS payload designers. These developments were motivated by the conclusions of groups contracted to study and model the acoustic environment of earlier flights, who stated that higher resolution frequency and spatial data were needed to understand acoustic source and reactive pressure distributions within the cargo bay. They raised questions about the validity of flight data to date, due to the possibility that vibration isolation mounts were mechanically resonant within the bandwidth of the processed data. The NPS proposal would improve upon earlier studies by:

1. Designing vibration isolation mounts for the microphones which were resonant well below the lowest frequency of acoustic interest to guarantee a low vibrationally induced noise floor.

2. Providing non-volatile, non-perturbable data storage in solid state form circumventing problems (flutter, start-up lag, etc.) and expense encountered by using analog (magnetic tape) storage.

3. Sampling above the Nyquist rate for the highest frequency of interest and providing narrowband processing with 1 Hz resolution over a 30-780 Hz bandwidth. This would provide a substantial improvement over the one-third octave processing produced by the previous studies of the Dynamic Acoustic and Thermal Environments (DATE) group of NASA Goddard Space Flight Center [Ref. 2] and the Bolt, Beranek and Newman Corporation of Canoga Park, California [Ref. 3].

4. Using the trigonal aperture to discern modal distributions and spatially determine propagation vectors to the strongest discrete sources. This capability is considered necessary to resolve the hypothesis proposed by Carol Tanner of the Aerospace Corporation that high intensity sound sources at frequencies within the 315 Hz one-third octave band are produced by the coupling of aerodynamic flow along the fuselage to the acoustic modes of the cargo bay in one or more of the eight bay vents, producing flow induced resonances [Ref. 4]. Earlier intensity measurements provided no signal cross-correlation directional processing, requiring Carol Tanner to extrapolate the intensity of the propagating wavefront

inside the bay from information in one-third octave bins to infer relative range to the speculated source [Ref. 5].

5. Providing an active sweep to determine the resonant standing wave ratios at the microphone locations as a function of frequency to aid in identifying reactive field (standing wave) contributions to the narrowband signal analysis.

The first task of designing low frequency response isolation mounts for the measuring microphones was addressed by CDR. C. D. Stehle, resulting in his September 1985 thesis [Ref. 6] which detailed the design and vibrational testing of the mounts currently adopted for this project. The mounts meet the durability and isolation requirements of the most stringent expected space environment, placing the vibrationally induced noise floor below 85 microvolts, peaking in the 315 Hz one-third octave band [Ref. 6, figure 3.3], which is equivalent to 102 dB SPL, 40 dB below the expected ambient sound environment.

Specifications for the magnetic bubble memory recorder are outlined in the March 1986 thesis by LT T. M. D'Ercole [Ref. 7], and the 32 bit processor interface in a separate March 1986 thesis by LT T. J. Frey [Ref. 8]. A successful prototype has been built and tested by the team of D'Ercole, Frey, and Mr. Dave Rigmaiden, who has been indispensable in providing continuity to this project. Mr. Rigmaiden has also written the data retrieval software for IBM PC

compatible signal processing software. LT D. W. Jordan has provided a matched filter designed to activate the data storage upon detection of the operation of the Shuttle Auxiliary Power Unit (APU), just prior to Solid Rocket Booster (SRB) ignition. Details are provided in his June 1985 thesis [Ref. 9]. The electrical power supply for the entire experiment has been designed and tested by LT B. Kosinski and proven flight ready within NASA safety specifications. The 60 rigidly constrained Gates brand lead acid cells mounted in the battery pack are rated at 600 watt-hours. LT S. Dee has recently completed the design and testing of the accelerometer launch detector system used to activate the experiment autonomously at SRB ignition. LCDR A. W. Boyd has managed the project development, and has been the point of contact with NASA, overseeing the administrative and logistic requirements of this project during his tour at the Naval Postgraduate School. Dr. A. Fuhs and Dr. R. Panholzer have provided valuable advice and expertise in the areas of Space Systems and Electrical Engineering, guiding the students' efforts mentioned thus far. Drs. S. L. Garrett and O. B. Wilson have overseen the acoustic development of the project. A synopsis of the project history may also be found in the 1987 Naval Research Reviews [Ref. 10].

C. SCOPE

The remainder of this thesis describes the development of the microphone, pre-amplifier, and anti-aliasing filter used in the NASA G-313 project and provides a signal analysis model and computerized implementation capable of analyzing flight data retrieved from the magnetic bubble memory recorder.

II. HARDWARE DESIGN AND TESTING

A. MICROPHONE SELECTION

The process of selecting a microphone for the cargo bay environment was quickly narrowed down to a comparison of two possibilities, the already NASA flight approved and tested Endevco model 2510 (specification sheet in Appendix A) and PCB model 106B50. Both piezoelectric microphones were designed to have flat frequency response and linear sensitivity up to the maximum expected sound pressure levels of 160 dB narrowband within the cargo bay (based on 140 dB one-third octave band ambient design levels with a crest factor of 5).

A rectangular wooden comparison calibrator box with internal dimensions of 40 inches by 6 inches by 2 inches was constructed of one-half inch pine and used with a General Radio sound level meter (model 1565-B) to make sensitivity and noise comparisons between the two microphones. An ALS model 120S shaker table was used to measure vibration sensitivity of the microphones without isolation mounting. The measured sensitivity of both microphones was reasonably close to the manufacturer's calibration curves. At the second plane wave longitudinal resonance of the calibrator box, 395 Hz, the incident pressure was set at 1 Pa or 94 dB SPL upon both microphones. The output of the PCB was

measured at 86 microvolts or -81.3 dB re 1V/Pa, giving an open circuit sensitivity of 592 mV/psi measured compared to a nominal 565.4 mV/psi given by the manufacturer's calibration data. The Endevco open circuit output was measured at 34 microvolts or -89.4dB re V/Pa, giving an open circuit sensitivity of 234 mV/psi, compared to 152 mV/psi nominal sensitivity for the microphone.

The experiment in the calibrator box revealed that the PCB microphone was at least 10 dB noisier in signal to noise ratio than the Endevco, whose noise level was verified to be ambient acoustic noise. In subsequent experimentation using an Ithaco model 1201 low noise amplifier, set to give the Endevco and PCB the same absolute output level in the same sound field, the Endevco was verified to have a 10 dB lower noise floor than the PCB with its internal electronics. The PCB microphone was also shown to have much greater sensitivity to vibration. Measurements were made on a shaker table at one g (9.8 m/s) at frequencies of 20, 50, 100, and 200 Hz, with results summarized in Table I. The PCB sensitivity to vibration was observed to be 500 mV per peak g in the high frequency limit versus the 3.5 mV per peak g for the Endevco. The PCB, being about 4 times as pressure signal sensitive, at high frequencies, would have produced over 25 times the vibrational noise as the Endevco, performing even more poorly at lower frequencies. Because of the better signal to noise response due to lack of

internal electronics, and much greater vibration rejection properties, the Endeveco model 2510 was chosen as the better microphone for this application.

TABLE I. SHAKER TABLE TEST RESULTS AT ONE G. PEAK.

FREQUENCY (Hz)	DRIVE VOLTAGE (mV)	PCB RESPONSE (mV)	ENDEVCO RESULTS (mV)
20	510	2300	9
50	920	4.5	4.5
100	120	540	3.4
200	180	530	3.5

B. PREAMPLIFIER AND ANTI-ALIASING FILTER DESIGN

The basic preamplifier design, suggested by Dr. David Gardner, uses a Burr Brown low-noise OPA-111 Difet (Specifications in Appendix B) operational amplifier. The gain of 11 was set to provide a ± 5 volt peak signal at 160 dB SPL microphone input to comply with the A/D requirements for maximum input voltage (Specifications in Appendix C). The design was shown to have a noise floor around -100 dBV at a 2.5 Hz bandwidth, and verified to be Johnson noise limited by the (room temperature 300°K) 2 megohm input bleedoff resistor [Ref. 11]. The Johnson noise voltage is calculated according to

$$V_{rms} = \sqrt{4KT R \Delta f} = 286nV/\sqrt{Hz}$$

where K is Boltzman's constant (1.38×10^{-27} J/K), T is absolute temperature in K, R is the resistance in ohms, and Δf is the bandwidth of the preamplifier. A 0.01 microfarad

capacitor was added to block the D.C. pyroelectric effects of the input bias voltage produced by the piezoelectric microphone [Ref. 12]. The final design is shown schematically in Figure 2.1.

The anti-aliasing filter was designed by LT Mike Ziegler to roll-off below 1250 Hz allowing for the 2500 Hz sample digitization rate. A schematic is provided as part of Figure 2.1. The entire microphone/preamplifier/filtering front end was assembled by Mr. Dave Rigmaiden and tested in a calibration experiment discussed next.

C. MEASUREMENT OF FRONT END CHARACTERISTICS

In experiments conducted on October 19 and October 21, 1987, Mr. Rigmaiden's prototype front end (Figure 2.2) was tested to verify that it met the design criteria of ± 5 volt maximum peak voltage output to the A/D converter at 160 dB SPL acoustic input, linear pressure to voltage response up to the maximum design level, and anti-aliasing roll-off at less than 1250 Hz with fairly flat frequency response from 50 to 700 Hz. The measurements were made using a calibration tube designed by CPT Michael Muzzerall (Canadian Forces) and described in his 1987 thesis [Ref.13]. The tube was 90 cm long with a 6.2 cm I. D. and was driven by a JBL model 2445J compression driver. The results are tabulated below.

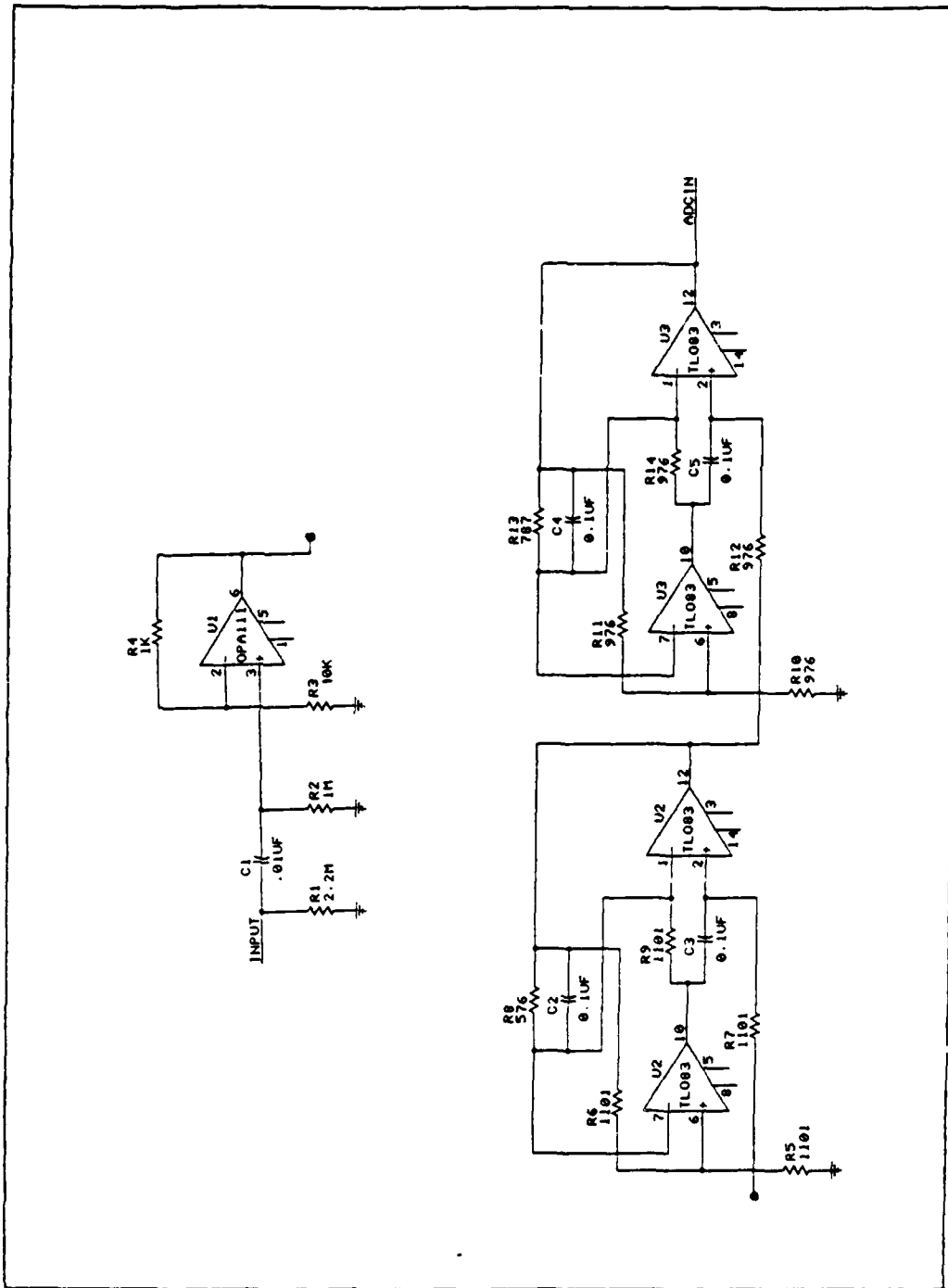


Figure 2.1 Pre-amplifier and Anti-aliasing Filter

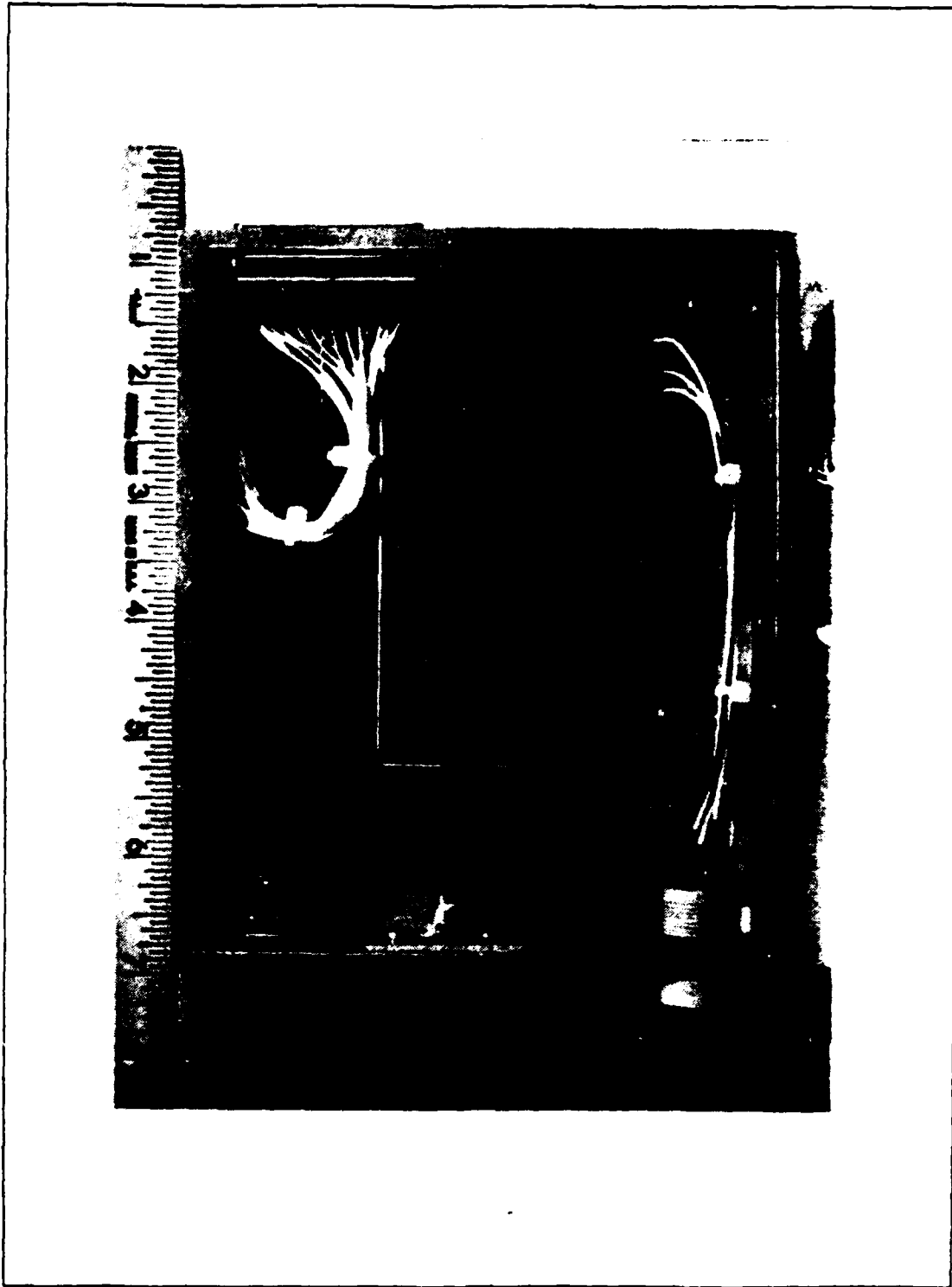


Figure 2.2 Photograph of Front End Assembly

Tables II and III compare a standard General Radio Model 1961-9611 perpendicular incidence one-half inch electret condenser microphone with power supply GR Model 1560-P62 and Model 1560-P42 pre-amplifier, to the Endevco 2510 described in this chapter. The front end pre-amplifier did not have the pyroelectric pre-filter. Table II contains data taken in the wooden calibrator box in the frequency range 50-800 Hz with pressures up to 25 dB re 1 Pa. Table III presents data taken in the Muzzerall calibration tube to extended frequency ranges to 100-2000 Hz and higher pressure levels to 50 dB re 1 Pa. The response of the front end output was verified to be linear to 160 dB SPL input acoustic signal with 3 dBV electrical output.

As seen from Table III, the final design has fairly flat response in the base band range from 50 Hz to 600 Hz rolling off 3 dB down around 1000 Hz. All prerequisite design specifications have been met by circuitry shown in Figure 2.1.

Date: 21 October 1987

TABLE II. FRONT END RESPONSE DATA IN CALIBRATOR BOX.

<u>Freq.</u> (Hz)	<u>Absolute Output</u> $\frac{1}{2}$ " GR (dBV)	<u>dB Difference</u> (Endevco-GR)	<u>Phase Difference</u> (Endevco-GR) (degrees)
50	-59.8	-16.6	6
100	-53.7	-18.6	15
125	-51.2	-18.6	-5.5
150	-48.3	-18.2	-9
175	-40.4	-17.1	-13.8
200	-36.6	-16.93	-16.6
225	-41.2	-16.74	-23.85
250	-43.3	-16.73	-22.6
275	-43.8	-16.36	-28.70
300	-43.5	-16.38	-29.70
325	-42.3	-16.20	-35.60
350	-39.2	-16.45	-38.25
375	-37.5	-16.1	-41.85
400	-40.0	-16.80	-39.40
425	-44.4	-15.6	-46.66
450	-46.4	-15.4	-57.73
475	-47.0	-17.4	-60.73
500	-46.3	-17.87	-54.4
525	-44.5	-17.36	-57.12
550	-40.7	-17.72	-61.90
575	-39.7	-18.10	-59.75
600	-45.0	-18.40	-63.60
625	-48.4	-18.90	-57.66
650	-51.4	-16.88	-59.0
675	-50.9	-17.06	-68.3
700	-48.4	-17.65	-73.6
725	-44.4	-17.86	-76.00
750	-38.7	-18.73	-84.5
775	-81.9	-20.3	-81.9
800	-49.40	-19.85	-81.6

Comparison Calibration GenRad one-half inch mic vs
Endevco 2510. GR one-half inch mic Frequency
Independent Sensitivity is -39.3 dB re 1V/Pa.

Date: 21 October 1987

TABLE III. FRONT END RESPONSE DATA IN MUZZERALL CALIBRATION TUBE.

<u>Freq.</u> (Hz)	<u>Absolute Output</u> $\frac{1}{2}$ " GR (dBV)	<u>dB Difference</u> (Endevco-GR)	<u>Phase Difference</u> (Endevco-GR) (degrees)
100	-6.98	-20.3	-2.0
200	7.3	-20.3	-16.3
300	2.64	-20.3	-27.9
400	8.45	-20.5	-39.3
500	6.06	-20.7	-50.2
600	9.21	-21.0	-60.9
700	6.04	-21.3	-71.5
800	7.57	-21.78	-81.6
900	7.47	-22.3	-92.6
1000	6.11	-22.8	-102.9
1100	10.1	-23.4	-113.4
1200	6.53	-24.2	-123.4
1300	8.19	-24.98	-133.1
1400	9.44	-26.02	-142.8
1500	4.44	-26.8	-151.8
1600	9.30	-27.8	-160.58
1700	2.74	-29.0	-168.5
1800	3.56	-30.14	-175.8
1900	4.09	-31.32	-177.3
2000	1.13	-32.52	-171.2

Comparison Calibration GR one-half inch mic vs Endevco 2510
GR one-half inch mic Sensitivity is -39.3 dB re 1V/Pa.

III. THEORY AND ANALYSIS

A. RECEIVED SIGNAL THEORY

1. Introduction

This section will discuss the capabilities and limitations of the sparse, trigonal co-planar array [Fig. 3.1, 3.2] for the analysis of complicated acoustic pressure distributions inside the Space Shuttle Cargo bay. From the general mathematical expression, derived below, only the cases of constant spectral amplitude or constant spectral phase (modulo π) lead to resolvable solutions given the many limitations imposed by the three element array. For comparison, processing techniques used by prior experimenters for NASA (BBN and DATE) will be presented after an explanation of the NPS approach.

2. Development

It is expected that the output voltage from each microphone will very nearly represent the point field pressure at the microphone location since the microphone and its housing assembly (see Fig. 3.1, 3.2) are much smaller than acoustic wavelengths of interest as examined by C. D. Stehle [Ref. 6]. By carefully measuring the amplitude and phase response characteristics of each microphone, preamplifier, and anti-aliasing filter assembly in a

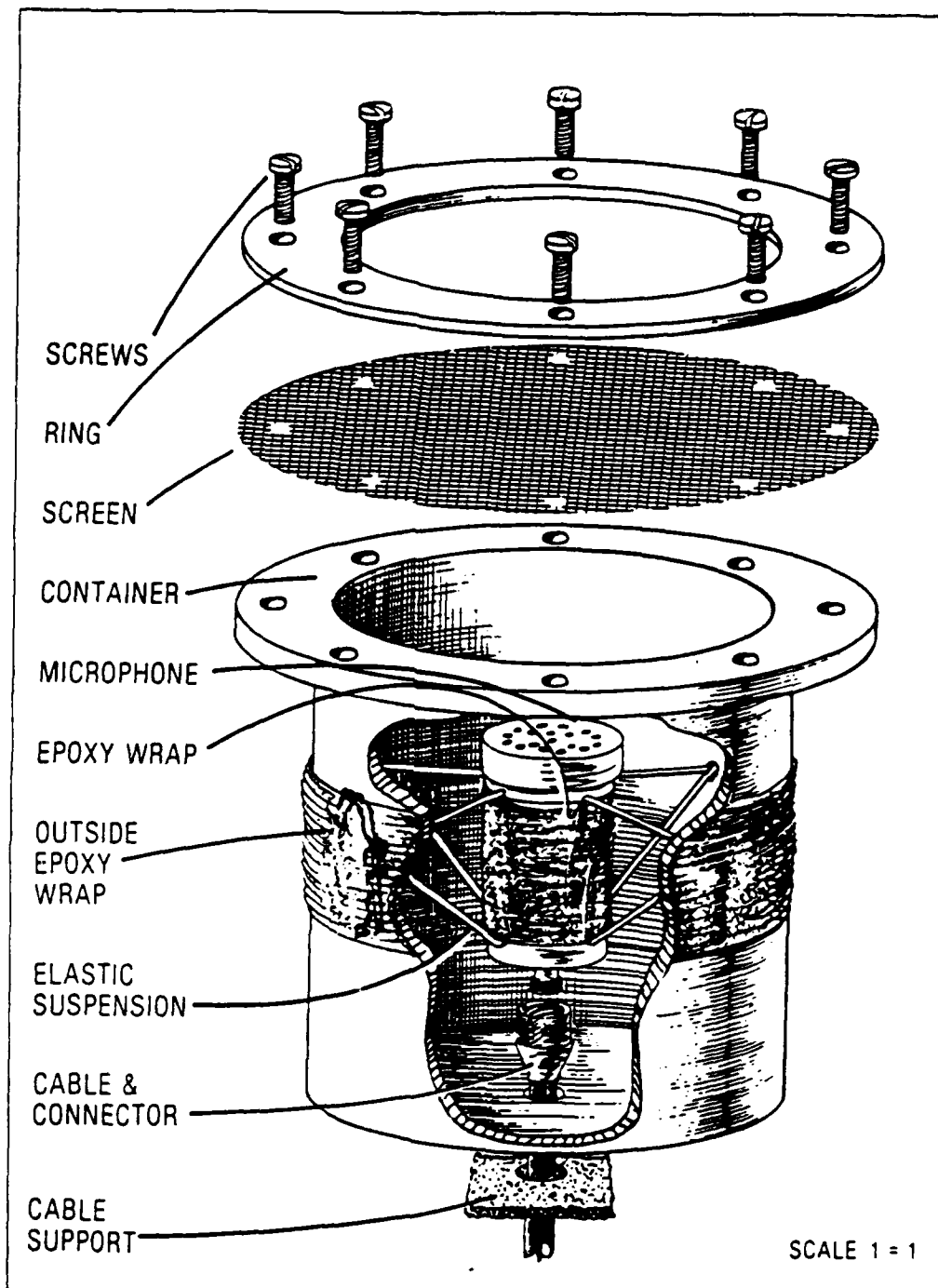


Figure 3.1 Microphone Isolation Cannister

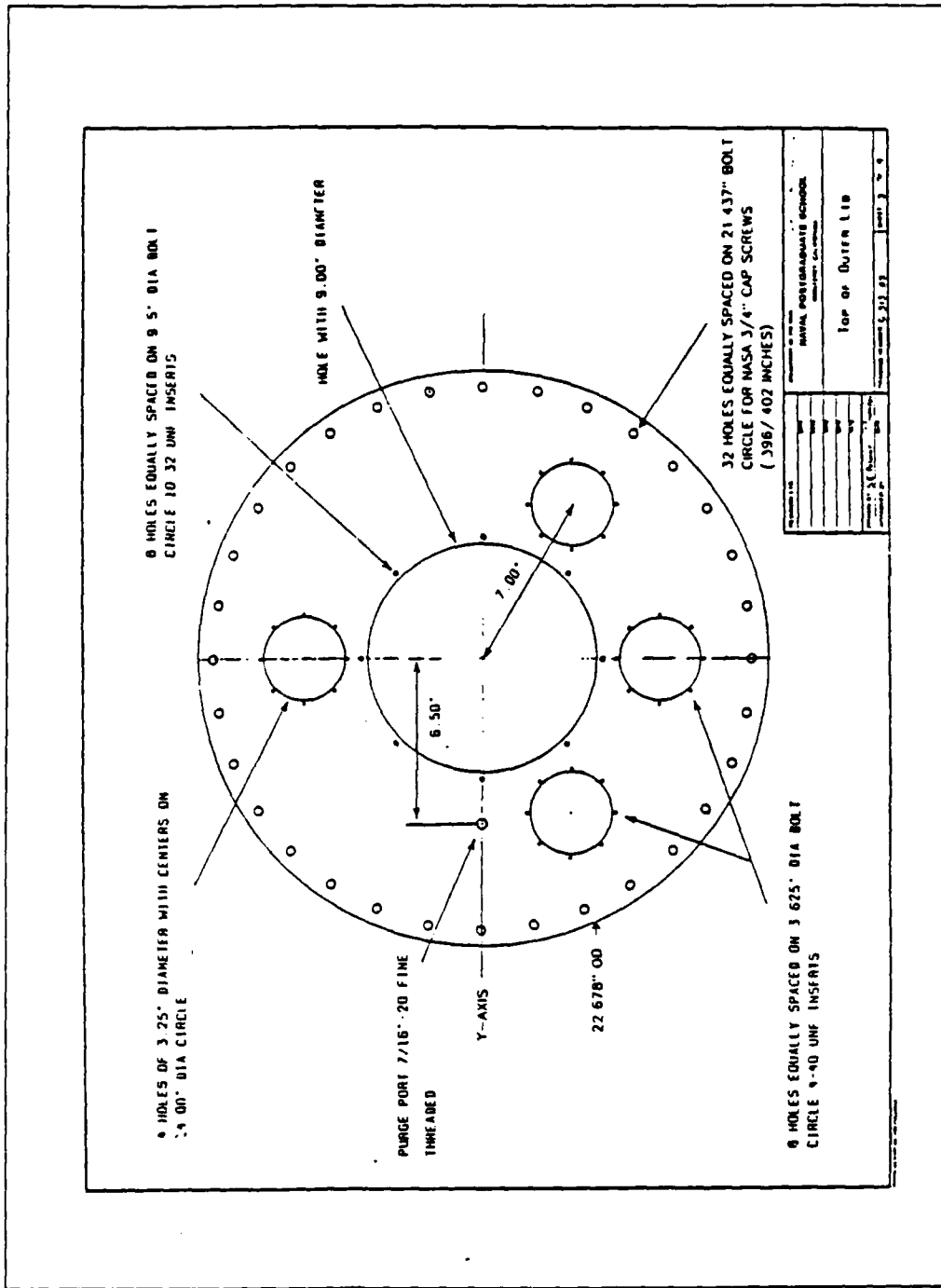


Figure 3.2 GAS CAN Lid Assembly

controlled calibrator experiment, it is possible to use the software described in the next chapter to provide the differential gain and phase for each of the three front end inputs. This information may be used to eliminate the effects of unmatched front end response characteristics when solving for the dynamic pressure amplitude and phase at the microphone locations.

In developing a mathematical model, the pressure distribution is assumed to have propagated through a medium of homogeneous sound speed throughout the cargo bay (isoceleric) and be the linear superposition of all active and reactive sources. All sources are assumed to be in the far field to eliminate the effects of wavefront curvature, undetectable by a three element array, and therefore, all wavefronts impinging on the array are assumed to be plane wavefronts. Spherical divergence is modeled from all active and reactive sources, so that the monochromatic pressure from a single source is given by

$$P_o = \frac{A}{|\vec{r}|} \exp [j(\omega_o t + \vec{k}_o \cdot \vec{r} + \phi_o)]$$

where A/r is the pressure amplitude [Ref. 15, Eq. 5.57, pg 114], ω_o is the angular source frequency, $k_o = \omega_o/c$, c is the speed of sound (assumed constant), and ϕ_o is an arbitrary phase constant. Using the monochromatic result of Ziomek's equation 4.7-10 [Ref. 14], and applying the inverse spatial transform to this equation for a receiving vice

transmitting planar circular array ($z = 0$, $r = a$ = distance of microphone from center) for a far field source distribution

$$D(f, \theta, \psi)$$

we get,

$$P_o(f, r, \phi) = e^{j\omega t} \int_0^\pi \int_0^{2\pi} D(f, \theta, \psi) \exp[jka \sin(\theta) \cos(\psi - \phi)] d\theta d\psi$$

To perform the forward transform, as in Ziomek's equation 4.7-10, for a sparse array of only three directional samples (ϕ) it is impossible to get a complete representation of the $D(f, \theta, \psi)$ as an output. With a higher number of sampled directions it would be possible to obtain a discrete representation of the far field source distribution. There are, however, two special cases of interest which are recognizable by the array. These cases are explained in the next three sections:

3. Resonance

At an acoustic resonance the outputs of all three microphones will be in phase (modulo π) with varying peak amplitudes corresponding to the homogeneous standing wave ratios within the cavity. The array must be far enough away from driving sources as described by the critical distance cited in Kinsler, Frey, Coppens and Sanders equations 13.7 and 13.24 [Ref. 15], which represents the distance at which the direct and reverberant intensities are equal. For this

distance to be small, the cavity must have low absorption corresponding to a high resonance quality factor, Q .

In general, the analytical solution to the homogeneous wave equations is not known for irregular boundary geometries. Such is the case for the Space Shuttle cross-section of the unloaded cargo bay, which is further complicated by varying loading configurations. With the information attainable from the sparse trigonal array, it is impossible to solve for all possible conditions of pressure distribution throughout the cargo bay, without an a priori comparison to a numerical model of homogeneous eigenfunctions or an experimental scale model.

The approach taken in this project is to make an active, pure tone frequency sweep of the quiet pre-launch cargo bay using the sinusoidal output of a voltage controlled oscillator (VCO) driven loudspeaker (JBL Model LE10-H) and monitoring the return for frequencies at which the received pressure signals are co-phased modulo π . Upon recognition of this resonance criterion, the amplitude levels for each microphone data channel are corrected for the electrical differences in gain and recorded. An attempt will be made to use this standing wave ratio information to identify the general modal patterns based on prior knowledge about the resonances of cylinders and the results of a small scale model experiments. It is worthy to note that the stated resonance recognition criteria of cophased elements

is indistinguishable from a single active source (travelling wave) directly above or below the planar array. The effect of system Q, controlled primarily by boundary incidence losses, is an important factor in determining the relative importance of cavity resonance. For a low Q environment, direct path radiation from a source will play the more important role in its vicinity, even near resonant frequency, because the driver is within the previously mentioned critical distance. The choice of a driver equidistant from all three array elements should preserve the cophase definition of resonant frequencies, but will perturb the standing wave ratio values by an offset constant, once again, highly Q dependent.

4. Modal Model

To the simplest approximations, the Space Shuttle cargo bay resembles a cylinder. The analytic solution for a cylinder is well known and cited in Morse, [Ref. 16, pg 398]. The longitudinal solution (Z), radial (r) and the azimuthal (ϕ) pressure distribution functions are given in terms of integer ordered Bessel functions, J_m , cited by Morse to be:

$$P(r, \phi, z) = \cos(m\phi) \cos\left(\frac{\omega z}{c}\right) J_m\left(\frac{\omega r}{c}\right) e^{-2\pi i \omega t}$$

$$v = \frac{1}{2\pi} \left[\omega_z^2 + \omega_r^2 \right]^{1/2}$$

Since the cargo bay is of constant cross-section, the longitudinal (z) part of the cargo bay solution,

$$\cos \left[\frac{\omega_z Z}{c} \right]$$

is identical to the cylindrically symmetric solution. The radial and azimuthal cargo bay solution will be similar to, but differ slightly from, the cylinder solution because the cargo bay's cross-section is not quite circular.

To assist in identifying resonant modes when flight data are analyzed, the eigenfunctions for the first five cross-sectional modes were determined by experimental scale modeling. The empty shuttle cargo bay geometry is shown in Figure 3.3 and 3.4. The model used was constructed of one inch thick Plexiglass with dimensions as shown in Figure 3.5, and is an exact cross-sectional replica of scale 1:14.7. A photograph of the model is shown in Figure 3.6. A Panasonic Model P9932 omni-directional Electret condenser microphone with internal FET and bias circuitry shown in Figure 3.7, was used to measure the pressure distributions throughout the model at resonance for the first five modes. The microphone was moved by a magnet so that the system

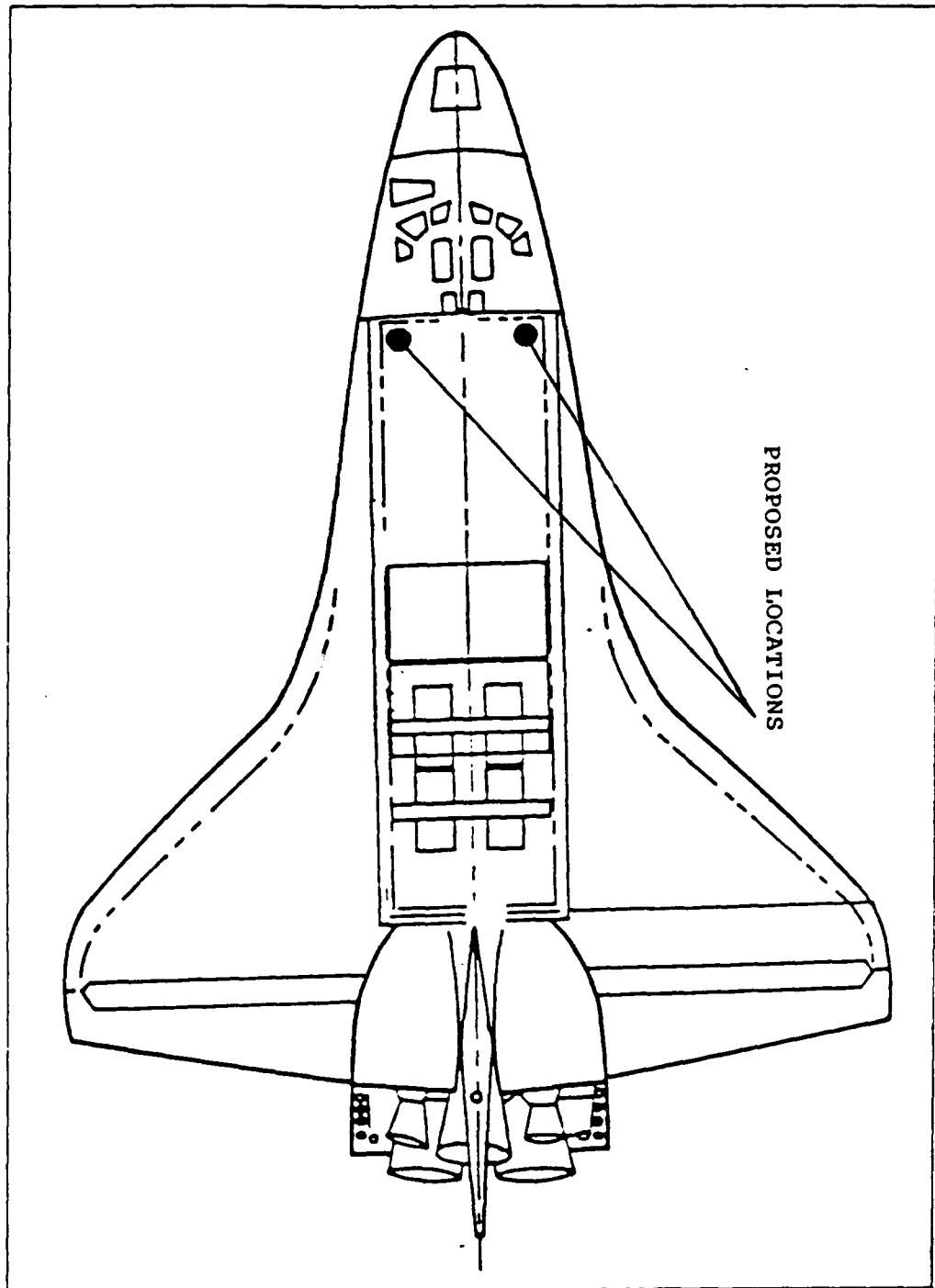


Figure 3.3 Top View of Space Shuttle Cargo Bay

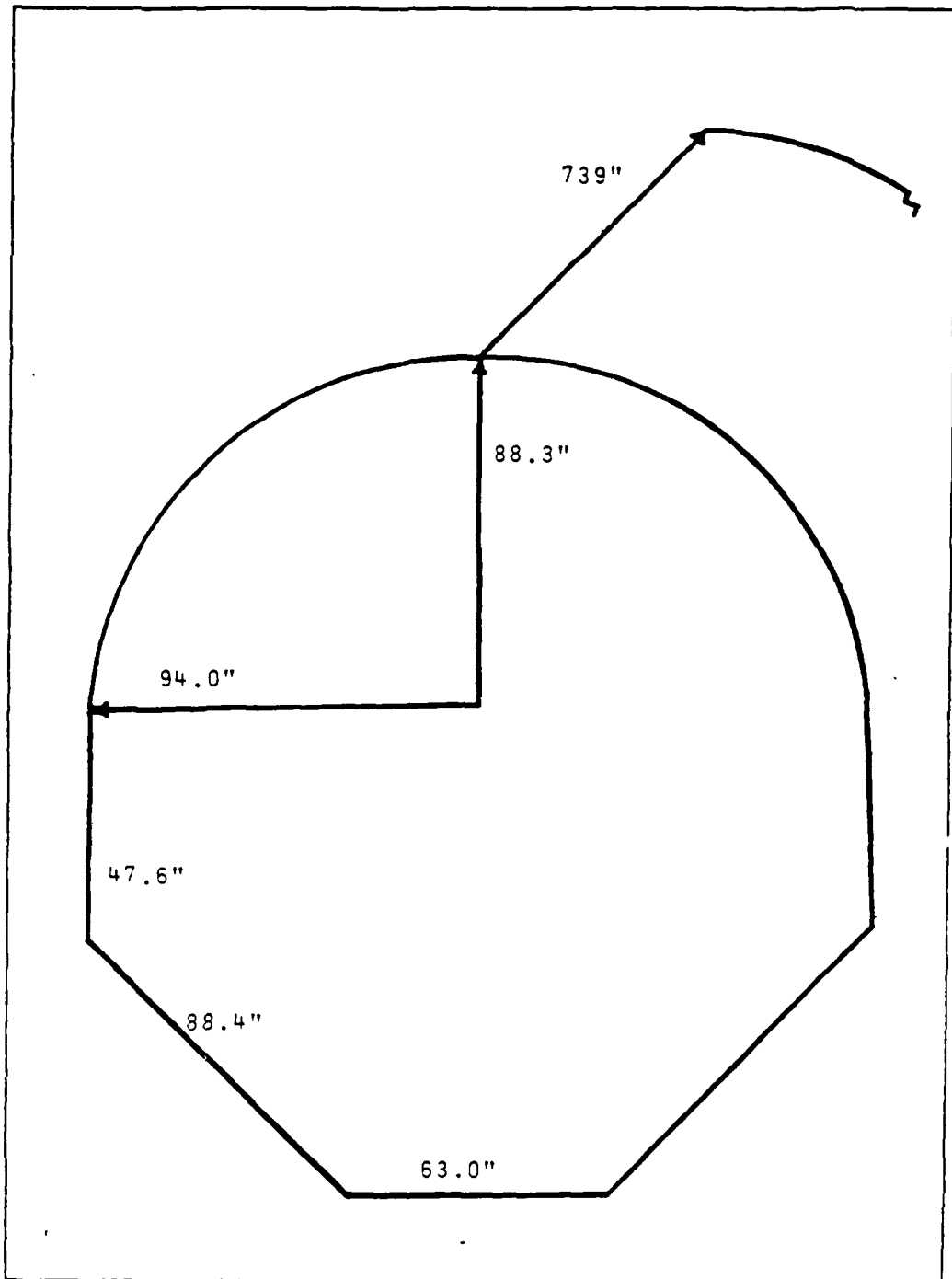


Figure 3.4 Shuttle Cargo Bay Dimensions

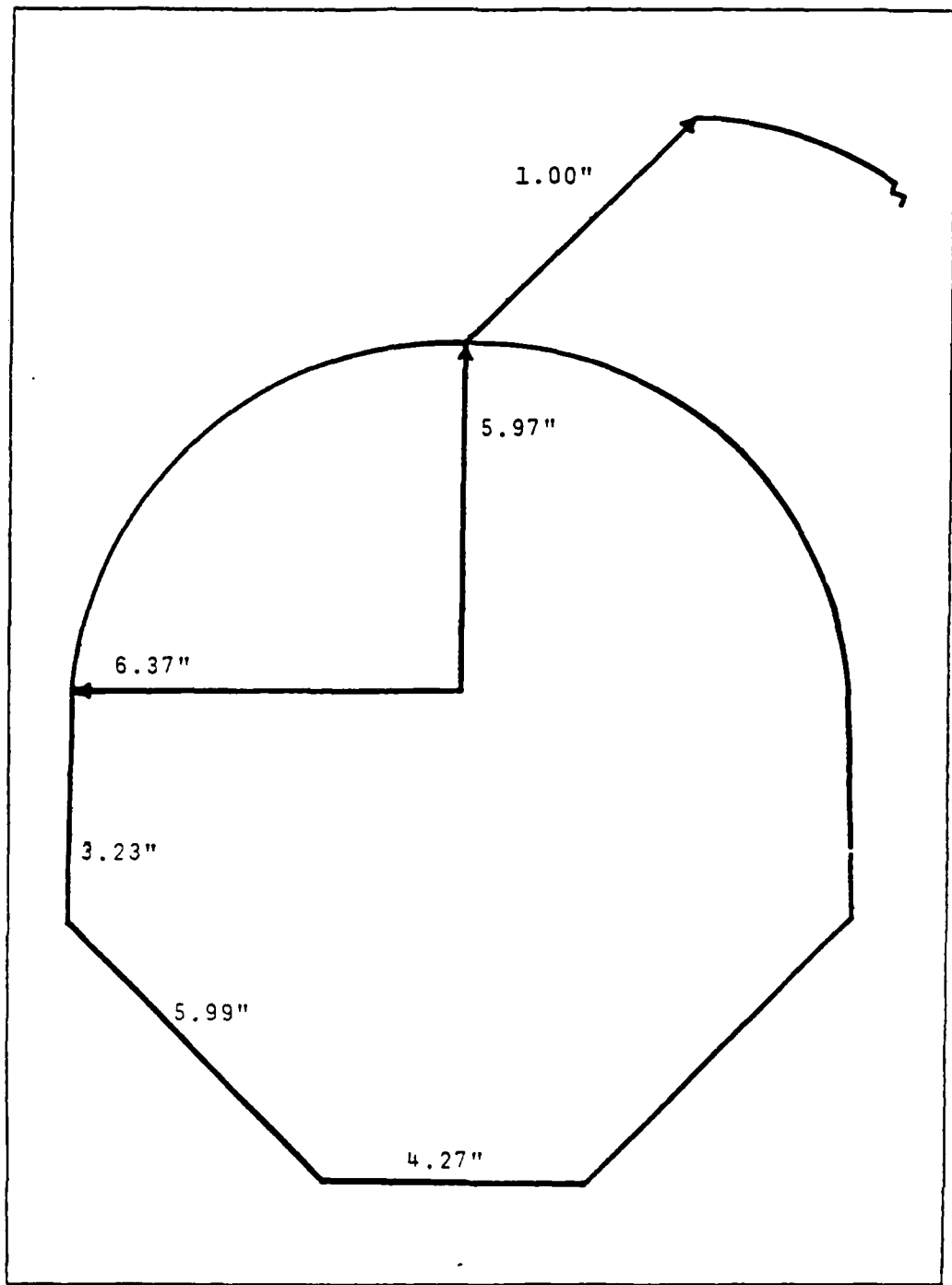


Figure 3.5 Plexiglass Model Experiment Dimensions



Figure 3.6 Photograph of Plexiglass Model

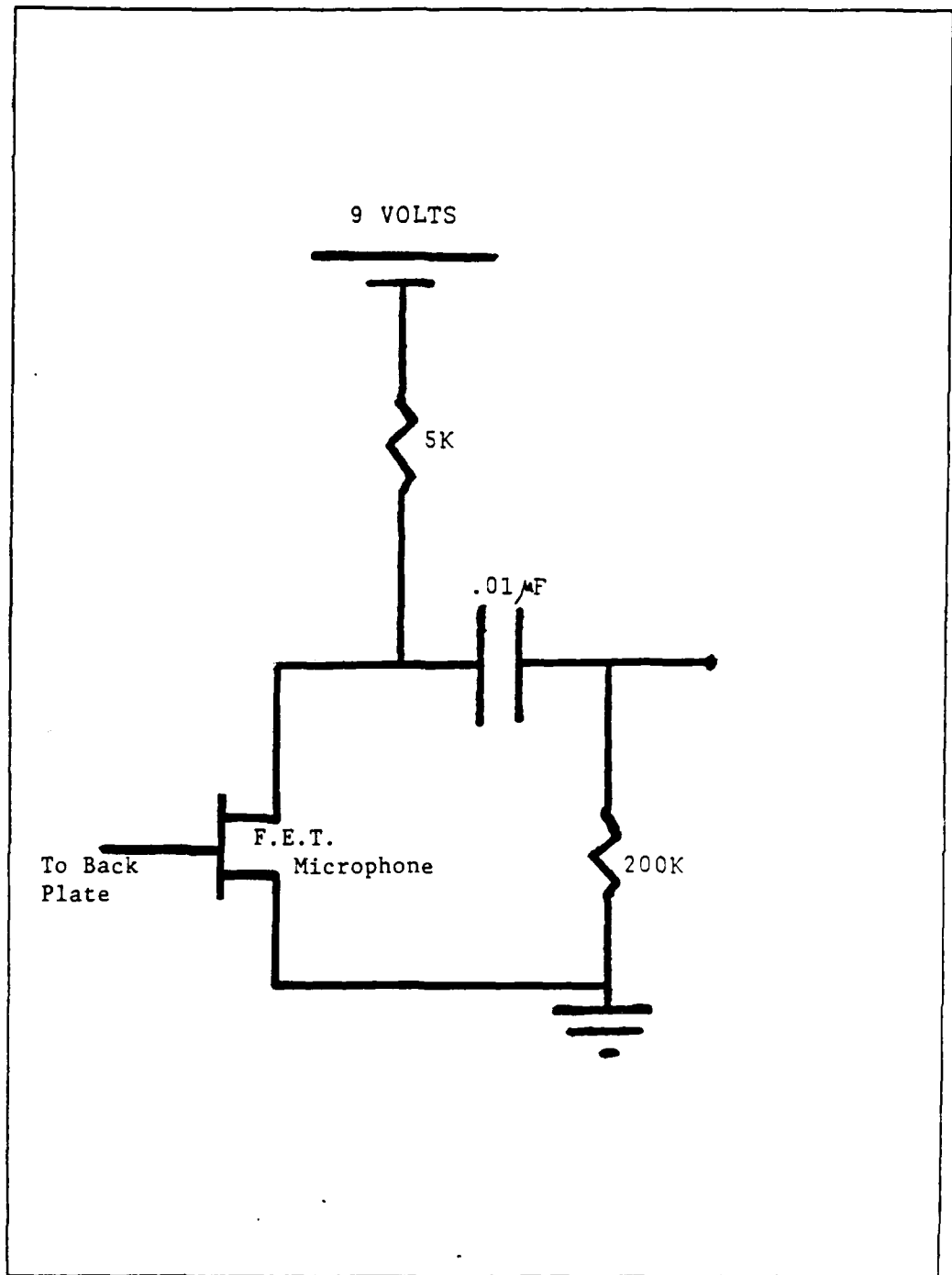


Figure 3.7 Microphone Bias Circuitry for Model

could remain tightly sealed throughout the data taking procedure.

The resulting modal pressure eigenfunctions are presented in Figures 3.8 to 3.12. The measured resonance frequencies of the model compared at worst to within four percent (average 1.2 %) to the harmonicity of the first five eigenvalues of a cylinder of equivalent cross-sectional area, calculated using the cited Morse equation.

The principle of adiabatic invariance, discussed by Greenspan [Ref. 17], guarantees that small deformations of the shape of the resonator which do not change the volume may perturb the eigenfunctions without changing the eigenfrequencies. This is required because no work ($W = PdV$) has been done against the radiation pressure, and consequently, there is no change in frequency since the ratio of energy to frequency is the adiabatic invariant. Because of the similitude, the theory presented for modal density in a resonant cylinder, given by Morse in Reference 16 starting page 399, can be applied to this geometry. It is used to derive an approximate density of modes within a specified frequency band as

$$\Delta N/\Delta F = 4\pi f^2 V/c^3 + \pi fA/2c^2 + L/8c$$

for a cylinder of volume V , Surface Area A , perimeter $L = 4\pi a + 4l$ (radius a and length l), and speed of sound c . The resulting resonant frequencies for the model, calculated resonant frequencies for the Space Shuttle

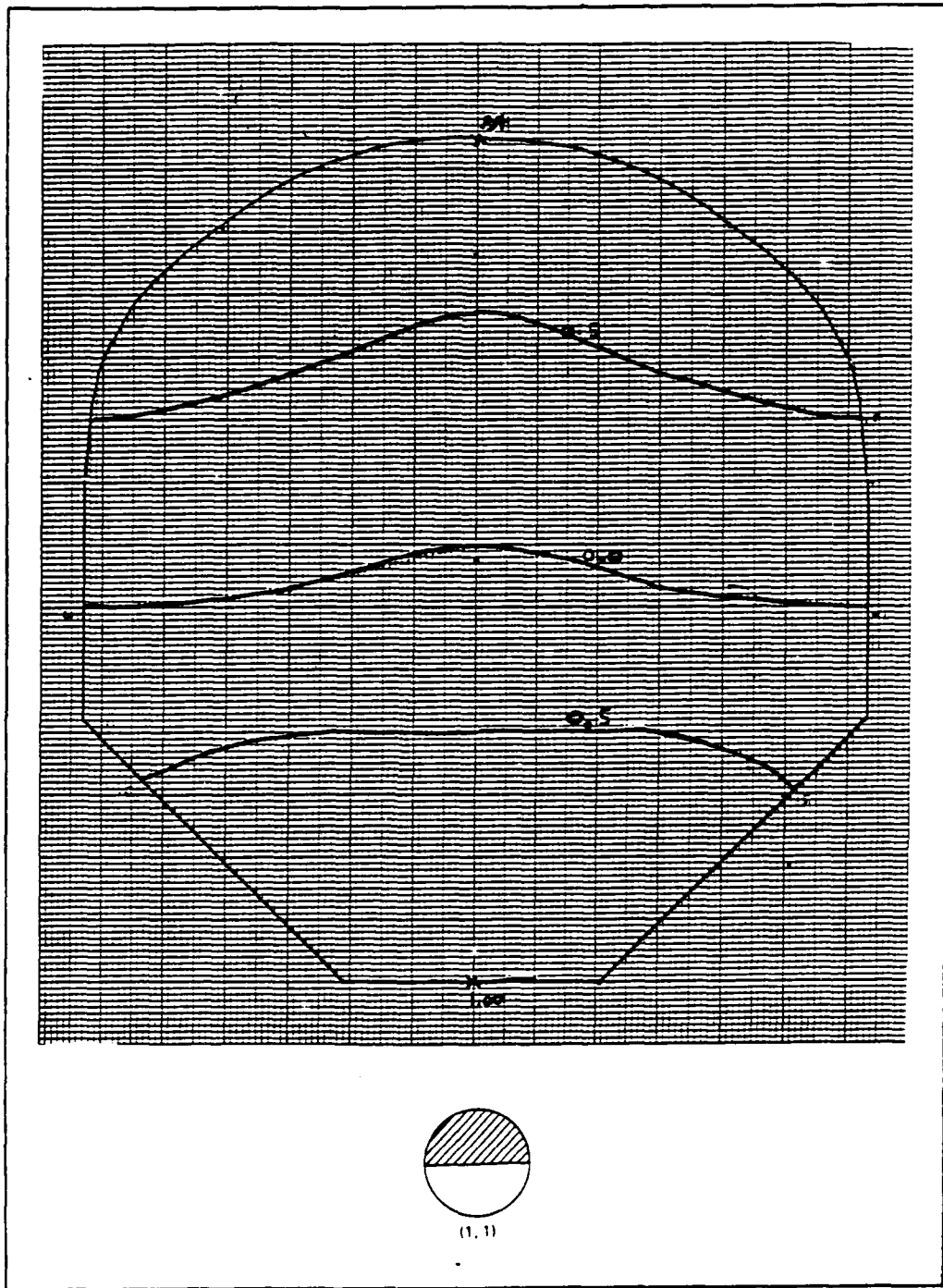


Figure 3.8 Equal Amplitude Contours First Mode
of Plexiglass Model and Cylinder

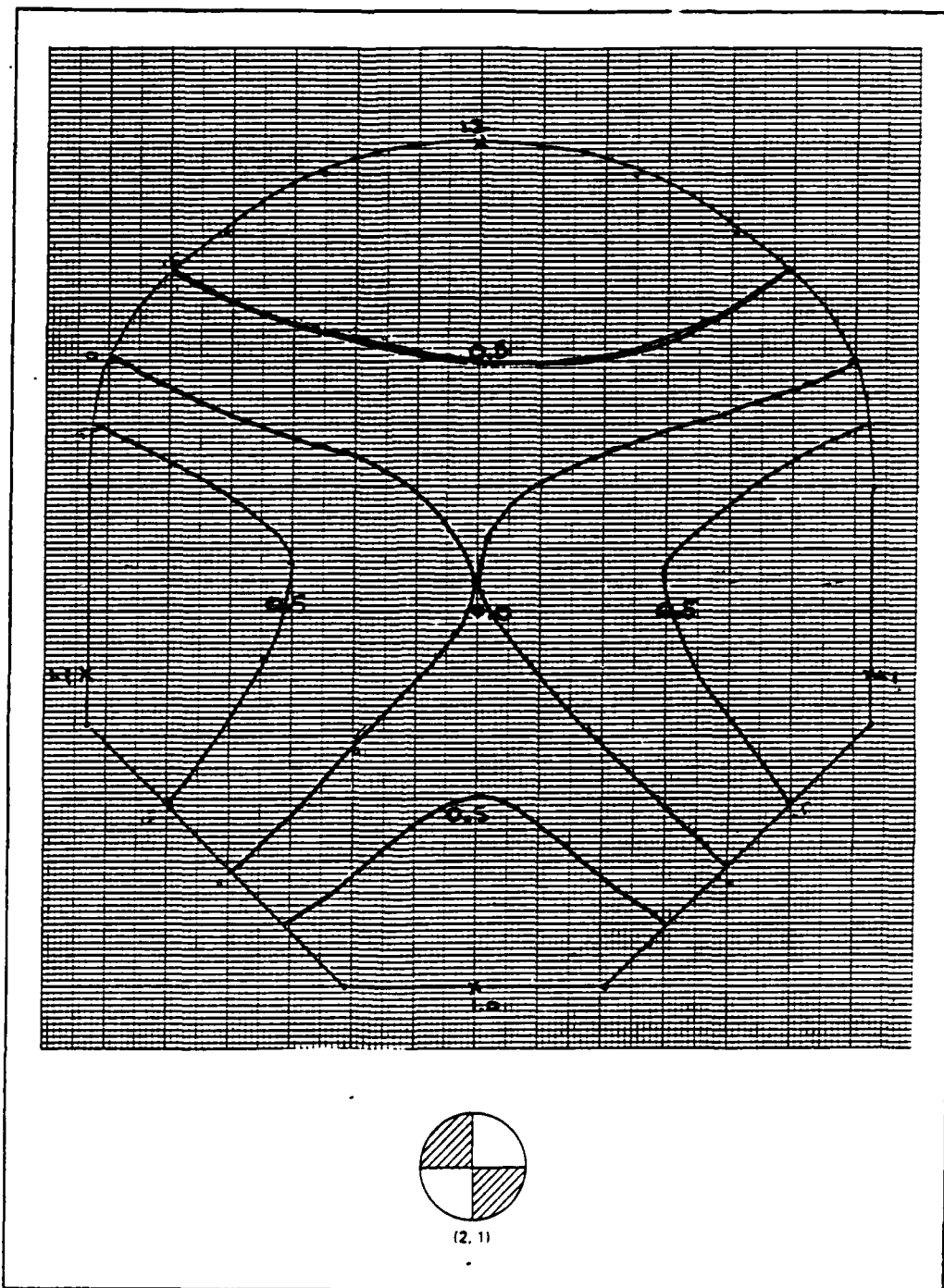


Figure 3.9 Equal Amplitude Contours Second Mode
of Plexiglass Model and Cylinder

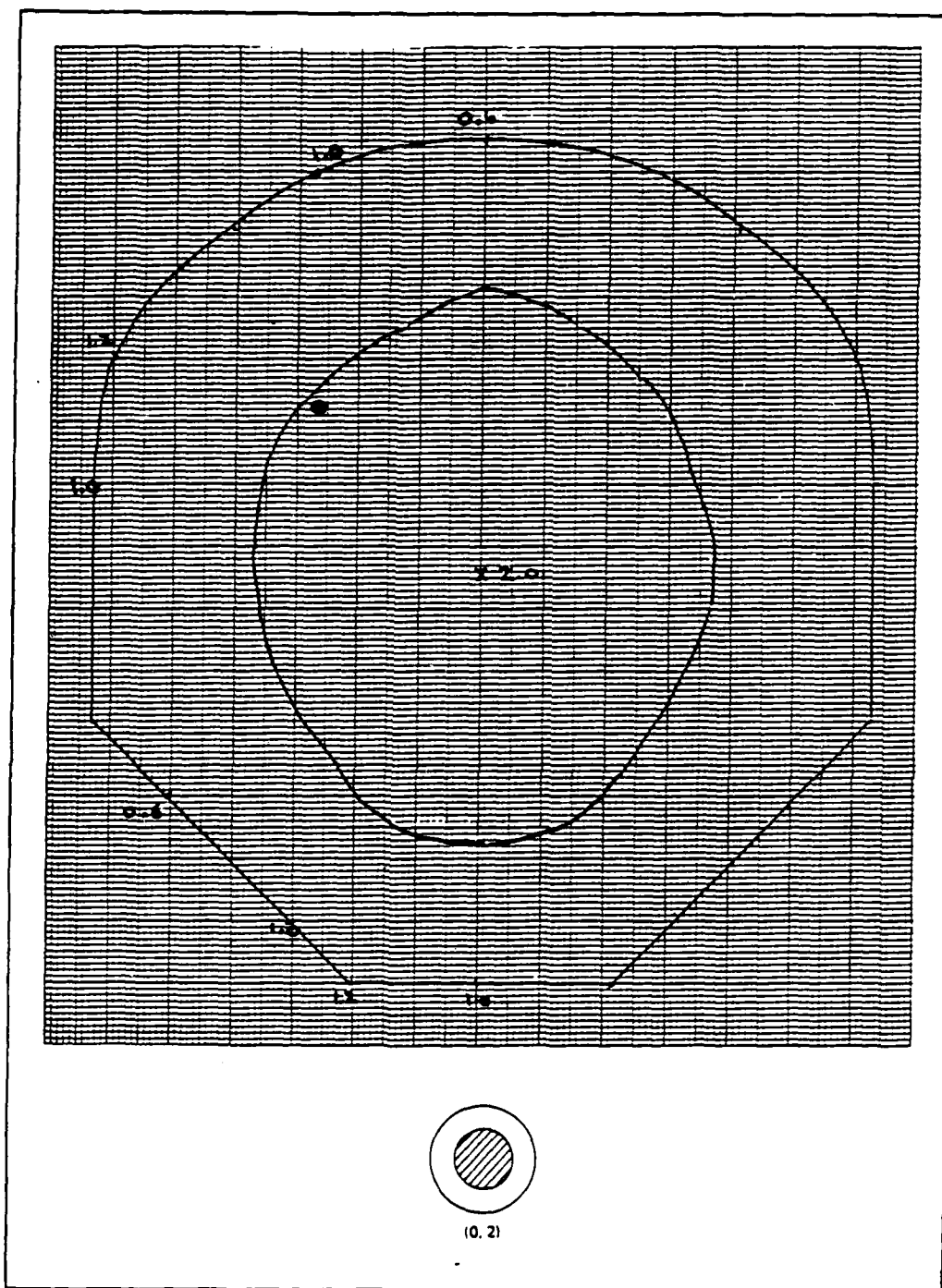


Figure 3.10 Equal Amplitude Contours Third Mode
of Plexiglass Model and Cylinder

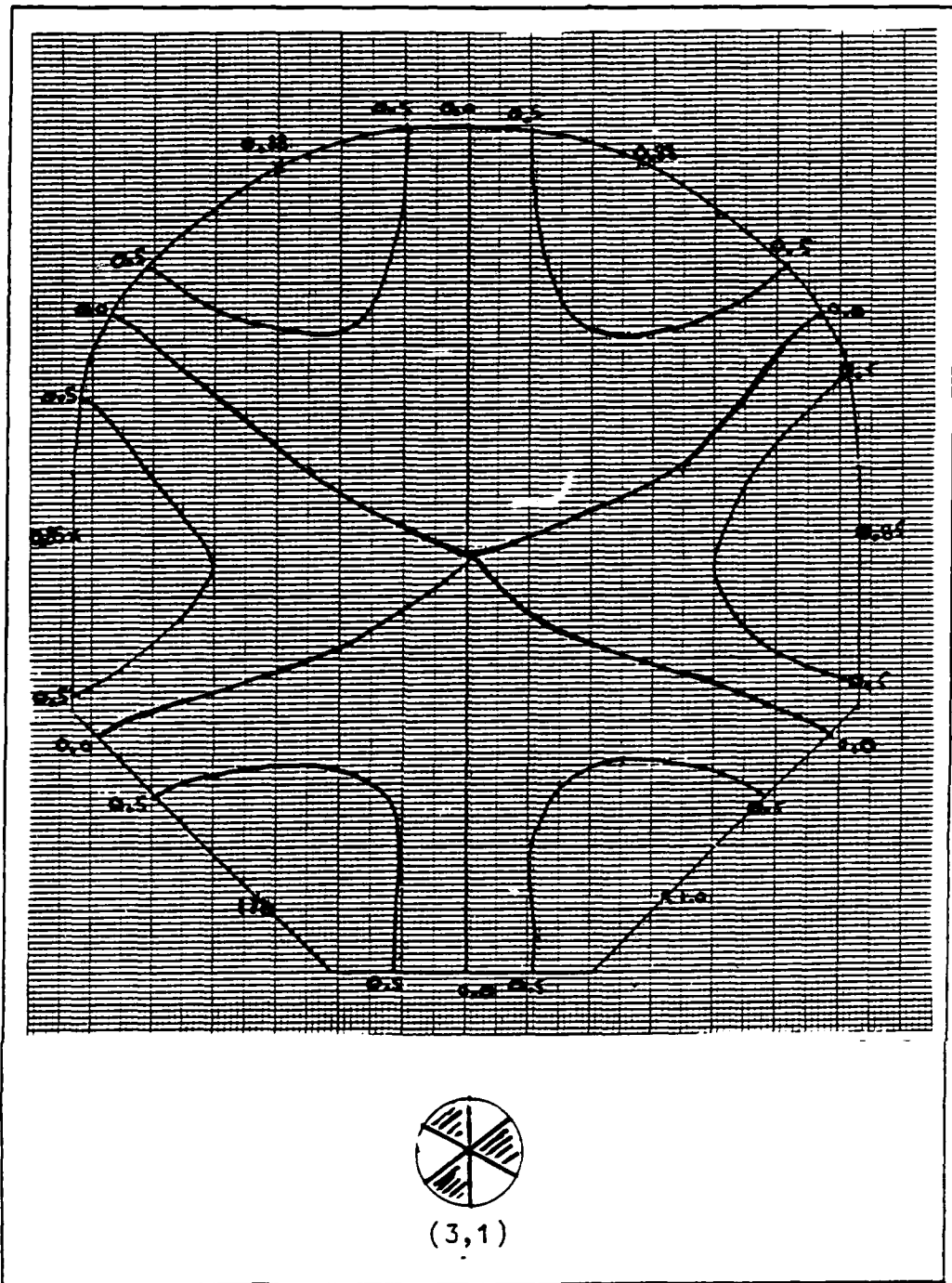


Figure 3.11 Equal Amplitude Contours Fourth Mode
of Plexiglass Model and Cylinder

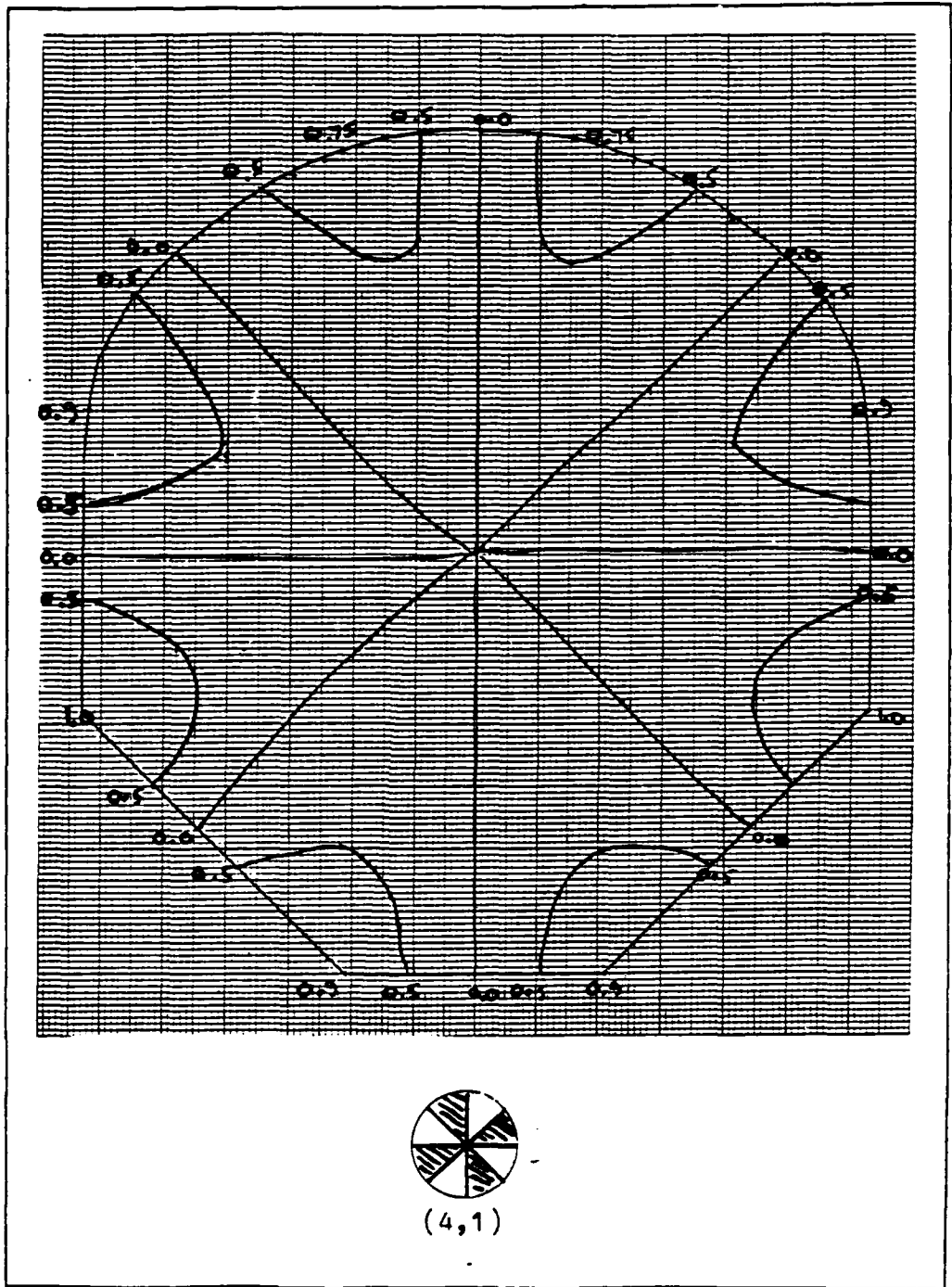


Figure 3.12 Equal Amplitude Contours Fifth Mode
of Plexiglass Model and Cylinder

TABLE IV. RESULTS OF 1/14.7 SCALE MODEL COMPARED WITH
CYLINDRICALLY SYMMETRIC APPROXIMATION.

Mode	Model Freq (Hz)	Shuttle Freq (Hz)	Modal Density (Hz ⁻¹)	Harmonicity (measured)	Cylindrical Harmonicity (theory)	$\Delta\%$	Model Q
1,1	606	41.07	0.85	1.0	1.0	0	26.3
2,1	995	67.4	1.95	1.635	1.658	-1.4	45.2
0,2	1259	85.3	2.98	2.076	2.082	-0.3	53.6
3,1	1387	94.0	3.56	2.287	2.283	+0.2	42.0
4,1	1690	114.5	5.14	2.782	2.891	-3.8	62.5

The modal density is calculated for the actual shuttle dimensions.

$$f_{\text{shuttle}} = f_{\text{model}}/14.757,$$

and harmonicity comparisons to an equivalent cylinder are presented in Table IV. Harmonicity is the ratio of the sequential values of resonant frequencies to the value of the first resonance. A rigid cylinder of 2.4 meters radius is shown to have harmonicity within 4% of the shuttle bay geometry as cited earlier.

5. Strong Point Sources in the Far Field

In this case a sparse co-planar array will be exposed to a nearly planar fronted travelling wave. Each element will record a phase shifted, equal amplitude spectral pressure component. The phase shift is given by the argument of the received spectral signal, hence, the time shift T is given by:

$$T = \frac{Kd \sin\phi \cos(\psi - \phi_0)}{\omega}$$

The above expression is useful in cross-correlation tracking of far field sources. Note that if ϕ is modulo π , or the wavefront enters normal to the array plane, the elements are cophased and a condition exists which is indistinguishable from a standing wave resonance. The problems with zeros in $\cos(\psi - \phi)$ can be circumvented by having more than two non-colinear elements. Grating lobes [Ref. 14] caused by spatial aliasing will exist for frequencies above $f = c/2d$ (where d is the spacing between elements), giving an upper bound on the ability to process spectral information.

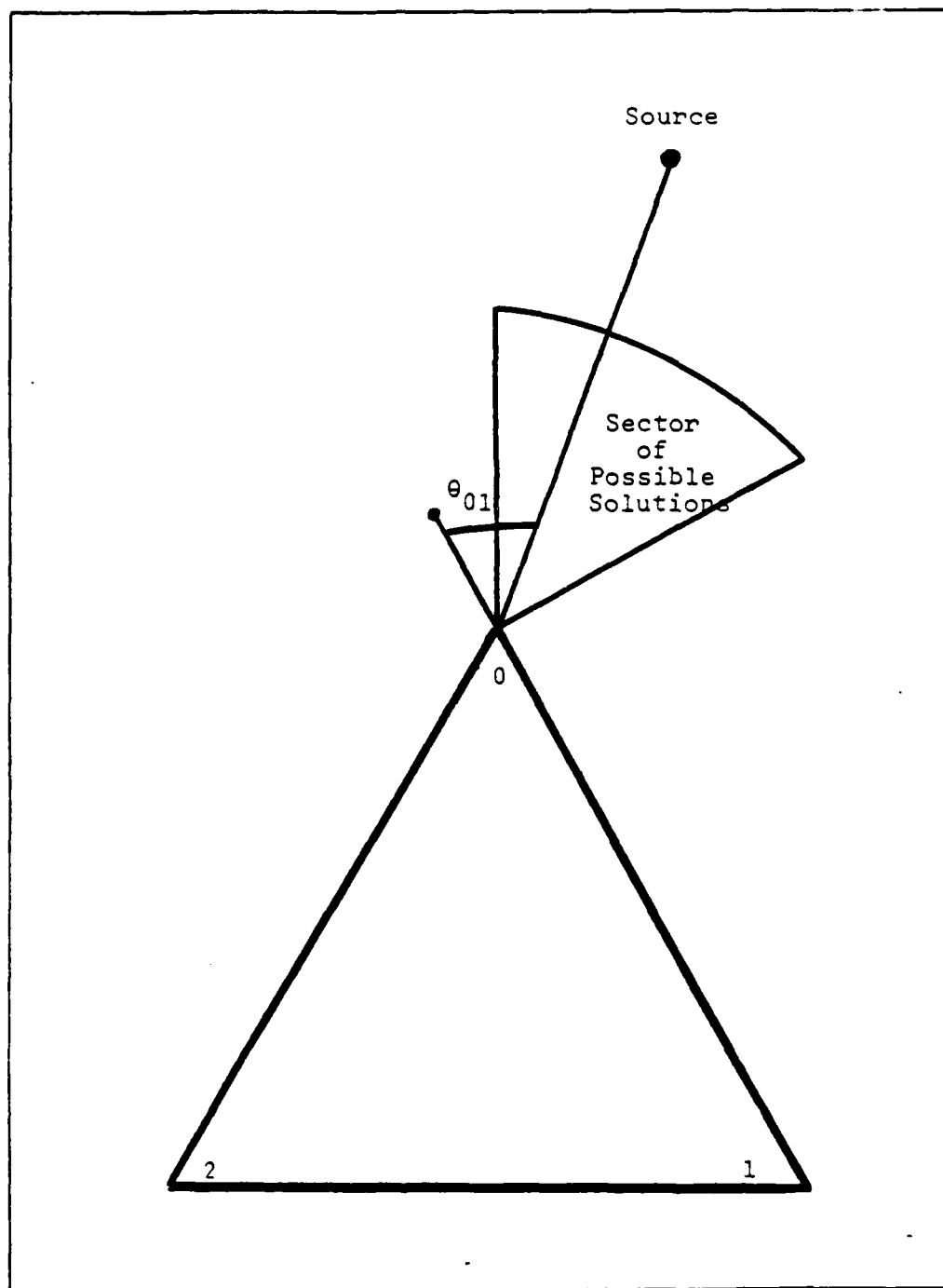


Figure 3.13 Arrival Angle of Plane Wave Incident
Upon Co-planar Trigonal Array

For this experiment $d = 12.1$ inches, placing an upper bound of 550 Hz for spatial processing. Note that the modal density at this frequency exceeds 108 modes per Hz, saturating the one Hz processing resolution.

To process this information, first, the temporal order of arrival of the wavefront at each element is used to restrict the direction to a sixty degree sector [See figure 3.13]. The resultant phase shifts are recorded by a FFT using the time series of interest for each microphone output corrected for differential amplitude and phase response of the microphone and input stages. The corrected phase information is used in the following equations (variables defined by Figure 3.13):

1) Azimuth

$$30^\circ \leq \theta_{01} = \tan^{-1} \left[\frac{\Delta\phi_{12}/\Delta\phi_{01} - \cos(120)}{\sin(120)} \right] \leq 90^\circ$$

2) Elevation

$$0 \leq \phi = \cos^{-1} \left[\frac{(\Delta\phi_{01} * c)}{d \cos(\theta_{01}) 2\pi f} \right]$$

where $\Delta\phi$ is the phase difference between the subscripted elements. The solution reference shifts to accommodate the temporal order of arrival. The solution may be shifted back to the absolute cargo bay reference geometry. These two equations resolve source azimuth and elevation.

Two experiments were performed to test the above technique in the NPS anechoic chamber using the experimental apparatus diagrammed in Figure 3.14. In the first experiment the signals from the two Bruel and Kjaer (Model 4177) one-half inch microphones spaced 5 cm apart were cross-correlated. The time shifts found in the cross-correlated signals agreed with the solution presented earlier in this section. The two signals were graphed in the time domain for five configurations of offset azimuth. The results are presented in Figures 3.15 to 3.19. The phase shift agrees with $\Delta\phi = 2\pi fT$ of the first experiment which is the solution used for directional processing. Time shifts were verified using the cross-correlation function of the HP 3562A Dual Channel Dynamic Signal Analyzer with its cursor function.

B. ANALYSIS TO DATE

There have been two approaches to the analysis of flight data on previous STS missions. The Dynamic Acoustic and Thermal Environments (DATE) group of NASA Goddard Space Flight Center [Ref. 2] has taken analog magnetic tape recorded pressure transducer voltage output readings and processed the power spectra in one-third octave bandwidths. This point receiver power spectral density approach has provided no narrowband information about modal patterns and

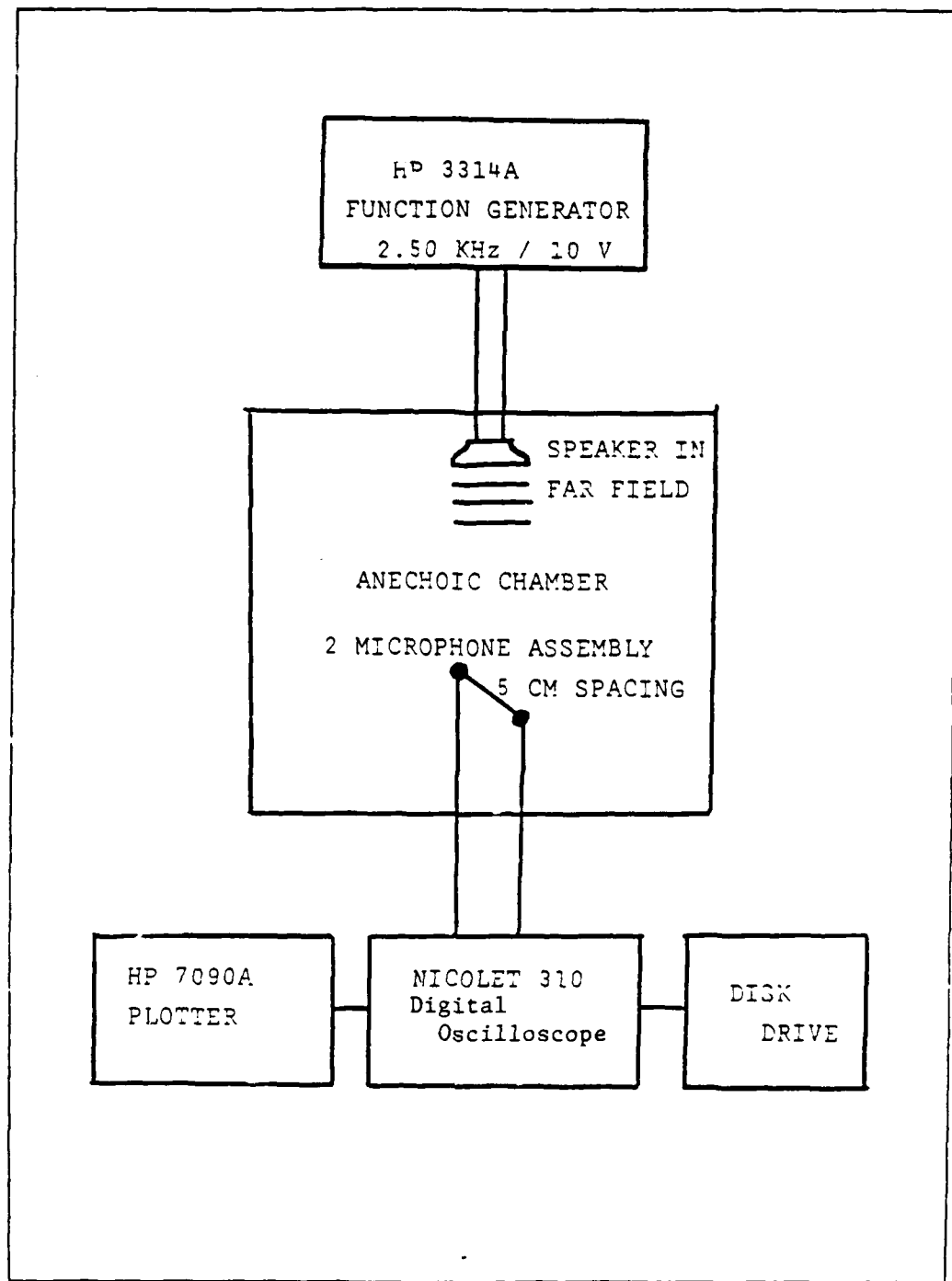


Figure 3.14 Experimental Apparatus used in 2 Element Array Phase Experiment

ANECHOIC CHAMBER



PLANE WAVES FROM SOURCE
IN THE FAR FIELD



MIC CH2 MIC CH1

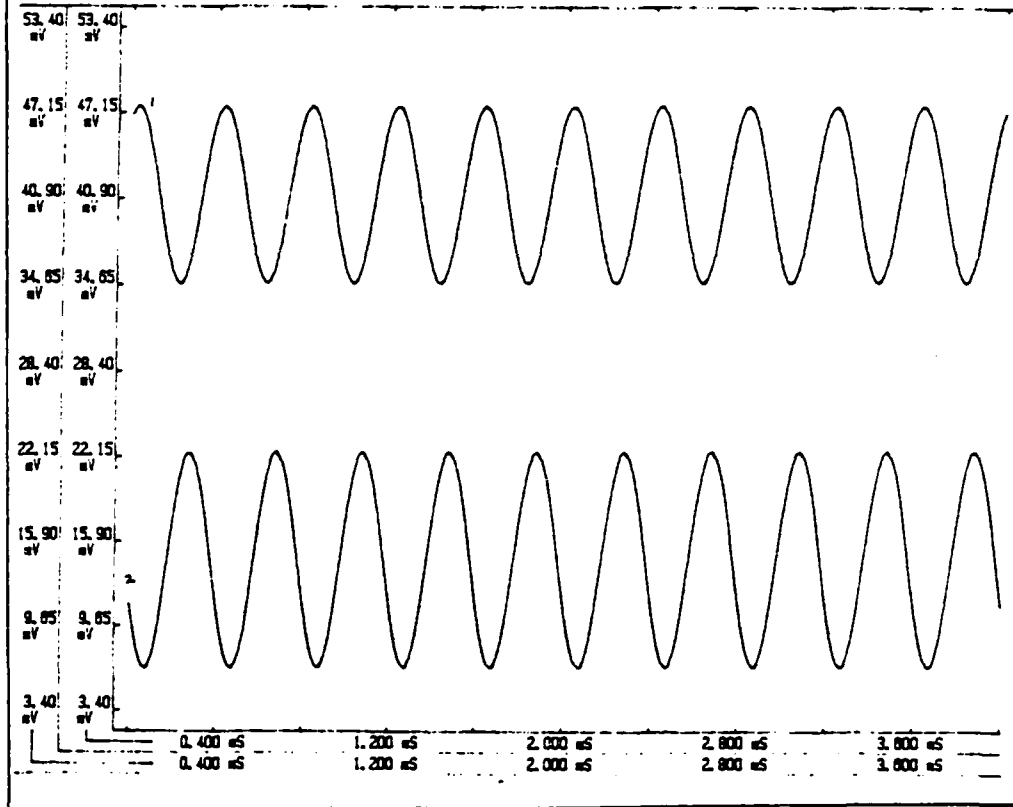


Figure 3.15 Time Series Comparison of Received
Signal by 2 Element Array (0° Offset)

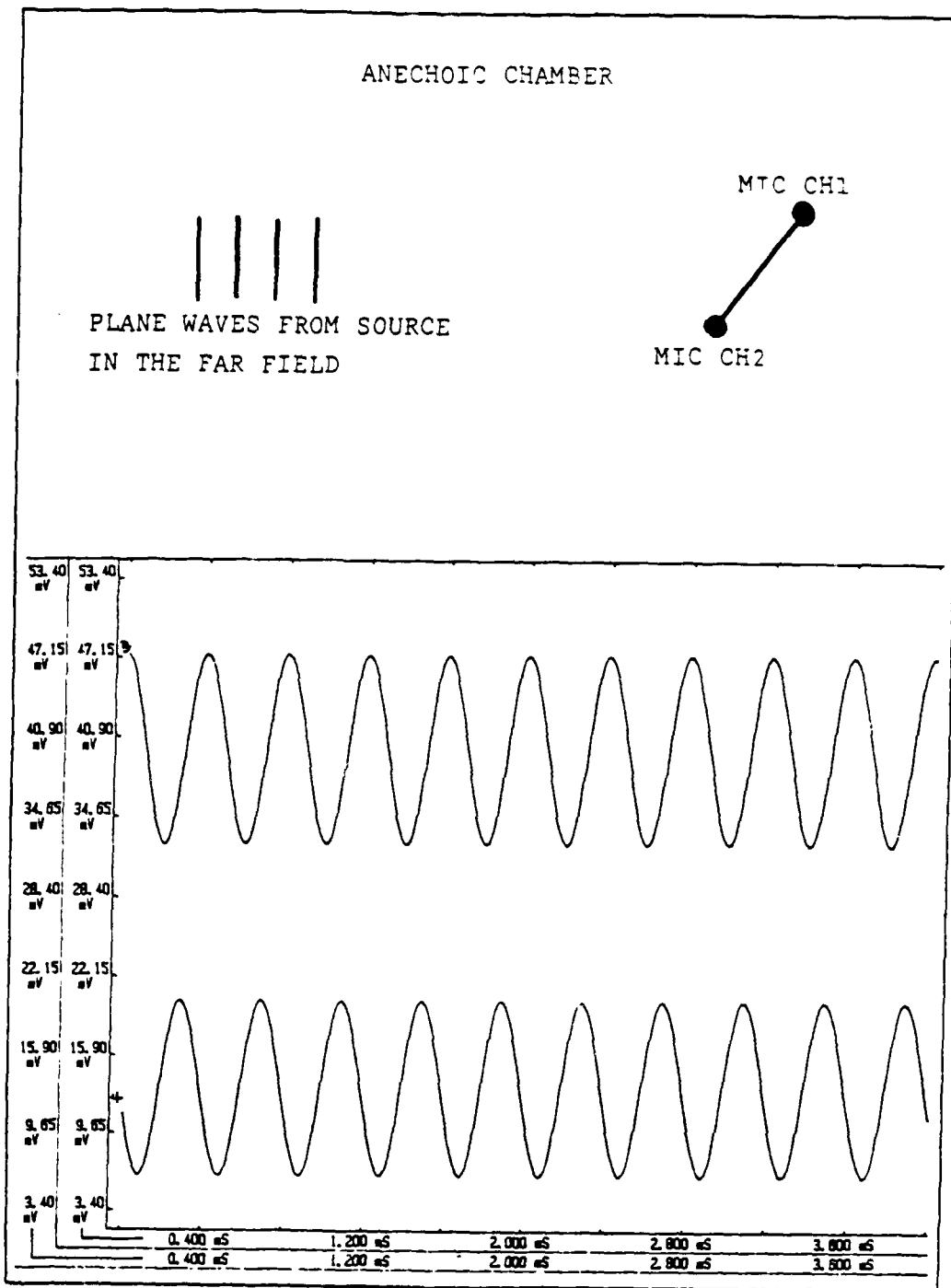


Figure 3.16 Time Series Comparison of Received
Signal by 2 Element Array (45° Offset)

ANECHOIC CHAMBER

PLANE WAVES FROM SOURCE
IN THE FAR FIELD

MIC CH1
MIC CH2

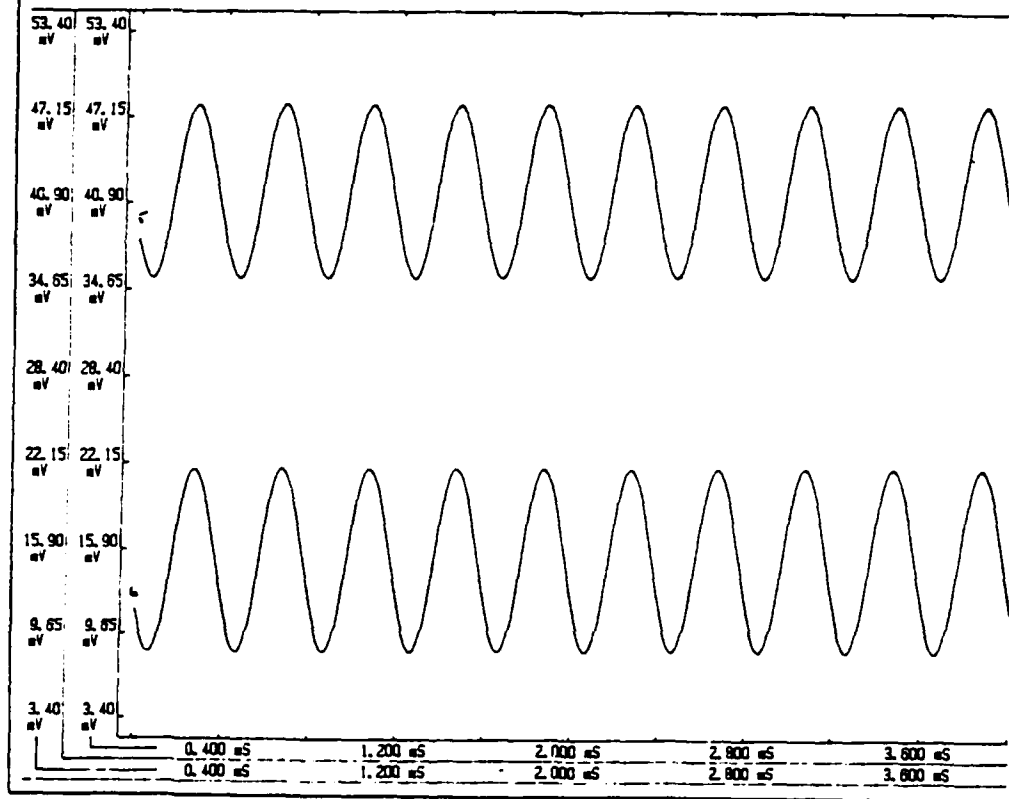


Figure 3.17 Time Series Comparison of Received
Signal by 2 Element Array (90° Offset)

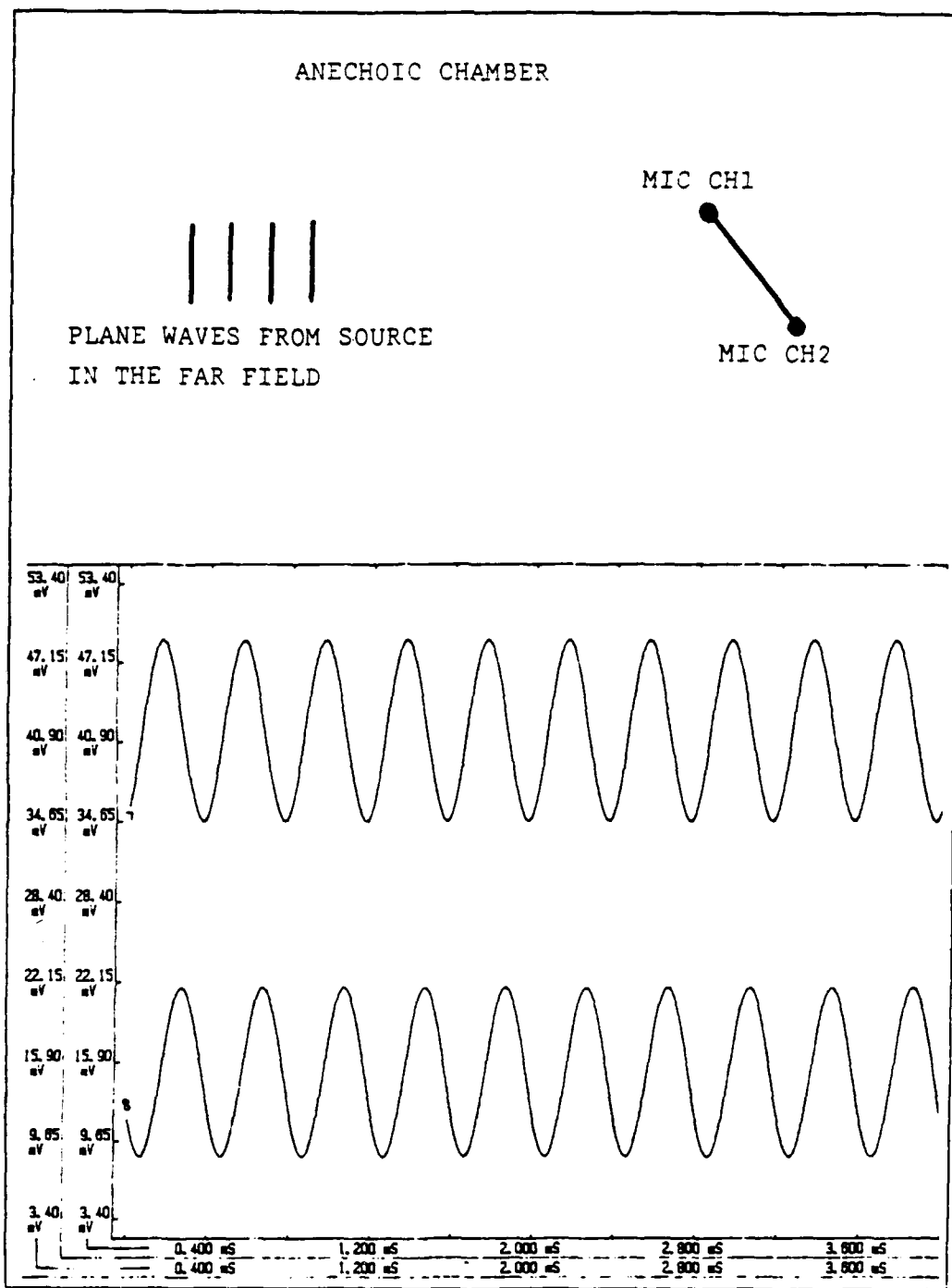


Figure 3.18 Time Series Comparison of Received
Signal by 2 Element Array (135° Offset)

ANECHOIC CHAMBER



PLANE WAVES FROM SOURCE
IN THE FAR FIELD



MIC CH1 MIC CH2

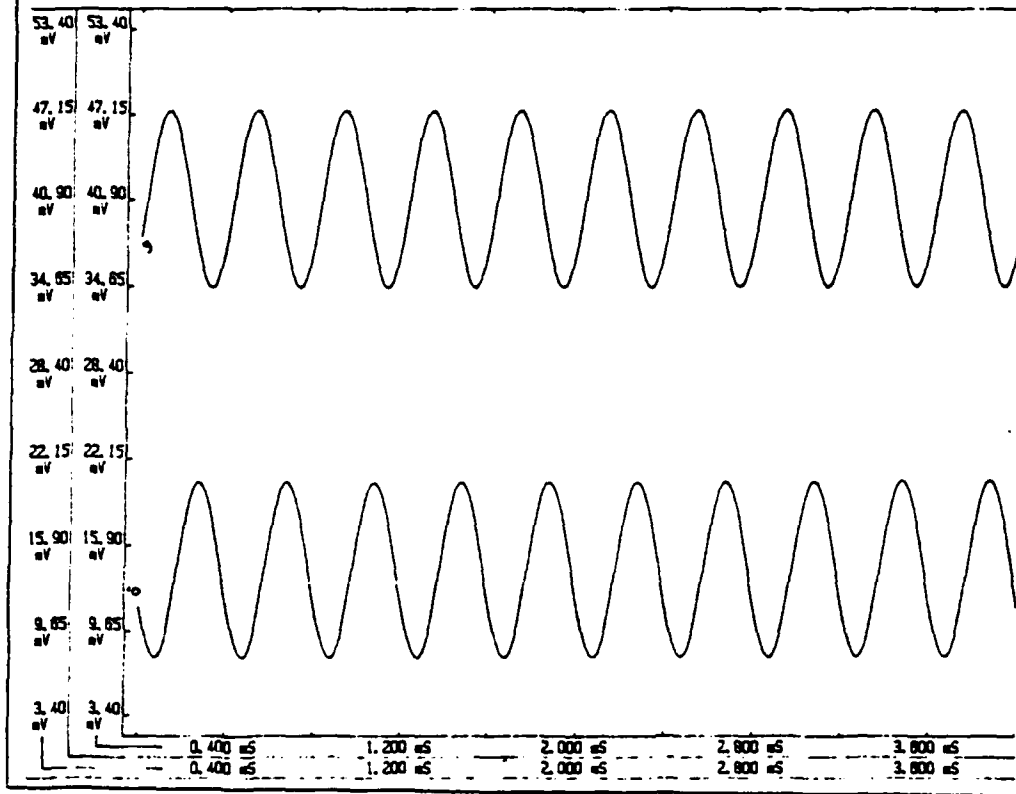


Figure 3.19 Time Series Comparison of Received
Signal by 2 Element Array (180° Offset)

gives no directional information about high intensity sources.

A question has been raised about the mechanical response of the vibration isolation mounts by C. D. Stehle [Ref. 6]. CDR Stehle's analysis suggested that there are isolator resonances within the 110 and 315 Hz analysis bands, which may have permitted vibrationally coupled signals to corrupt the data. This could account for the reported peaks in the power spectra [Ref. 2].

The Aerospace Corporation of El Segundo, California, has developed a model to help STS orbiter payload bay users design for the expected acoustic environment of any particular mission, and to help NASA planners optimally to configure payloads within the cargo bay. This model divides the cargo bay into seven subvolumes of adiabatically perturbed rectangular parallelepipeds and maintains a power balance of the space averaged mean square pressure for the steady state solution within each subvolume. The input power into each subvolume is provided by the exterior engine noise field through the joint acceptance function of the structural panels. The internal modal density for one-third octave bandwidths is computed as the eigenvalues of the homogeneous Helmholtz equation for a perturbed boundary rectangular parallelepiped with walls of slight, constant curvature. Hence:

$$\nabla^2 \phi + k^2 \phi = 0$$

where

$$k^2 = \left[\begin{array}{ccc} (p\pi)^2 & + & (q\pi)^2 & + & (r\pi)^2 \\ \frac{\quad}{a} & & \frac{\quad}{b} & & \frac{\quad}{c} \end{array} \right]$$

of the p, q, r, mode for dimensions (adjusted for perturbations) a x b x c. This modeling approach provides designers with only spatially and frequency averaged mean square pressures and does not address modal eigenfunctions or high intensity narrowband sources, where localized pressure may be well above averaged values. The NPS experiment is designed to identify these tendencies towards localizing the distribution of dynamic pressure in both frequency and space. Once verified, this experiment could show the value of developing a finite element analysis for resonant modes which may help to identify high intensity noise sources, for example hydrodynamically induced or mechanically resonant structures, with the NPS experiment's directional processing narrowband capability.

IV. FLIGHT DATA PROCESSING

A. DISCUSSION

This chapter will describe procedures to record and retrieve data from the bubble memory recorder. A software procedure is developed to measure the differential electrical front end response spectra (amplitude and phase) for each of the three elements as described in Chapter II. A discussion of software used to recognize resonance and strong travelling waves as described in Chapter III is presented. The entire data reduction development is accomplished using the capabilities of the ILS software available for IBM personal computers. Batch data file listings are provided and discussed using an example of output data for a test case.

B. ILS

Interactive Laboratory System (ILS) is a software system for digital signal processing in the PC-DOS and MS-DOS environment. Features supported by ILS include data display and editing, digital filtering, spectral analysis, speech processing, and pattern classification. ILS also supports data acquisition, file management, data manipulation, and graphics, thus offering a system capable of handling large

sequential data files for batch processing with a minimum of coding effort. ILS has the advantage of being both general and versatile. The ILS system is easily understood by persons of moderate signal processing background and is well documented. For the understanding of the syntax presented in the batch file listings provided, the reader is referred to the ILS command Reference Guide v6.0 [Ref. 18].

C. FRONT END ELEMENT DIFFERENTIAL ANALYSIS

The goal of this analysis is to determine differential amplitudes between data channels and correct phase differences by bin shifts in the input time series. To obtain differential gain/phase between data element channels, it is necessary first to know how to operate the bubble memory recorder with its own interface peripheral computer and input the sequential data into the IBM PC.

The following abbreviations apply:

IBM PC = PC

Bubble Memory Interface Computer = BMI

↑ = Return

- = Blank

The following sequence will record and send the data to the IBM PC.

<u>Device</u>	<u>Command</u>	<u>Comments</u>
PC		<Load disk for ILS Data>
	cd Bubdata † ILS I †	
BMI	H W O 07 00 A B O 0600	<Commands sent automatically>
PC	Convert †	<DOS ASCII file formatted>
BMI	E -	<Sends data to PC>
PC	a) INTDATA.BAT †	<Places headers on Files>

BATCH LISTINGS OF INTDATA
(IN ILS SYNTAX)

```

FIL  ANDR
FIL  100
INA  H
INA  SF2500
FIL  200
INA  H
INA  SF2500
FIL  300
INA  H
INA  SF2500

```

At this point all of the sequential data for the three front end channels is in the IBM PC in ILS sample data file format. To analyze the data it must be converted to complex valued record data by the RECORDDATA batch file.

BATCH LISTINGS OF RECORDATA

FIL 100
FIL S101
OPN S
SRE 1
FIL 200
FIL S201
OPN S
SRE 1
FIL 300
FIL S301
OPN S
SRE 1

Now files 100, 200, 300 contain sampled time domain data for channels 1, 2, 3; while files 101, 201, 301 contain complex valued record data. The data may be displayed by the following batch files SAMPLEDISPLAY and RECORDDISPLAY.

BATCH FILE SAMPLEDISPLAY

FIL 100
DSP
FIL 200
DSP
FIL 30
DSP

Each display may be reviewed and dumped to the printer if a hard copy is desired by hitting shift Print_send on the IBM keyboard before "returning" for the next display. The plot is automatically scaled and documented by file and location within the file.

BATCH FILE RECORDDISPLAY

FIL 101
DRE 1
FIL 201
DRE 1
FILE 301
DRE 1

Here the records are displayed as was the sampled data with an automatic offset between frames of length as specified by the context. In the case of the analysis presented, this consists of 64 data points.

The next batch file, CROSSCOMPARE superimposes the magnitude/phase vs. frequency of the three input channels for differential comparison.

BATCH FILE CROSSCOMPARE

```
FIL 101
FIL S400
OPN S
FFT P1,1,8,,
FIL 201
FFT P2, 1, 8,,
FIL 301
FFT P3, 1, 8,,
FIL 400
DRE GSCP 1, 3
C
-
R
```

This provides the comparison of a 256 point FFT for the 3 input channels. The peaks may be marked by the file PEAKS.

BATCH FILE PEAKS

```
XTR 1, 1
XTR 2, 1
XTR 3, 1
```

The values for the peaks may be found for magnitude and phase (radians) by paging through to the bin indicated by the peak marker using the file GRABVALUES.

BATCH FILE GRABVALUES

DTO R SC 1
DTO R SC 2
DTO R SC 3

The final part of determining differential amplitude (now documented) and phase information is to convert phase differentials to bin shifts for each processing frequency bin using the formula.

$$\text{Bin shift} = \text{INT} \left[\left[\frac{(\text{Phase1} - \text{Phase2}) \times 2^n}{2 * \text{PI} \times \text{Frequency bin \#}} \right] \right]$$

where n=8 for a 256 point FFT. Note that differential amplitudes arise from different phase offsets which may occur due to complex impedance differences between the input electrical front ends of the channels. Also note that the ability of the software to provide phase adjustments by shifting input time records is inversely proportional to frequency favoring lower frequencies where the modal density is less. Adjustments to amplitude standing wave ratios are performed manually by using the differential results (in dB) produced by the input channel analysis as described in this section.

D. RESONANCE RECOGNITION

As described in Chapter III, resonance will be recognized by cophasing modulo pi of the three data channels corrected for any differential electrical response. This condition is readily visible from a slightly modified

version of CROSSCOMPARE using the calculated Bin Shift Values (BSV) in the new batch file analyze.

```
BATCH FILE ANALYZE
FIL 101
FIL S400
OPN S
FPT P1, 1, 8,, BSV1
FIL 201
FFT P2, 1, 8,, BSV2
FIL 301
FFT P3, 1, 8,, BSV3
FIL 400
DRE GSCP 1, 3
      C
      -
      R
```

where BSV1 = 0; BSV2 and BSV3 are values from the differential element measurements compared to channel 1. By looking in the vicinity of the frequency bin of interest the cophasing is readily apparent. The standing wave ratios and closeness of cophasing may be read using the GRABVALUES file as presented earlier.

E. STRONG SOURCE RECOGNITION

The following batch file will show where strong spectral amplitudes occur, and by noting the data frames where the phenomena is strongest ANALYZE may be used to calculate a corresponding direction (as presented in Chapter III) to the source.

```
BATCH FILE STRONGSOURCE
FILE 100
SDI
FIL 200
SDI
FIL 300
SDI
```

Using Batch file strong source, the SDI command gives a waterfall spectral display of FFT frequency vs. time for each data channel. If a strong spectral source occurs (not identified as a resonance) ANALYZE may be used along with GRABVALUES to get the Acoustic phase differential between channels and the direction calculated as shown in chapter three directly.

F. EXAMPLE PROBLEM

In this section a sample problem is provided to demonstrate the capabilities and usage of the software developed in sections C, D, and E. A resonant calibrator box (described in Chapter II.A) was driven at its second resonant mode of frequency 381 Hz with two microphone channels recording the pressure signal at the maximum located at the rear face of the calibrator. The two channels were recorded, transferred, transformed into analysis and record data, displayed and cross-compared as described in section C. The time domain analysis data is shown in Figure 4.1 for channel 1 and Figure 4.2 for channel 2 using the SAMPLEDISPLAY file. Note that channel 2 has

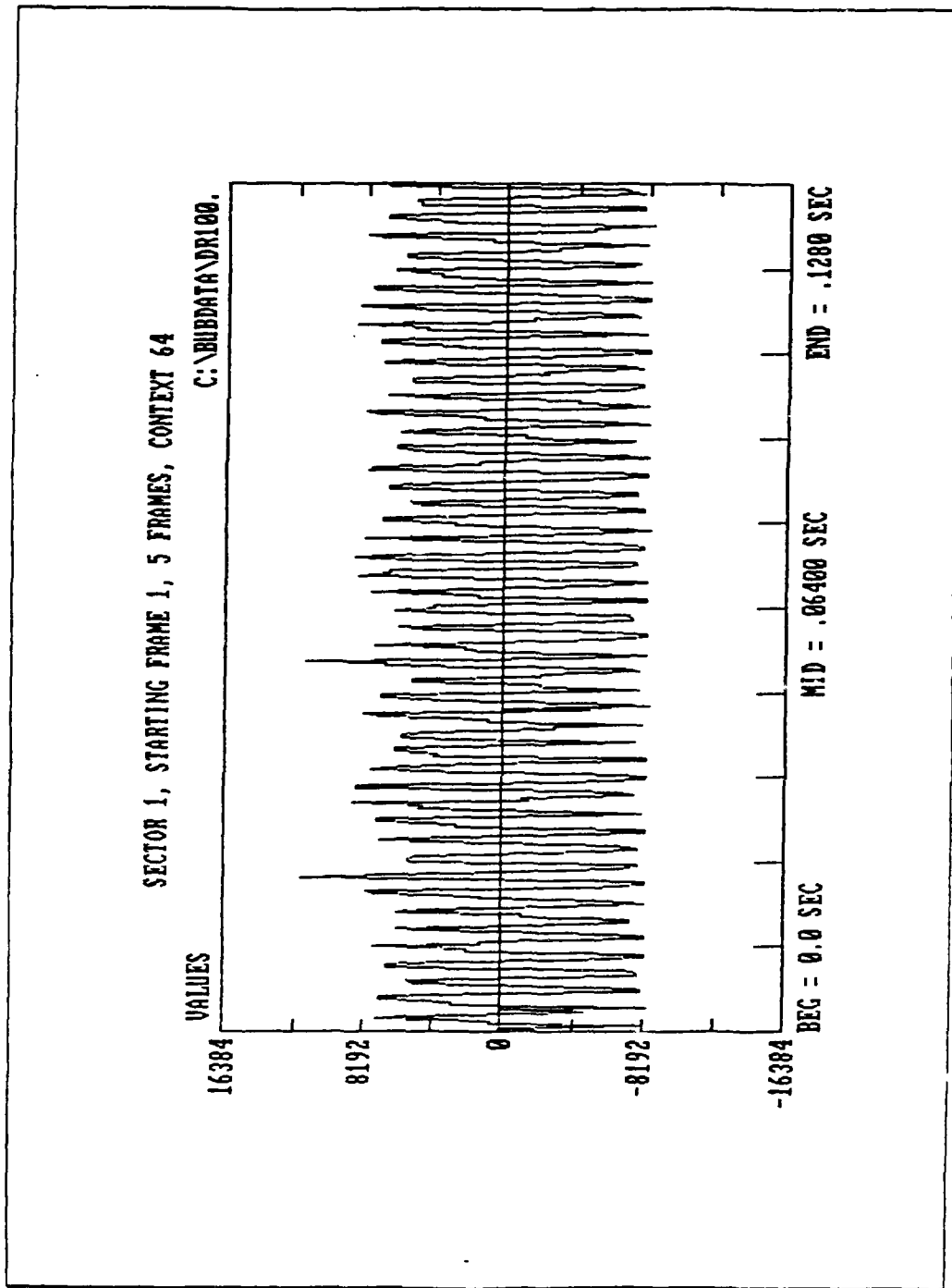


Figure 4.1 Sample Data Channel 1 for Test Case

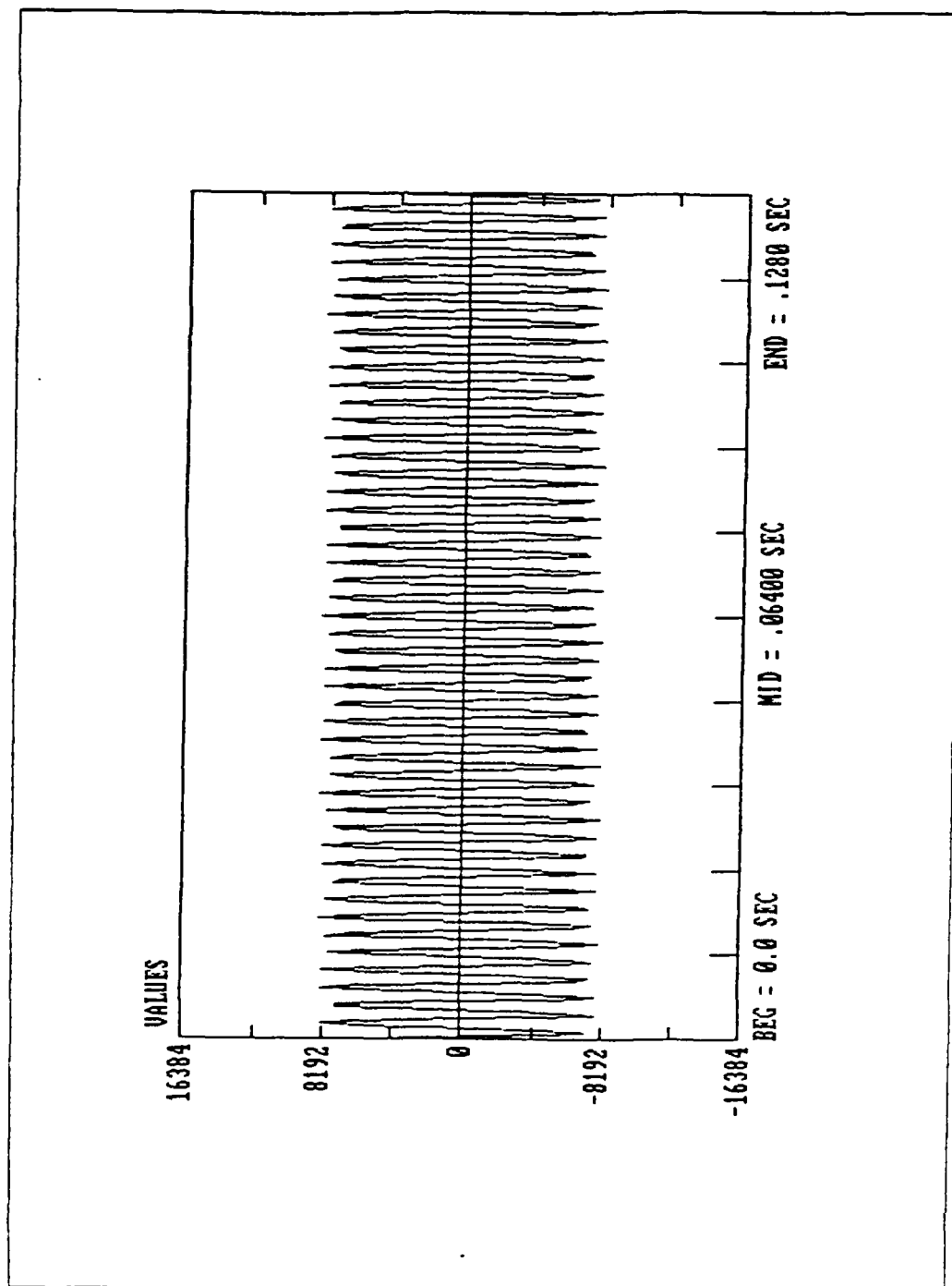


Figure 4.2 Sample Data Channel 2 for Test Case

much lower noise in the channel input. Fortunately, the averaging property of the Fourier Transform helps diminish the effects of random noise in the channels. The record data is shown in Figures 4.3 for channel 1 and 4.4 for channel 2, produced by the RECORDDISPLAY file. File records of 64 points each are displayed. The file RECORDATA had been previously run to produce the record data from the analysis data files. The batch file CROSSCOMPARE was then executed to produce a comparison record file 400 shown in Figure 4.5. The peak amplitudes occur at bin 39 corresponding to 380 Hz ($39 \times 2500/256 = \text{Bin number} \times \text{FFT length/sample rate}$) with an error of \pm one-half bin is equivalent to ± 5 Hz. Using the peak marking routine PEAKS the values and bin number of the maxima for channels 1 and 2 were found in bin 39 to be 107 dB and 108 dB respectively, for a differential of about 1 dB (see Figure 4.6). Using the routine GRABVALUES, the phase for bin 39 was found to be 1.698 radians for channel 1 and -1.859 radians for channel 2 for a differential phase of -3.557 (see Figure 4.7). This corresponds to a bin shift in time domain (BSV2) of

$$\text{INT} \left[\frac{-3.557}{2\pi} \times \frac{2^8}{39} \right] = -4$$

for a 256 point FFT using the first four 64 point records concatenated. The integer bin shift in this case causes an error of 0.3 bins or 0.159 radians (9.1°). Note that using a longer FFT would produce more accurate phase matching

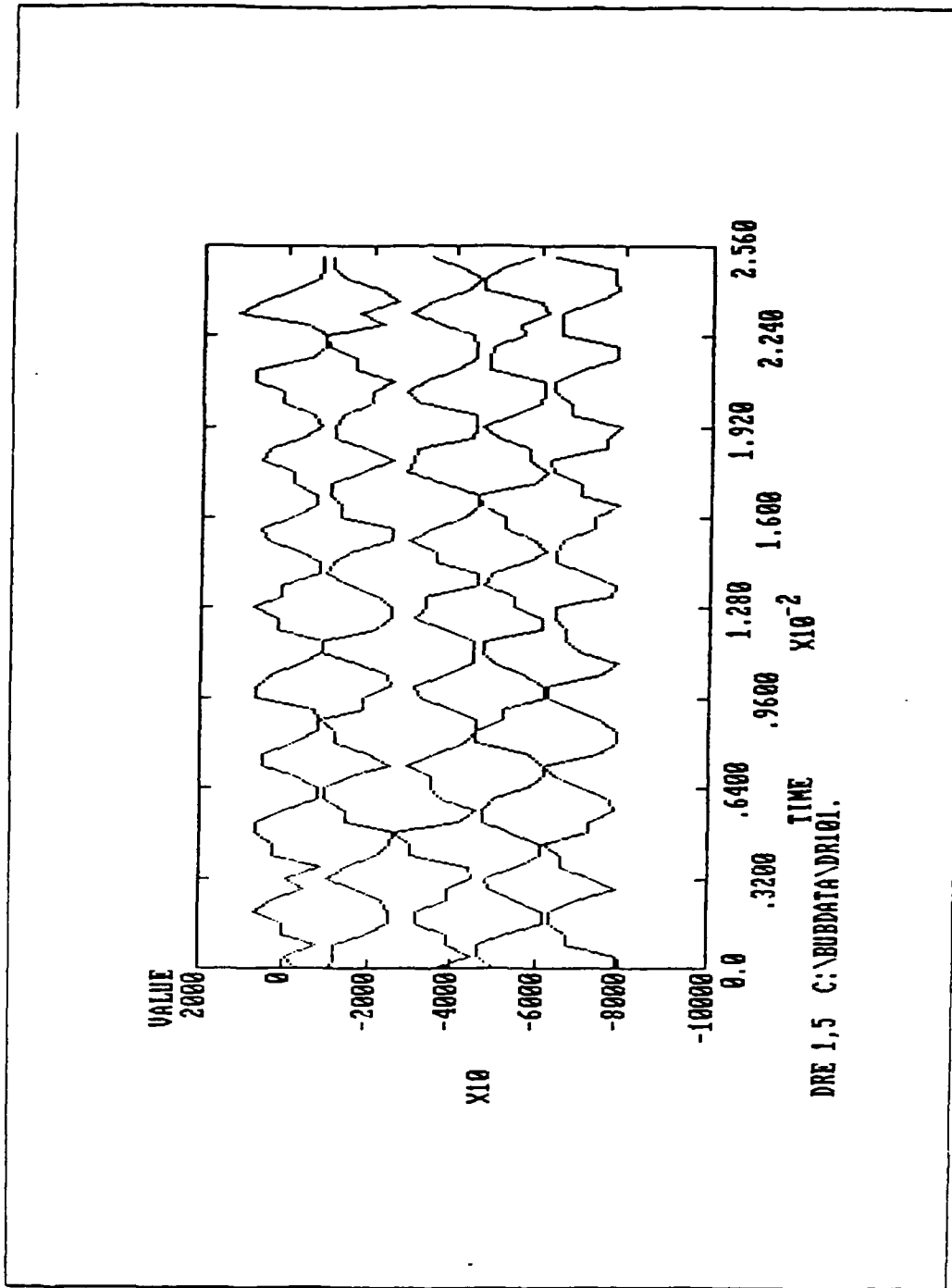


Figure 4.3 Record Data Channel 1 For Test Case

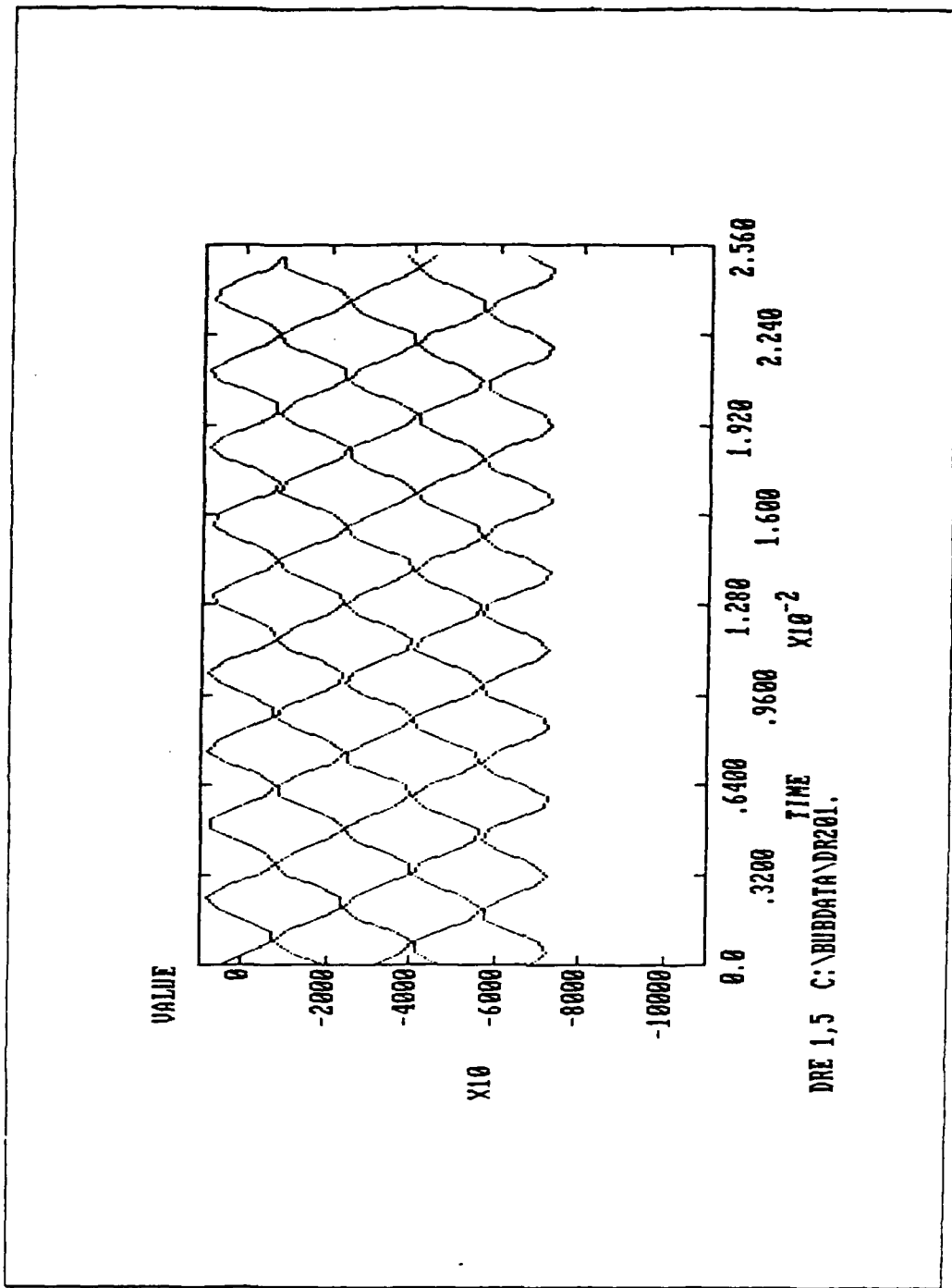
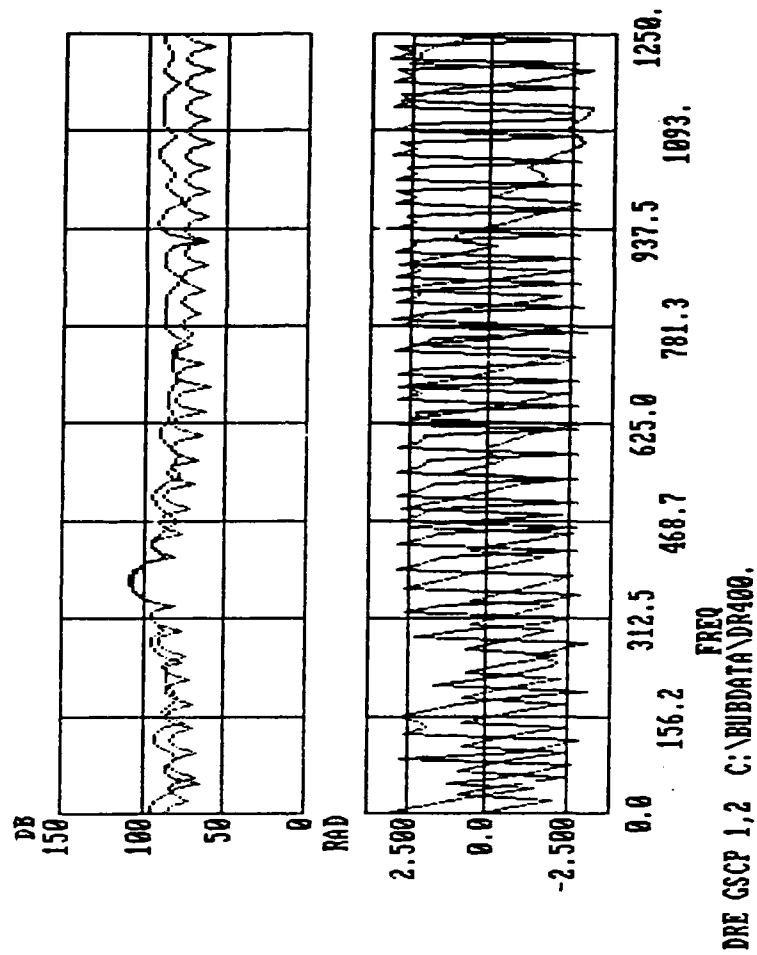


Figure 4.4 Record Data Channel 2 for Test Case



Upper Trace is Magnitude in dB as in Figure 4.6
 Lower Trace is Phase in Radians

Figure 4.5 FFT Comparison of Channels 1 and 2

```
ILS> xtr 1,1
```

```
ELEMENT NUMBER 1
```

ORDER	REC	ITEM	VALUE
1	1	39	1.0719260E+02

```
ILS> xtr 2,1
```

```
ELEMENT NUMBER 1
```

ORDER	REC	ITEM	VALUE
1	2	39	1.0829060E+02

```
ILS>
```

All dB values are referenced $20\text{Log}(\text{Integer Value}) + 10\text{Log}(\text{Processing Bandwidth})$. The Processing Bandwidth is one-half the sample frequency and in this case is 1250 Hz. For this example, channel 2 would have a dB value of $20\text{Log}(7900) + 10\text{Log}(1250) = 108\text{ dB}$. This plot gives the FFT bin number corresponding to the maximum dB value in the entire FFT.

Figure 4.6 Maximum Values Output by Batch File PEAKS

9.0335E+01	-1.4407E+00
9.5068E+01	-2.6629E+00
9.4920E+01	2.6414E+00
8.6063E+01	1.4558E+00
9.4041E+01	-1.9165E+00
1.0225E+02	-2.8713E+00
1.0586E+02	2.5466E+00
→ 1.0719E+02	1.6980E+00
1.0674E+02	8.5300E-01
1.0443E+02	5.6930E-03
9.9505E+01	-8.4797E-01
8.7425E+01	-1.7040E+00
8.8890E+01	5.1217E-01
9.4196E+01	-4.1351E-01
9.4018E+01	-1.4173E+00
9.1141E+01	-2.5531E+00
8.6247E+01	2.3747E+00
7.8735E+01	4.9370E-01
8.2933E+01	-2.2716E+00
9.0027E+01	2.6597E+00

ENTER C TO CONTINUE, E TO EXIT, N FOR NEXT RECORD

8.8953E+01	5.6472E-01
9.4606E+01	-2.6278E-01
9.4304E+01	-1.0729E+00
8.1469E+01	-1.9717E+00
9.5888E+01	5.2934E-01
1.0355E+02	-2.7683E-01
1.0704E+02	-1.0701E+00
→ 1.0829E+02	-1.8595E+00
1.0771E+02	-2.6462E+00
1.0513E+02	2.8533E+00
9.9483E+01	2.0765E+00
8.1891E+01	1.3936E+00
9.2310E+01	-2.6750E+00
9.5017E+01	2.8454E+00
9.1771E+01	2.0839E+00
7.5466E+01	1.5049E+00
8.7164E+01	-2.6979E+00
9.0513E+01	2.8412E+00
8.7758E+01	2.0939E+00
7.1760E+01	1.6182E+00

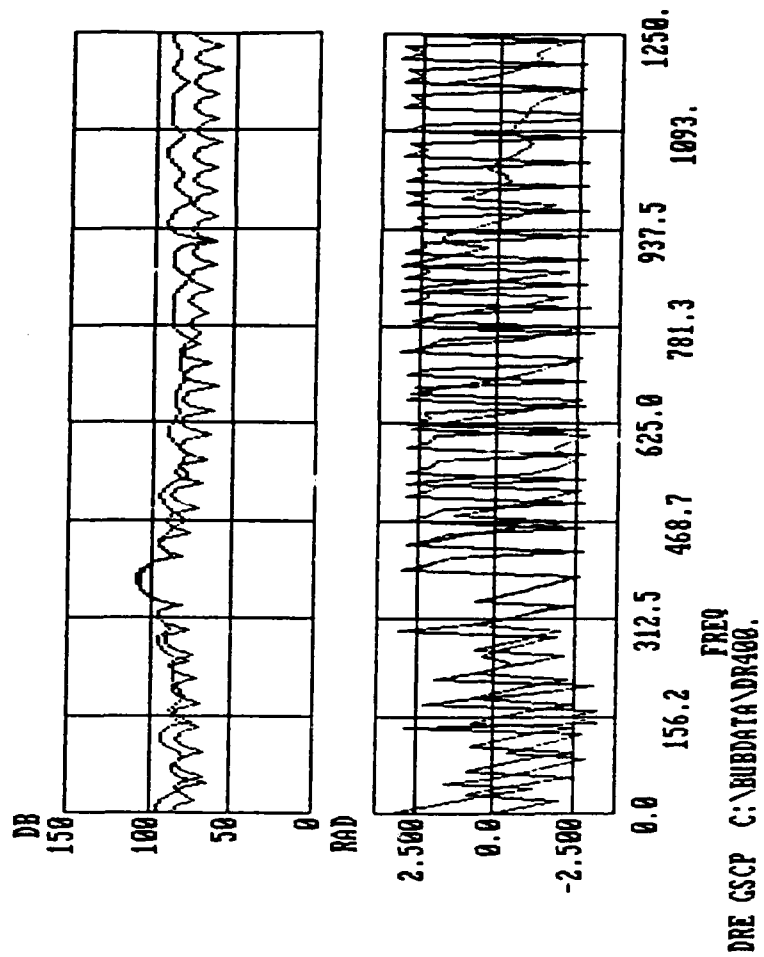
Left Column dB as in Figure 4.6
Right Column Phase in Radians

Figure 4.7 Bin Values Near Maxima Listed by GRABVALUES

qualities, as the time domain shifts must be discrete for digital data, hence, phase accuracy is proportional to FFT length at a given frequency. As mentioned earlier, phase matching correction accuracy is inversely proportional to frequency bin number.

The resonance recognition for the calibrator as described in section D was now possible using ANALYZE with $BSV1 = 0$, $BSV2 = -4$. The results are shown graphically in Figure 4.8 with the printed values around bin 39 in Figure 4.9. The display of phase vs frequency in Figure 4.8 is now nicely cophased in the vicinity of the 381 Hz resonance. To demonstrate the stability and ability of the software to recognize resonance once the channels were cross compared with offset values available, the experiment was run again several hours later with the microphones repositioned near the antinode (on the same side of the zero) where the signal amplitude would be greatly diminished. The analysis data signals for channel 1 and 2 are shown in Figures 4.10 and 4.11. The routine ANALYZE was run using the previous calibration comparison values ($BSV2 = -4$) and the phase matching is apparent as seen Figure 4.12. The differential phase in bin 39 was only .04 radians as shown in the values in Figure 4.13 GRABVALUE data.

The final demonstration shows the reaction of the microphone assembly pair to travelling waves from a strong



Upper Trace is Magnitude in dB as in Figure 4.6
 Lower Trace is Phase in Radians

Figure 4.8 FFT Comparison With Time Series Bin
 Shift Correction for Phase Differential

9.0335E+01	8.4190E-01
9.5068E+01	-3.0669E-01
9.4920E+01	-1.2119E+00
8.6063E+01	-2.3229E+00
9.4041E+01	6.6061E-01
1.0225E+02	-2.2063E-01
1.0566E+02	-1.0122E+00
→ 1.0719E+02	-1.7872E+00
1.0674E+02	-2.5586E+00
1.0443E+02	2.9509E+00
9.9505E+01	2.1709E+00
8.7425E+01	1.3885E+00
8.8890E+01	-2.6049E+00
9.4196E+01	2.8263E+00
9.4018E+01	1.8961E+00
9.1141E+01	8.3397E-01
8.6247E+01	-4.4781E-01
7.8735E+01	-2.2552E+00
8.2933E+01	1.3363E+00
9.0027E-01	5.8099E-02

ENTER C TO CONTINUE, E TO EXIT, N FOR NEXT RECORD

8.8953E+01	5.6472E-01
9.4606E+01	-2.6278E-01
9.4304E+01	-1.0729E+00
8.1469E+01	-1.9717E+00
9.5888E+01	5.2934E-01
1.0355E+02	-2.7683E-01
1.0704E+02	-1.0701E+00
→ 1.0829E+02	-1.8595E+00
1.0771E+02	-2.6462E+00
1.0513E+02	2.8533E+00
9.9483E+01	2.0765E+00
8.1891E+01	1.3936E+00
9.2310E+01	-2.6750E+00
9.5017E+01	2.8454E+00
9.1771E+01	2.0839E+00
7.5466E+01	1.5049E+00
8.7164E+01	-2.6979E+00
9.0513E+01	2.8412E+00
8.7758E+01	2.0939E+00
7.1760E+01	1.6182E+00

Left Column dB as in Figure 4.6
Right Column Phase in Radians

Figure 4.9 Bin Values Near Maxima for Phase
Corrected Data

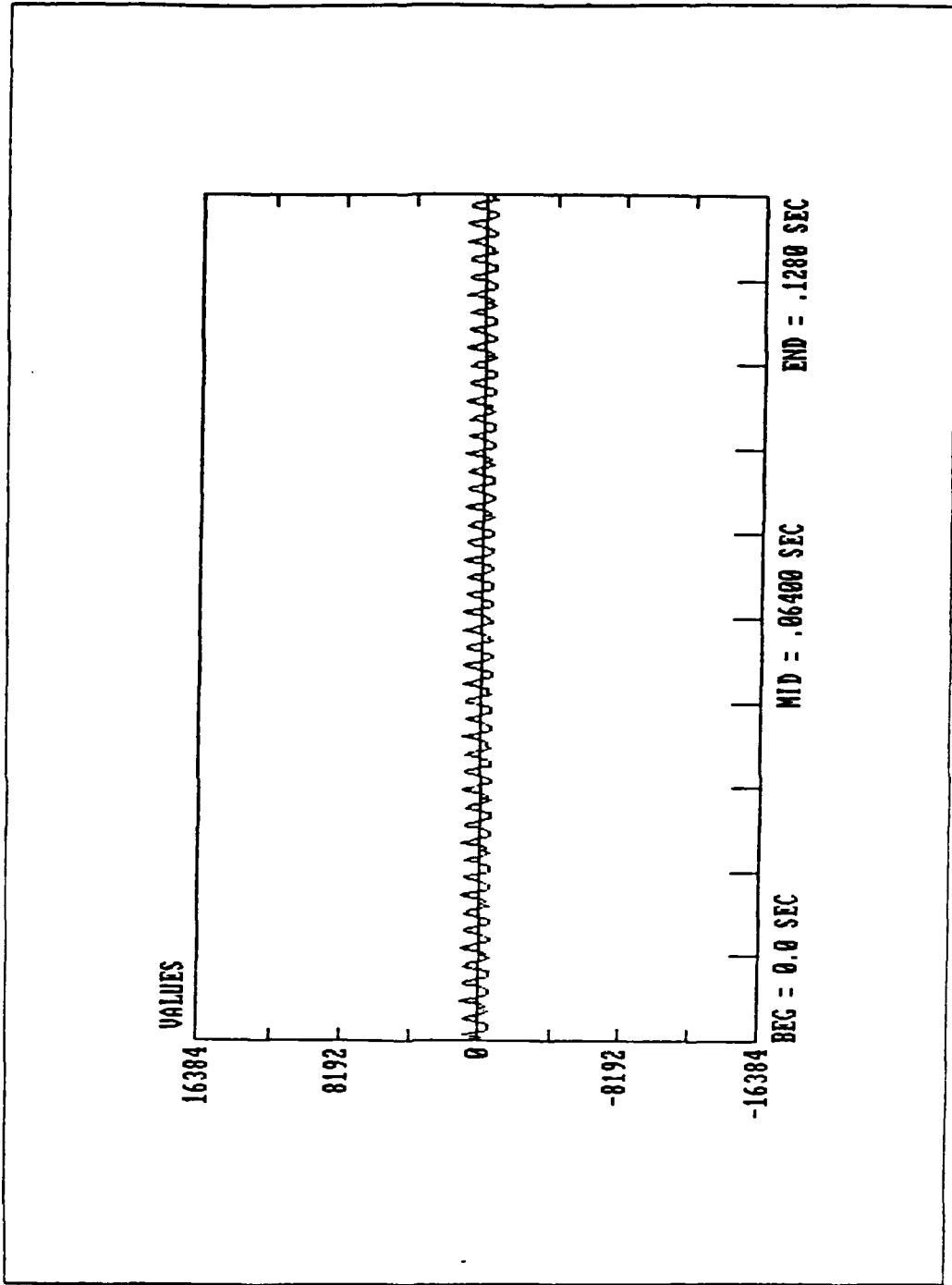


Figure 4.10 Sample Data Channel 1 Near Resonant
Mode Pressure Minima

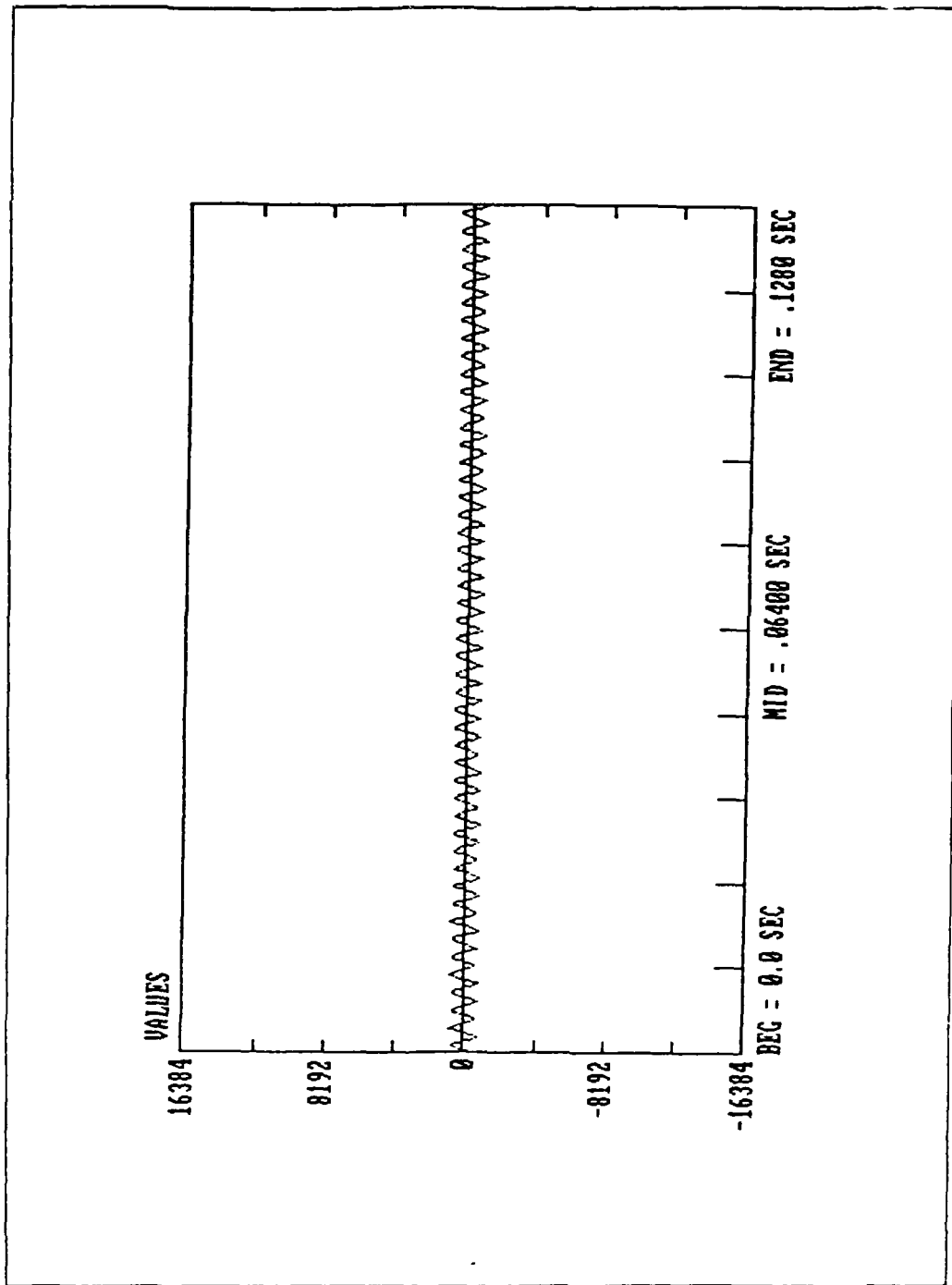
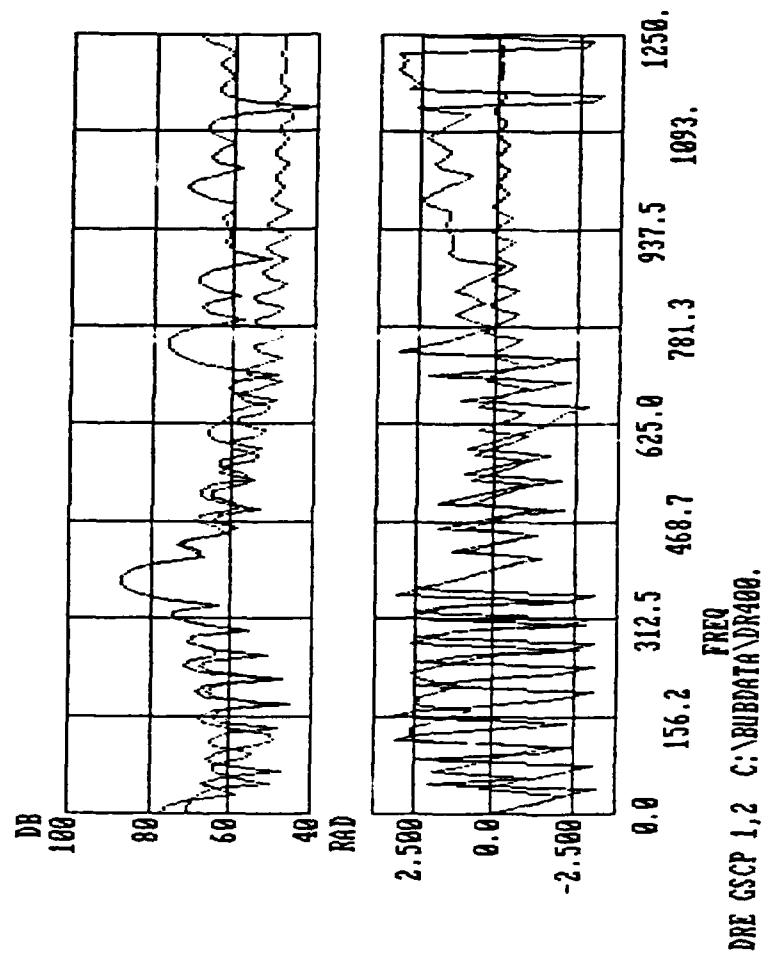


Figure 4.11 Sample Data Channel 2 Near Resonant
Mode Pressure Minima



Upper Trace is Magnitude in dB as in Figure 4.6
 Lower Trace is Phase in Radians

Figure 4.12 FFT Comparison Channels 1 and 2 for
 Phase Corrected Data at Pressure Minima

6.8810E+01	-2.7806E+00
7.4488E+01	2.8123E+00
7.4269E+01	2.1128E+00
6.3224E+01	1.4847E+00
7.4546E+01	-2.5099E+00
8.2454E+01	3.0766E+00
8.5945E+01	2.3629E+00
→ 8.7186E+01	1.6428E+00
8.6641E+01	9.1657E-01
8.4236E+01	1.8167E-01
7.9215E+01	-5.7154E-01
6.7377E+01	-1.4351E+00
6.7541E+01	1.2694E+00
7.2278E+01	4.2269E-01
7.0496E+01	-3.9531E-01
6.2397E+01	-1.3732E+00
5.8514E+01	1.7685E+00
6.4255E+01	6.5357E-01
6.3069E+01	-2.9977E-01
5.2783E+01	-2.1691E+00

ENTER C TO CONTINUE, E TO EXIT, N FOR NEXT RECORD

→

6.8032E+01	-2.1420E+00
7.3848E+01	-2.0076E+00
7.3805E+01	2.4584E+00
6.3493E+01	1.5857E+00
7.3900E+01	-2.2116E+00
8.2105E+01	-3.0193E+00
8.5786E+01	2.4741E+00
→ 8.7197E+01	1.6896E+00
8.6809E+01	9.0867E-01
8.4533E+01	1.3189E-01
7.9552E-01	-6.3673E-01
6.6961E+01	-1.3486E+00
6.9221E+01	8.8106E-01
7.3620E+01	1.4638E-01
7.1593E+01	-5.9642E-01
6.1658E+01	-1.2330E+00
6.2865E+01	8.1703E-01
6.8550E+01	1.5069E-01
6.7337E+01	-5.6048E-01
5.8579E+01	-1.1195E+00

Left Column dB as in Figure 4.6, Right Column is Phase Radians

Figure 4.13 FFT Bin Values for Phase Corrected Data
Near Pressure Minima

source in a non-reactive field. Using a speaker placed outdoors, operating at 381 Hz, the channel 2 microphone was placed 24 inches directly in front of the speaker and channel 1 microphone 15 inches directly behind the channel 2 microphone. The microphone could not be placed in the far field because signal levels there were too low to record, but because the microphones were along a direct radius from the front of the speaker it was expected that the phase would behave as a propagating plane wave and the amplitudes as a diverging wavefront making channel 2 levels higher. The analysis and record data displays for channels 1 and 2 are provided in Figures 4.14 through 4.17. Note that the channel 2 amplitude is higher, as expected. The phase difference between the channels was calculated to be

$$\text{phase} = 2 \times \pi \times \text{separation distance/wavelength}$$

$$\text{phase} = 2 \times \pi \times \{15.0"/(39.36 \text{ inches/meter})/[(345\text{meters/second})/(381 \text{ Hertz})]\}$$

$$\text{phase} = 2.64 \text{ radians (channel 2 leading channel 1)}$$

The ANALYZE routine was run as described in section E (see Figure 4.18) the GRABVALUES printout showed the phase differential to be channel 2 leading channel 1 by $.24 - (-)2.59 = 2.83$ radians (see Figure 4.19). The difference between measured and expected phase of .2 radians is within the digital time shifting capability of the 256 point FFT at the 381 Hz frequency where 1 bin = ± 0.5 radians of resolution.

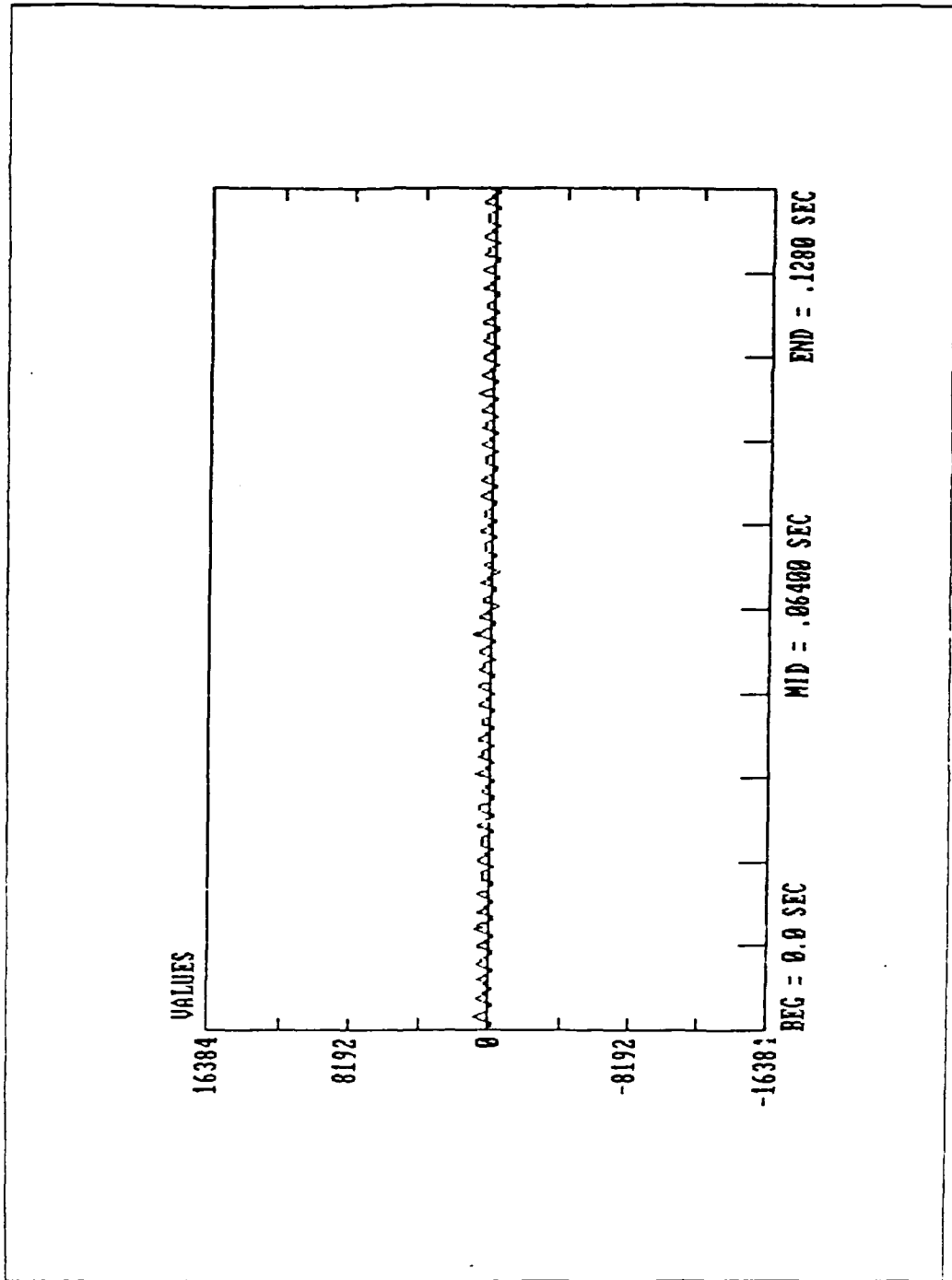


Figure 4.14 Travelling Wave Sample Data Channel 1

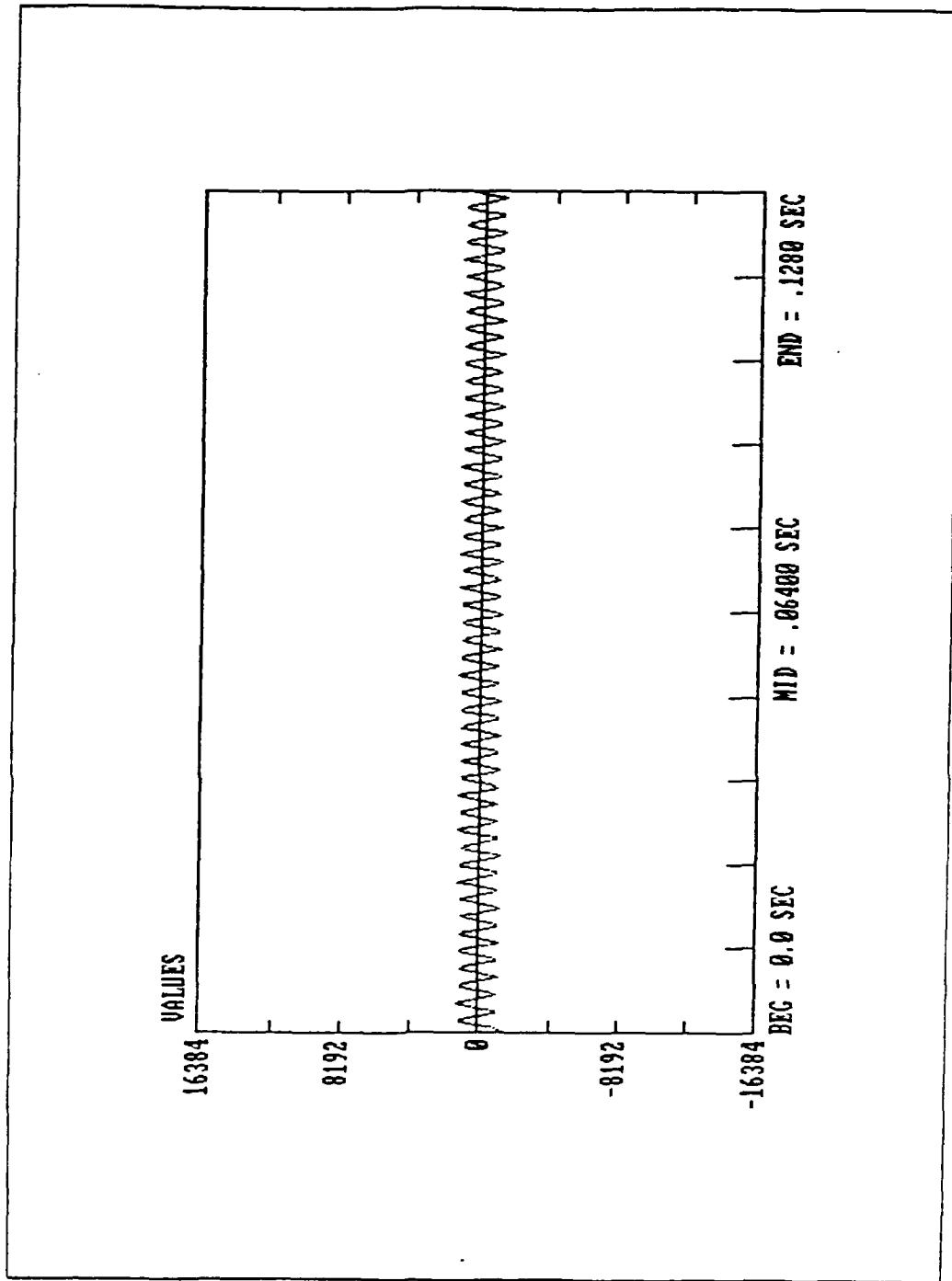


Figure 4.15 Travelling Wave Sample Data Channel 2

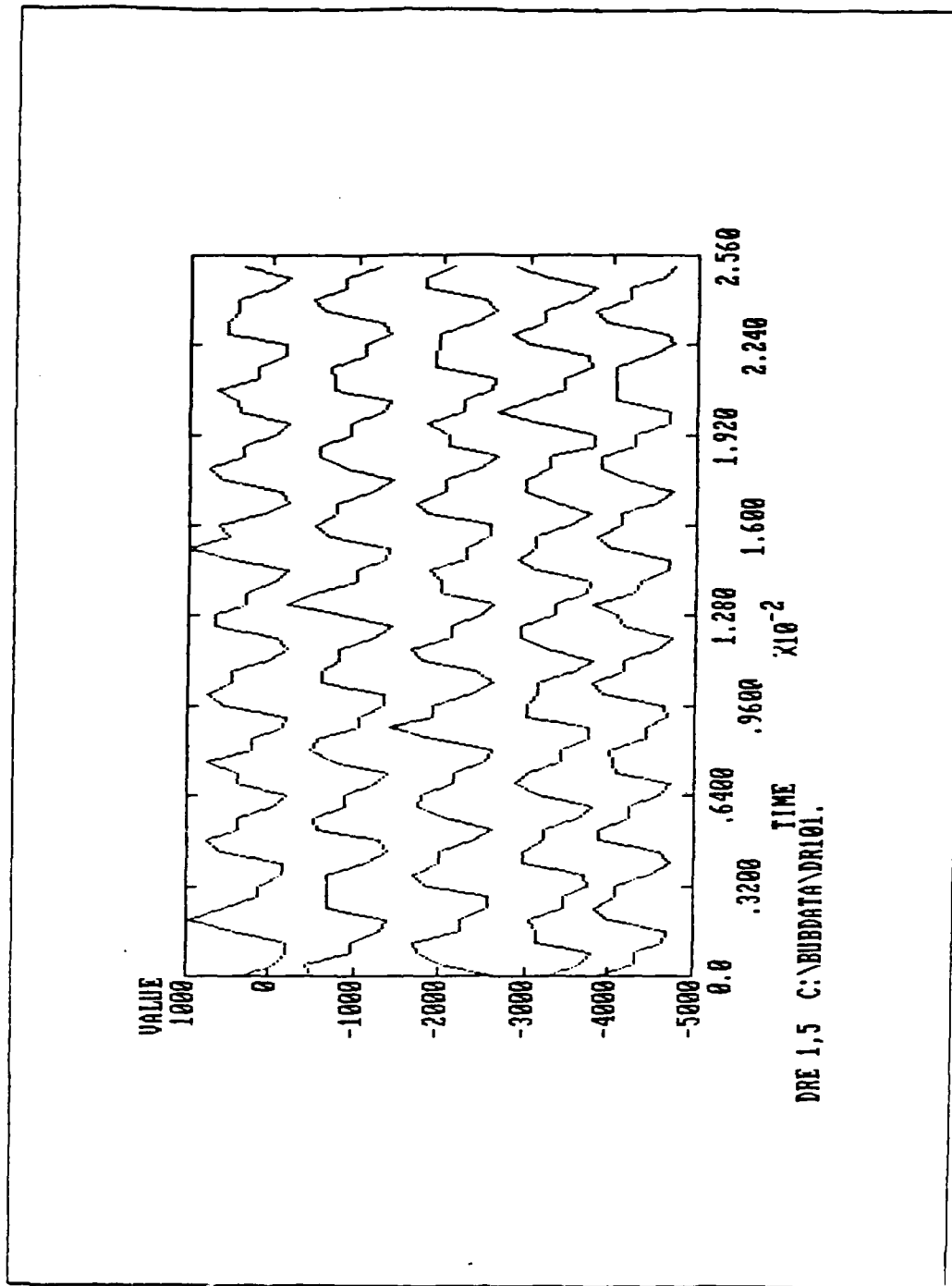


Figure 4.16 Travelling Wave Record Data Channel 1

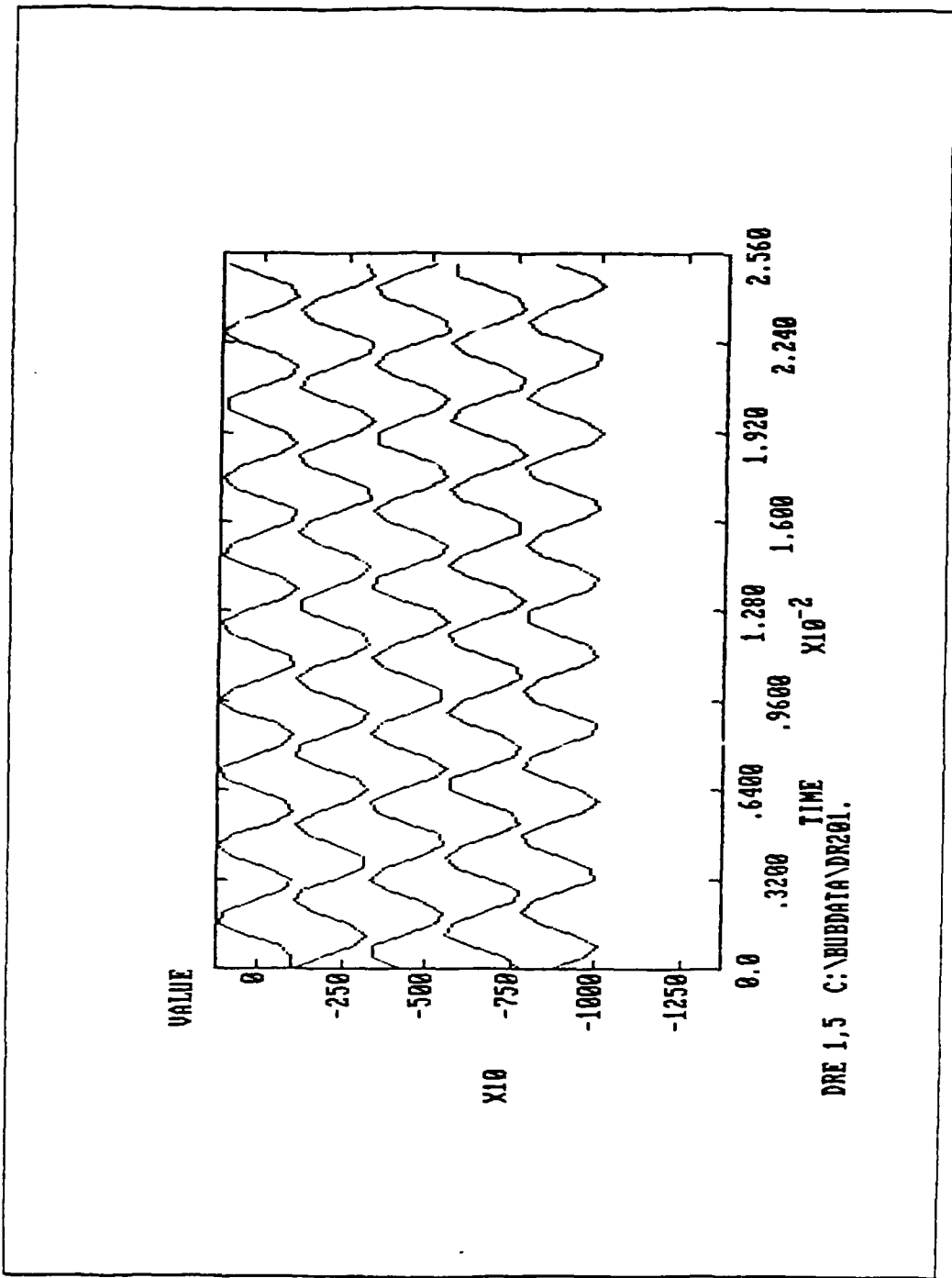
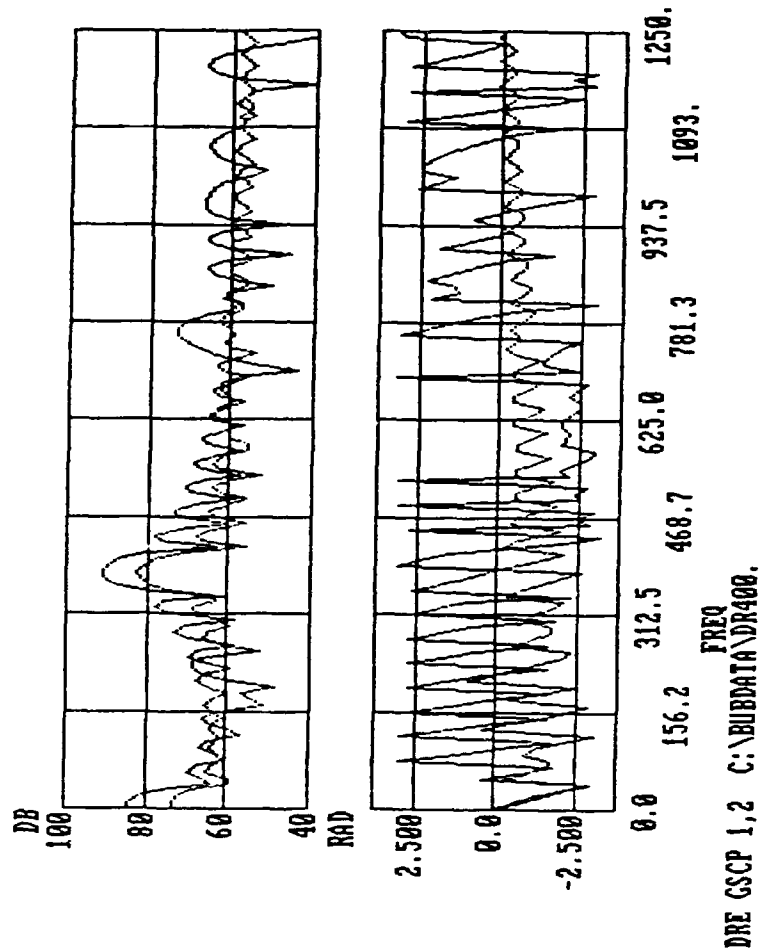


Figure 4.17 Travelling Wave Record Data Channel 2



Upper Trace is Magnitude in dB as in Figure 4.6
 Lower Trace is Phase in Radians

Figure 4.18 FFT Comparison Channels 1 and 2 for Phase
 Corrected Travelling Wave Data

6.2354E+01	-8.1524E-01
6.7921E+01	-1.1065E+00
6.8695E+01	-1.6315E+00
6.3135E+01	-2.0482E+00
6.4459E+01	-2.3957E-01
7.4832E+01	-6.6046E-01
7.9421E+01	-1.2764E+00
8.1581E+01	-1.9242E+00
→ 8.2001E+01	-2.5855E+00
8.0770E+01	3.0259E+00
7.7535E+01	2.3366E+00
7.0827E+01	1.5814E+00
5.5388E+01	-6.5381E-01
6.6999E+01	-2.4540E+00
6.8094E+01	-3.1393E+00
6.3735E+01	2.6599E+00
5.5762E+01	-2.8354E+00
6.3268E+01	-2.5203E+00
6.4522E+01	-2.9549E+00
6.0484E+01	3.0042E+00

ENTER C TO CONTINUE, E TO EXIT, N FOR NEXT RECORD
->

5.8477E+01	-1.7434E+00
7.3742E+01	2.6363E+00
7.7625E+01	1.7506E+00
7.5692E+01	8.9038E-01
6.1046E+01	-2.2059E+00
8.1549E+01	2.6209E+00
8.7624E+01	1.8052E+00
9.0417E+01	1.0180E+00
→ 9.1148E+01	2.4175E-01
9.0028E+01	-5.2600E-01
8.6700E+01	-1.2819E+00
7.9394E+01	-2.0008E+00
6.2966E+01	-1.9921E-01
7.7038E+01	-5.2442E-01
7.7561E+01	-1.2280E+00
7.2186E+01	-1.8820E+00
5.9866E+01	-3.8157E-01
7.2263E+01	-5.1763E-01
7.3277E+01	-1.1743E+00
6.8348E+01	-1.7663E+00

Left Column dB as in Figure 4.6, Right Column is Phase Radians

Figure 4.19 FFT Bin Values for Phase Corrected Data
for Travelling Wave Experiment

V. CONCLUSIONS AND RECOMMENDATIONS

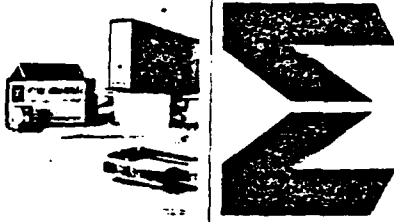
Using the equipment and signal processing software presented in this thesis it should be possible to recognize low frequency resonant modes and higher frequency travelling waves from a strong source in the far field within an active and reactive sound field.

All equipment has been tested and is determined capable of making autonomous acoustic measurements within the Space Shuttle Cargo Bay. The apparatus should be calibrated in an anechoic environment using the procedure outlined in this thesis to measure differential gain/phase corrections to be used when correcting for the different electrical input characteristics of each data channel. It is recommended that the on board loudspeaker be used when making acoustic calibration measurements.

APPENDIX A

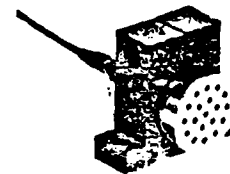
SPECIFICATIONS FOR MODEL 2510
ENDEVCO MICROPHONE

ENDEVCO - PRODUCT DATA



MODEL 2510
 Flight and Ground Measurement
 of High Intensity
 Sound Pressure Levels
**HIGH
 INTENSITY
 MICROPHONE**

The ENDEVCO Model 2510 Microphone¹ measures high intensity acoustic noise and very low pressure fluctuations. The rugged, hermetically sealed construction and extremely wide temperature range -65°F to $+500^{\circ}\text{F}$ (-54°C to $+260^{\circ}\text{C}$) make this transducer extremely useful over a wide range of environmental conditions. Unlike other microphones currently available, the Model 2510 is insensitive to altitude changes. The Model 2510 Microphone has a very thick diaphragm that prevents puncturing or damage due to particle impact, accidental mishandling, or high pressure pulses. Insulation between the transducer and mounting surface prevents data-degrading ground loops.



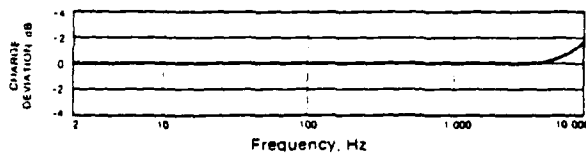
The Model 2510 is intended primarily to operate into preamplifiers that have a charge-to-voltage transfer characteristic (charge amplifiers). Its charge sensitivity vs. temperature characteristic is optimized through the proper choice of crystal material. Long cables may be used between the transducer and charge converter without affecting charge sensitivity. Although the basic design is directed toward maximizing charge characteristics, the Model 2510 also gives excellent results when operated into voltage amplifiers.

SPECIFICATIONS FOR MODEL 2510 MICROPHONE
 (According to ANSI and ISA Standards)

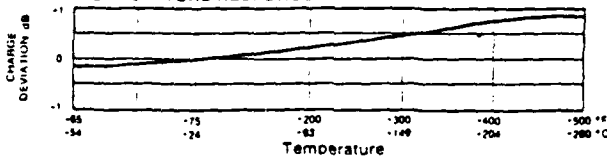
DYNAMIC	
CHARGE SENSITIVITY ²	23 rms pC (32.5 pk pC sinusoidal) at 140 dB ³ ; -15.8 dB re 1 pC at 1 N/m ² ; 793 pC/psi, typical
VOLTAGE SENSITIVITY	4.4 rms mV (6.2 pk mV sinusoidal) at 140 dB ³ ; -93 dB re 1 V at 1 N/m ² ; 152 mV/psi, typical; (open circuit)
DYNAMIC RANGE	Maximum useful SPL exceeds 180 dB ³
MOUNTED RESONANCE FREQUENCY	30 000 Hz, minimum
FREQUENCY RESPONSE (pressure calibration)	± 1 dB, 2 to 4 000 Hz; ± 3 dB, 2 to 10 000 Hz
AMPLITUDE LINEARITY (independent)	± 0.5 dB, max., 120 to 164 dB ³ ; ± 1 dB, max., 120 to 180 dB ³
TOTAL HARMONIC DISTORTION	5%, max., at 160 dB ³
TEMPERATURE RESPONSE (charge sensitivity)	± 1.5 dB, max., -65°F to $+500^{\circ}\text{F}$ (-54°C to $+260^{\circ}\text{C}$) reference -75°F ($+24^{\circ}\text{C}$)
TRANSDUCER CAPACITANCE	5 200 pF typical
RESISTANCE	20 000 M Ω , min., at $+75^{\circ}$ ($+24^{\circ}\text{C}$)

NOTES
¹The Model 2510 is a self-generating piezoelectric transducer and requires no external power for operation.
²Use ENDEVCO 2640, 2680, or 2700 Series Charge Amplifiers.
³Reference: 0 dB = 0.0002 μbar (dynes/cm²) = 20 $\mu\text{N/m}^2$ = 20 μPa .

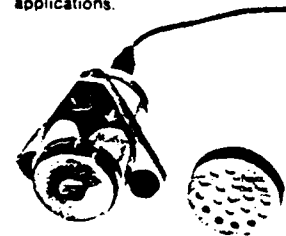
TYPICAL FREQUENCY RESPONSE



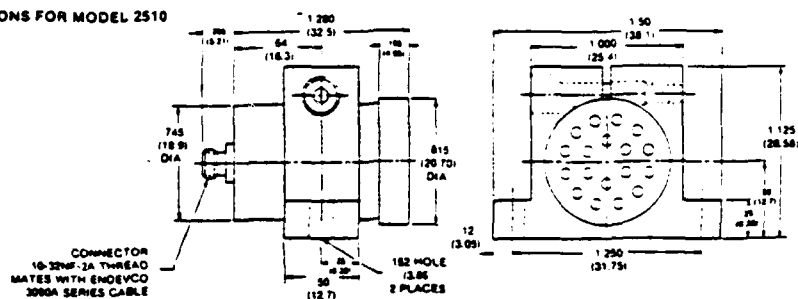
TYPICAL TEMPERATURE RESPONSE



The Model 2510M4A, illustrated below with electrical specifications identical to the basic Model 2510, provides a special mounting for flush diaphragm or other applications.



SPECIFICATIONS FOR MODEL 2510



DIMENSIONS IN INCHES (MILLIMETRES)

PHYSICAL

WEIGHT	2 oz (56.7 g) max., including mounting bracket
MATERIAL	Case — stainless steel; Bracket — hard anodized aluminum alloy
CRYSTAL MATERIAL	PIEZITE® Element Type P-8
CONNECTOR	Coaxial, 10-32 thrd.
MOUNTING	Two holes for No. 6 screws, 1/4" apart
GROUNDING	Case ground insulated from mounting bracket. Resistance from case to bracket is 1 MΩ minimum at 50 Vdc
ACCESSORIES INCLUDED	Model 3090A-120 Low Noise Cable Assembly, 10 ft (3 m); Two 6-32 x 1/4" cap screws; Removable grid

ENVIRONMENTAL

VIBRATION	150 g
VIBRATION SENSITIVITY	105 dB* max. SPL equivalent at 1 g pk
SHOCK	1 000 g
TEMPERATURE	-65°F to +500°F (-54°C to +260°C)
ALTITUDE SENSITIVITY	No change in sensitivity 0 to 100 000 feet
HUMIDITY	Hermetically sealed
SALT SPRAY	Meets MIL-E-5272C (with sealed cable connector)

NOTES *Reference 0 dB = 0.0002 μbar (dynes/cm²) = 20 μN/m² = 20 μPa

Continued product improvement necessitates that Endeveco reserve the right to modify these specifications without notice.

RELIABILITY: Endeveco maintains a program of constant surveillance over all products to ensure a high level of reliability. This program includes attention to reliability factors during product design, the support of stringent quality control requirements, and compulsory correction action procedures. These measures, together with conservative specifications have made the name Endeveco synonymous with reliability. Endeveco's Quality and Reliability system meets the requirements of MIL-Q-9858A and MIL-STD-785A.

CALIBRATION: Each unit is calibrated for acoustic pressure sensitivity and capacitance. Frequency response from 2 to 10 000 Hz, temperature calibration at -65°F (-54°C), +75°F (-24°C), and +500°F (+260°C), and amplitude linearity from 120 dB* to 180 dB*, are available at additional cost.

SYSTEMS: Airborne systems available providing 0-5 V or ±2.5 V full scale output from less than 140 dB to over 180 dB or from less than ±0.07 psi to above ±5.0 psi. Request Technical Data 501A for additional information on airborne acoustic systems. Inquiries on special systems are invited.



RANCHO VIEJO ROAD • SAN JUAN CAPISTRANO, CA 92675 • TELEPHONE (714) 493-8181

ANAHEIM CA • ATLANTA GA • BALTIMORE MD • BOSTON MA • CHICAGO IL • DAYTON OH • HARTFORD CT • HOUSTON TX • PALO ALTO CA • W. MYSTIC CT • WESTVILLE NJ
 FRANCE • SWEDEN • UNITED KINGDOM • W. GERMANY • ARGENTINA • AUSTRALIA • BRAZIL • CANADA • CHILE • FINLAND • INDIA • ITALY • JAPAN • MALAYSIA
 MEXICO • NETHERLANDS • NORWAY • S. AFRICA • S. KOREA • SPAIN • SWITZERLAND • TAIWAN • VENEZUELA • ALL COMECON COUNTRIES • U.S.S.R.
 TWX 910-500-1415 TELE 80-5400 PRINTED IN USA REV 1/81

APPENDIX B

SPECIFICATIONS FOR BURR-BROWN OPA 111
OPERATIONAL AMPLIFIER

BURR-BROWN®



OPA111

Low Noise Precision *Difet*™ OPERATIONAL AMPLIFIER

FEATURES

- LOW NOISE: 100% tested, $8nV/\sqrt{Hz}$ max at 10kHz
- LOW BIAS CURRENT: 1pA max
- LOW OFFSET: 250 μ V max
- LOW DRIFT: 1 μ V/°C max
- HIGH OPEN-LOOP GAIN: 120dB min
- HIGH COMMON-MODE REJECTION: 100dB min

APPLICATIONS

- PRECISION INSTRUMENTATION
- DATA ACQUISITION
- TEST EQUIPMENT
- PROFESSIONAL AUDIO EQUIPMENT
- MEDICAL EQUIPMENT—CAT SCANNER
- RADIATION HARD EQUIPMENT

DESCRIPTION

The OPA111 is a precision monolithic dielectrically-isolated FET (*Difet*™) operational amplifier. Outstanding performance characteristics allow its use in the most critical instrumentation applications.

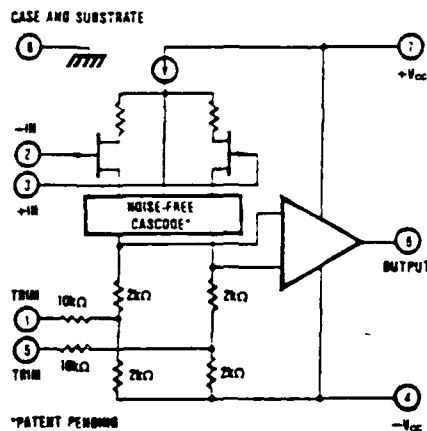
Noise, bias current, voltage offset, drift, open-loop gain, common-mode rejection, and power supply rejection are superior to BIFET® amplifiers.

Very-low bias current is obtained by dielectric isolation with on-chip guarding.

Laser trimming of thin-film resistors gives very-low offset and drift. Extremely-low noise is achieved with new circuit design techniques (patent pending). A new cascode design allows high precision input specifications and reduced susceptibility to flicker noise.

Standard 741 pin configuration allows upgrading of existing designs to higher performance levels.

BIFET® National Semiconductor Corp., *Difet*™ Burr-Brown Corp.



*PATENT PENDING

OPA111 SIMPLIFIED CIRCUIT

International Airport Industrial Park • P.O. Box 11400 • Tucson, Arizona 85734 • Tel. (602) 746-1111 • Twx: 910-952-1111 • Cable: BURCORP • Telex: 66-6401

Copy available to DTIC does not permit fully legible reproduction

SPECIFICATIONS

ELECTRICAL

At $V_{CC} = \pm 15\text{VDC}$ and $T_A = +25^\circ\text{C}$ unless otherwise noted. Pin 8 connected to ground.

PARAMETER	CONDITIONS	OP111AM			OP111BM			OP111SM			UNITS
		MIN	TYP	MAX	MIN	TYP	MAX	MIN	TYP	MAX	
INPUT											
NOISE Voltage $f_c = 10\text{kHz}$ $f_c = 100\text{kHz}$ $f_c = 1\text{kHz}$ $f_c = 10\text{kHz}$ $f_c = 10\text{kHz to } 100\text{kHz}$ $f_c = 0.1\text{kHz to } 10\text{kHz}$ Current $f_c = 0.1\text{kHz to } 10\text{kHz}$ $f_c = 0.1\text{kHz to } 20\text{kHz}$	100% tested		40	80		30	80		40	80	$\mu\text{V}/\sqrt{\text{Hz}}$
	100% tested		15	40		11	30		15	40	$\mu\text{V}/\sqrt{\text{Hz}}$
	100% tested		8	15		7	12		8	15	$\mu\text{V}/\sqrt{\text{Hz}}$
	100% tested		6	8		6	8		6	8	$\mu\text{V}/\sqrt{\text{Hz}}$
	100% tested		0.7	1.2		0.6	1.0		0.7	1.2	$\mu\text{V rms}$
	"		1.6	3.3		1.2	2.5		1.6	3.3	$\mu\text{V p-p}$
"		9.5	15		7.5	12		9.5	15	$\mu\text{A p-p}$	
"		0.5	0.8		0.4	0.6		0.5	0.8	$\mu\text{A rms}$	
OFFSET VOLTAGE ¹ Input Offset Voltage Average Drift Supply Rejection	$V_{CC} = 0\text{VDC}$ $T_A = T_{min} \text{ to } T_{max}$		-100	-500		-50	-250		-100	-500	μV $\mu\text{V}/^\circ\text{C}$ dB
		90	±2	±5	100	±0.5	±1	90	±2	±5	
			±3	±3		±3	±10		±3	±3	$\mu\text{V/V}$
BIAS CURRENT ² Input Bias Current	$V_{CC} = 0\text{VDC}$		-0.8	±2		-0.5	±1		-0.8	±2	pA
OFFSET CURRENT ² Input Offset Current	$V_{CC} = 0\text{VDC}$		-0.5	±1.5		-0.25	±0.75		-0.5	±1.5	pA
IMPEDANCE Differential Common-Mode			10^{11}	1		10^{11}	1		10^{11}	1	Ω pF
			10^{11}	3		10^{11}	3		10^{11}	3	Ω pF
VOLTAGE RANGE Common-Mode Input Range Common-Mode Rejection	$V_{CC} = \pm 10\text{VDC}$	±10	±11		±10	±11		±10	±11		V dB
90	110		100	110		90	110				
OPEN-LOOP GAIN DC											
Open-Loop Voltage Gain	$R_L = 2k\Omega$	114	125		120	125		114	125		dB
FREQUENCY RESPONSE											
Unity Gain Small Signal Full Power Response Slew Rate Settling Time 0.1% 0.01% Overload Recovery 50% Overdrive ³	20V p-p $R_L = 2k$ $V_o = \pm 10\text{V}$ $R_L = 2k$ Gain = 1 $R_L = 2k$ 10V step Gain = 1	16	2		16	2		16	2		MHz MHz V/ μSEC μSEC μSEC μSEC
		32			32			32			
		1	2		2			2			
		6	6		6			6			
		10	10		10			10			
		5	5		5			5			
RATED OUTPUT											
Voltage Output Current Output Output Resistance Load Capacitance Stability Short Circuit Current	$R_L = 2k\Omega$ $V_o = \pm 10\text{VDC}$ DC Load = 1000 Gain = 1	-10	-11		-10	-11		-10	-11		V mA Ω pF mA
		-5	-10		-5	-10		-5	-10		
		100	100		100	100		100	100		
		1000	1000		1000	1000		1000	1000		
		10	40		10	40		10	40		
POWER SUPPLY											
Rated Voltage Voltage Range Derated Performance Current Quiescent			±15			±15			±15		VDC VDC VDC mA
		-5		-18	±5	-18		-5		-18	
	0mA DC	2.5	3.5		2.5	3.5		2.5	3.5		
TEMPERATURE RANGE											
Specification Operating Storage Junction-Ambient	Ambient temp Ambient temp Ambient temp	25		-85	-25		-85	-55		-125	$^\circ\text{C}$ $^\circ\text{C}$ $^\circ\text{C}$ $^\circ\text{C/W}$
		55		-125	55		-125	55		-125	
		-65		-150	-65		-150	-65		-150	
		200		200	200		200	200		200	

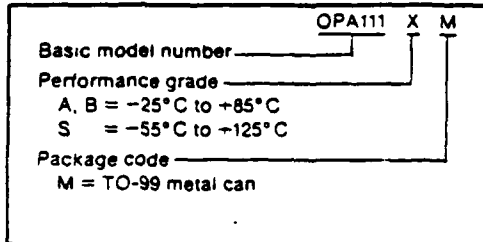
NOTES: (1) Sample tested—this parameter is guaranteed. (2) Offset voltage, offset current, and bias current are measured with the units fully warmed up. (3) Overload recovery is defined as the time required for the output to return from saturation to linear operation following the removal of a 50% input overdrive.

Copy available to DTIC does not permit fully legible reproduction

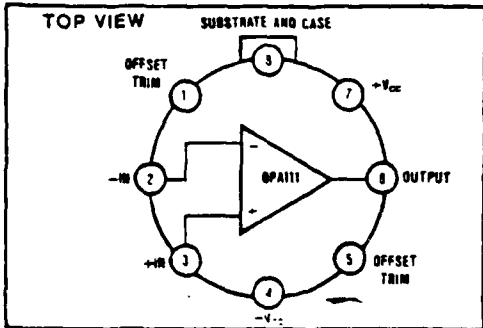
PARAMETER	CONDITIONS	OPA111AM			OPA111M			OPA111SM			UNITS
		MIN	TYP	MAX	MIN	TYP	MAX	MIN	TYP	MAX	
TEMPERATURE RANGE											
Specification Range	Ambient temp	-25		+85	25		+85	55		+125	°C
INPUT											
OFFSET VOLTAGE Input Offset Voltage Average Offset Supply Rejection	$V_{in} = 0VDC$		±220	+1000		-110	-500		±300	+1500	μV
			-2	±5	90	-0.5	±1	88	±2	-5	$\mu V/°C$
			88	100	±50		-10	-32		±10	+50
BIAS CURRENT Input Bias Current	$V_{in} = 0VDC$		±50	+250		±30	-130		±820	+4100	pA
OFFSET CURRENT Input Offset Current	$V_{in} = 0VDC$		±30	+200		±15	-100		±510	+3100	pA
VOLTAGE RANGE											
Common-Mode Input Range		-10	-11		-10	-11		+10	±11		V
Common-Mode Rejection	$V_{in} = -10VDC$	88	100		90	100		86	100		dB
OPEN-LOOP GAIN, DC											
Open-Loop Voltage Gain	$R_L = 2k\Omega$	110	120		114	120		110	120		dB
RATED OUTPUT											
Voltage Output	$R_L = 2k\Omega$	-10	-11		-10	-11		-10	-11		V
Current Output	$V_o = -10VDC$	-5	-10		-5	-10		-5	-10		mA
Short-Circuit Current	$V_o = 0VDC$	10	40		10	40		10	40		mA
POWER SUPPLY											
Current Quiescent	$V_o = 0VDC$		2.5	3.5		2.5	3.5		2.5	3.5	mA

NOTES: (1) Offset voltage, offset current, and bias current are measured with the units fully warmed up.

ORDERING INFORMATION



CONNECTION DIAGRAM



ABSOLUTE MAXIMUM RATINGS

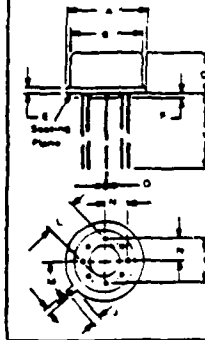
Supply	±18VDC
Internal Power Dissipation	500mW
Differential Input Voltage	±36VDC
Input Voltage Range	±18VDC
Storage Temperature Range	-95°C to +150°C
Operating Temperature Range	-55°C to +125°C
Lead Temperature (soldering, 10 seconds)	+300°C
Output Short-Circuit Duration	Continuous
Junction Temperature	+175°C

NOTES

- Packages must be derated based on $\theta_{JC} = 150°C/W$ or $\theta_{JA} = 200°C/W$.
- For supply voltages less than ±18VDC, the absolute maximum input voltage is equal to the supply voltage.
- Short circuit may be to power supply common only. Rating applies to +25°C ambient. Observe dissipation limit and T_J.

MECHANICAL "M" PACKAGE TO-99 (Hermetic)

NOTE: Leads in true position within 010° (25mm) at MMC at seating plane.



Pin numbers shown for reference only. Numbers may not be marked on package.

Pin material and plating composition conform to Method 2003 (solderability) of MIL-STD-883 (except paragraph 3.2).

DIM	MIL-883		MIL-STD-883	
	MIN	MAX	MIN	MAX
A	2.29	2.73	0.91	0.98
B	2.50	2.75	0.75	0.83
C	0.60	0.80	0.10	0.10
D	0.10	0.31	0.01	0.13
E	0.10	0.60	0.11	0.17
F	0.10	0.60	0.11	0.17
G	2.00 BASIC	1.00 BASIC		
H	0.28	0.34	0.11	0.08
I	0.20	0.60	0.14	0.10
J	0.60		0.17	
K	0.10	0.60	0.10	0.20
L	0.50 BASIC	0.50 BASIC		
M	0.70	0.70	0.11	0.11

APPENDIX C
SPECIFICATIONS FOR ANALOG DEVICES DAS 1153
A/D CONVERTER



14-Bit & 15-Bit Sampling Analog To Digital Converter

FEATURES

Complete with High Accuracy Sample/Hold and A/D Converter
 Differential Nonlinearity: $\pm 0.002\%$ FSR max (DAS1153)
 Nonlinearity: DAS1152: $\pm 0.005\%$ FSR max
 DAS1153: $\pm 0.003\%$ FSR max
 Low Differential Nonlinearity T.C.: $\pm 2\text{ppm}/^\circ\text{C}$ max
 High Throughput Rate: 25kHz min (DAS1152)
 High Feedthrough Rejection: -96dB
 Byte-Selectable Tri-State Buffered Outputs
 Internal Gain & Offset Potentiometers
 Improved Second Source to A/D/A/M 824 and A/D/A/M 825 Modules
 Low Cost

APPLICATIONS

Process Control Data Acquisition
 Automated Test Equipment
 Seismic Data Acquisition
 Nuclear Instrumentation
 Medical Instrumentation
 Robotics

GENERAL DESCRIPTION

The DAS1152/DAS1153 are 14-/15-bit sampling analog-to-digital converters having a maximum throughput rate of 25kHz/20kHz. They provide high accuracy, high stability, and functional completeness all in a $2" \times 4" \times 0.44"$ metal case.

Guaranteed high accuracy system performance such as nonlinearity of $\pm 0.005\%$ FSR (DAS1152) $\pm 0.003\%$ FSR (DAS1153) and differential nonlinearity of $\pm 0.003\%$ FSR (DAS1152) $\pm 0.002\%$ FSR (DAS1153) are provided. Guaranteed stability such as differential nonlinearity T.C. of $\pm 2\text{ppm}/^\circ\text{C}$ (DAS1153) maximum, zero T.C. of $\pm 80\mu\text{V}/^\circ\text{C}$ maximum, gain T.C. of $\pm 8\text{ppm}/^\circ\text{C}$ maximum and power supply sensitivity of $\pm 0.001\%$ FSR/ $\% V_s$ are also provided by the DAS1152/DAS1153.

The DAS1152/DAS1153 make extensive use of both integrated circuit and thin film components to obtain their excellent performance, small size, and low cost. The devices contain a precision sample/hold amplifier, high accuracy 14-/15-bit analog-to-digital converter, tri-state output buffers, internal gain and offset trim potentiometers, and power supply bypass capacitors (as shown in Figure 1).

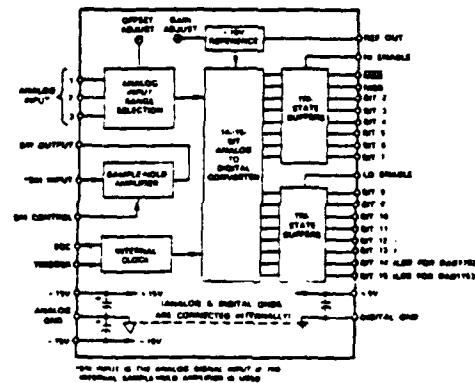


Figure 1. DAS1152/DAS1153 Block Diagram

Four analog input voltage ranges are selectable via user pin programming: 0 to $+3\text{V}$, 0 to $+10\text{V}$, $\pm 5\text{V}$, and $\pm 10\text{V}$. Unipolar coding is provided in true binary format with bipolar coding displayed in offset binary and two's complement. Tri-state buffers provide easy interface to bus structured applications.

Information furnished by Analog Devices is believed to be accurate and reliable. However, no responsibility is assumed by Analog Devices for its use; nor for any infringements of patents or other rights of third parties which may result from its use. No license is granted by implication or otherwise under any patent or patent rights of Analog Devices.

P.O. Box 280; Norwood, Massachusetts 02062 U.S.A.
 Tel: 617/329-4700 Twx: 710/394-6577
 Telex: 924491 Cables: ANALOG NORWOODMASS

Copy available to DTIC does not
 permit fully legible reproduction

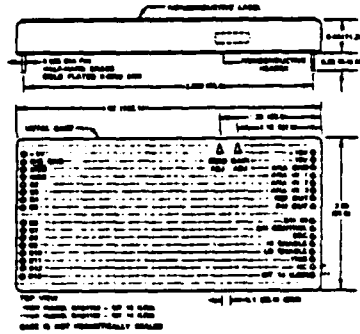
SPECIFICATIONS

(typical @ +25°C unless otherwise specified)

MODEL	DAS1152	DAS1153
RESOLUTION	14 Bits	15 Bits
DYNAMIC PERFORMANCE		
Throughput Rate	25k Hz max	20k Hz max
Conversion Time	35µs max	44µs max
S/H Acquisition Time	4µs max	5µs max
S/H Aperture Delay	50ns	•
S/H Aperture Uncertainty	1ns	•
Feedthrough Rejection	-96dB	•
Drump Rate	0.05µ V rms @ 0.1µ V rms max	•
Dielectric Absorption Error	± 0.007% of Input Voltage Change	•
ACCURACY		
Integral Nonlinearity ¹	± 0.005% FSR ¹ max	± 0.007% FSR ¹ max
Differential Nonlinearity	± 0.003% FSR ¹ max	± 0.002% FSR ¹ max
No Missing Codes	Guaranteed	•
± 3σ Noise (S/H plus A/D)	75µ V rms	•
± 3σ Noise (A/D)	56µ V rms	•
STABILITY		
Differential Nonlinearity T.C.	± 2ppm/°C max	•
Gain T.C.	± 8ppm/°C max	•
Zero T.C.	± 30µ V/°C typ, ± 80µ V/°C max	•
Power Supply Sensitivity	± 0.001% FSR/% V	•
ANALOG INPUT		
Voltage Range		
Bipolar	± 5V, ± 10V	•
Unipolar	0 to +5V, 0 to +10V	•
ADC Input Impedance 0 to +5V	2.5kΩ	•
0 to +10V, ± 5V	5kΩ	•
± 10V	10.0kΩ	•
S/H Input Impedance	100MΩ±5pF	•
DIGITAL INPUTS		
Convert Command ²	1TTL Level, Positive Pulse	•
	Negative Edge Triggered	•
S/H Control	HOLD = Logic 0	•
	SAMPLE = Logic 1	•
Low Enable, High Enable	ENABLE = Logic 0	•
DIGITAL OUTPUTS		
Parallel Data Outputs		
Unipolar	Biunary	•
Bipolar	Offset Biunary, 2's Complement	•
Output Drive	7TTL Loads	•
Status	Logic "1" During Conversion	•
Output Drive	7TTL Loads	•
INTERNAL REFERENCE VOLTAGE		
External Load Current (Rated Performance)	-10V, ± 0.3%	•
Temperature Stability	2µA max	•
	± 5ppm/°C max	•
POWER REQUIREMENTS		
Rated Voltages	± 15V (± 3%), ± 5V (± 3%)	•
Operational Voltages ³	± 12V to ± 17V, + 4.75V to + 5.25V	•
Supply Current Drain ± 15V	± 37mA	•
- 5V	80mA	•
TEMPERATURE RANGE		
Specified	0 to +70°C	•
Operating	- 25°C to + 85°C	•
Storage	- 25°C to + 85°C	•
Relative Humidity	Meets MIL-STD-202E, Method 103B	•
Shielding	Electromagnetic (RFL) 14 Sides	•
	Electromagnetic (EMI) 15 Sides	•
SIZE	2" x 4" x 0.44" Metal Package	

OUTLINE DIMENSIONS

Dimensions shown in inches and (mm)



NOTES

- ¹Measurement taken at DAS1152.
- ²Measured at 10k Hz, using 20V µs-rs or 100ns.
- ³Measurement taken at 5 Hz and A/D conversion errors.
- ⁴FSR means Full Scale Range.
- ⁵When calculating the Current Limitation and the S/H current consumption, the data sheet should be used as the basis for the S/H current to determine the total current to the converter (current) has. Also, DAS1152 has a 100µs (DAS1153) if the A/D converter is used, the Current Limitation data sheet should be used as the basis for the Power 2).
- ⁶To use the A/D portion in unit, the reference power supply voltage can be maintained at ± 12V to ± 17V. One of the 5V output is required, the reference voltage must be maintained at ± 15V ± 3% or the S/H input voltage must be limited to ± 7V to ± 10V and ± 1.7V supply voltage.
- ⁷Recommended Power Supply: Analog Devices Model 923.
- ⁸Measurement taken at 100µs reference source.

OPERATION

The DAS1152/DAS1153 are functionally complete data acquisition subsystems being fully characterized as such. All the necessary data acquisition and microprocessor interface elements are provided internal to these devices. Accuracy and performance criteria are tested and specified for the entire system. Thus, design time and associated high accuracy problems are minimized because layout and component optimization have already been performed.

For operation, the only connections necessary to the DAS1152/DAS1153 are the $\pm 15V$ and $+5V$ power supplies, analog input signal, trigger pulse, and the HI-ENABLE/LO-ENABLE tri-state controls.

ANALOG INPUT SECTION

The analog input can be applied to just the A/D converter or to the internal sample/hold amplifier ahead of the A/D converter. When using just the A/D converter, apply the analog input per the voltage range pin programming shown in Table 1. When using the sample/hold amplifier in conjunction with A/D converter, apply the analog input to the S.H INPUT terminal and connect the S.H OUTPUT terminal to the appropriate A/D converter analog input.

Analog Voltage Input Range	Connect V_{IN} or S.H Out To	Connect Analog Common To	Connect Ref Out To
0 to +5V	ANA IN 1, ANA IN 2, ANA IN 3	Ground	NC*
0 to +10V	ANA IN 2, ANA IN 3	Ground, ANA IN 1	NC*
$\pm 5V$	ANA IN 1	Ground, ANA IN 3	ANA IN 2
$\pm 10V$	ANA IN 3	Ground, ANA IN 1	ANA IN 2

*No Connection

Table 1. Analog Input Pin Programming

Errors due to source loading are eliminated since the sample/hold amplifier is a high-impedance unity-gain amplifier. High feedthrough rejection is provided for either single-channel or multichannel applications. Feedthrough rejection can be optimized, in multichannel applications, by changing channels at the rising or falling edge of the S.H control pulse.

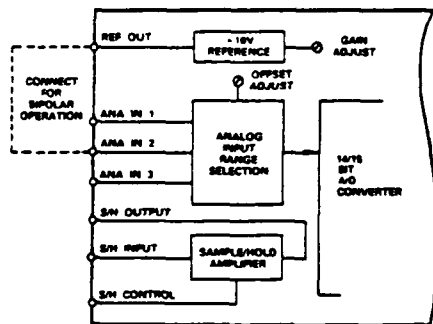


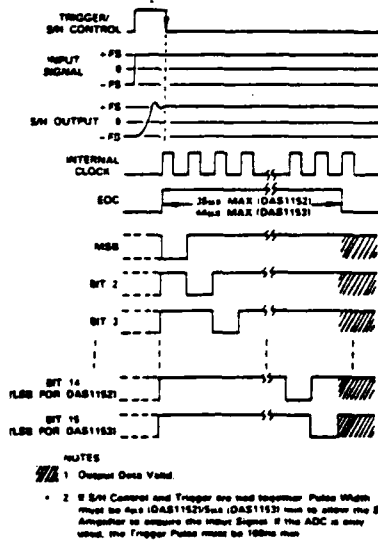
Figure 2. Analog Input Block Diagram

TIMING DIAGRAM

The timing diagram for the DAS1152/DAS1153 is illustrated in Figure 3. This figure also includes the sample/hold amplifier acquisition time.

If the sample/hold amplifier is required, the TRIGGER input and S.H CONTROL terminal can be tied together providing only one conversion control signal. When the trigger pulse goes high, it places the sample/hold amplifier in the sample mode allowing it to acquire the present input signal. The trigger pulse must remain high for a minimum of $4\mu s$ (DAS1152) $5\mu s$ (DAS1153) to insure accuracy is attained. If the sample/hold amplifier is not used, the trigger pulse needs to be only 100ns (min) in length to satisfy the A/D converter trigger requirements. At the falling edge of the trigger pulse, the sample/hold amplifier is placed in the hold mode, the A/D conversion begins, and all internal logic is reset. Once the conversion process is initiated, it cannot be retriggered until after the end of conversion.

With this negative edge of the trigger pulse the MSB is set low with the remaining digital outputs set to logic high state, and the status line is set high and remains high through the full conversion cycle. During conversion each bit, starting with the MSB, is sequentially switched low at the rising edge of the internal clock. The DAC output is then compared to the analog input and the bit decision is made. Each comparison lasts one clock cycle with the complete 14-15-bit conversion taking $35\mu s$ / $44\mu s$ maximum for the DAS1152/DAS1153 respectively. At this time, the STATUS line goes low signifying that the conversion is complete. For microprocessor bus applications, the digital output can now be applied to the data bus by enabling the tri-state buffers. For maximum data throughput, the digital output data should be read while the sample/hold amplifier is acquiring the new analog input signal.



NOTES

1 Output Data Valid

2 If S.H Control and Trigger are tied together Pulse Width must be $4\mu s$ (DAS1152) $5\mu s$ (DAS1153) min to allow the S.H Amplifier to acquire the Input Signal. If the ADC is only used, the Trigger Pulse must be 100ns min.

Figure 3. DAS1152/DAS1153 Timing Diagram

GAIN AND OFFSET ADJUSTMENT

The DAS1152/DAS1153 contain internal gain and offset adjustment potentiometers. Each potentiometer has ample adjustment range so that gain and offset errors can be trimmed to zero.

Since offset calibration is not affected by changes in gain calibration, it should be performed prior to gain calibration. Proper gain and offset calibration requires great care and the use of extremely sensitive and accurate reference instruments. The voltage standard used as a signal source must be very stable and be capable of being set to within $\pm 1/10$ LSB of the desired value at any point within its range.

OFFSET CALIBRATION

For a 0 to +10V unipolar range set the input voltage precisely to +305 μ V for the DAS1152 and +153 μ V for the DAS1153. For a 0 to +5V unipolar range set the input to +153 μ V for the DAS1152 and +76 μ V for the DAS1153. Then adjust the zero potentiometer until the converter is just on the verge of switching from 000.....000 to 000.....001.

For the ± 5 V bipolar range set the input voltage precisely to +305 μ V for the DAS1152 and +153 μ V for the DAS1153. For a ± 10 V bipolar range set the input voltage precisely to +610 μ V for the DAS1152 and +305 μ V for the DAS1153. Adjust the zero potentiometer until the offset binary coded units are just on the verge of switching from 000.....000 to 000.....001 and the two's complement coded units are just on the verge of switching from 100.....000 to 100.....001.

GAIN CALIBRATION

Set the input voltage precisely to +9.99909V (DAS1152) +9.99954V (DAS1153) for the 0 to +10V units, +4.99954V (DAS1152) +4.99977V (DAS1153) for 0 to +5V units, +9.99817V (DAS1152) +9.99909V (DAS1153) for ± 10 V units, or +4.99909V (DAS1152) +4.99954V (DAS1153) for ± 5 V units. Note that these values are 1/2LSBs less than nominal full scale. Adjust the gain potentiometer until binary and offset binary coded units are just on the verge of switching from 11.....10 to 11.....11 and two's complement coded units are just on the verge of switching from 011.....10 to 011.....11.

DAS1152/DAS1153 INPUT/OUTPUT RELATIONSHIPS

The DAS1152/DAS1153 produces a true binary coded output when configured as a unipolar device. Configured as a bipolar device, it can produce either offset binary or two's complement output codes. The most significant bit (MSB) is used to obtain the binary and offset binary codes while $\overline{\text{MSB}}$ is used to obtain two's complement coding. Table 2 shows the DAS1152/DAS1153 unipolar analog input/digital output relationships. Tables 3 and 4 show the DAS1152/DAS1153 bipolar analog input/digital output relationships.

NOMINAL BIPOLAR INPUT-OUTPUT RELATIONSHIPS

ANALOG INPUT			
0 to +5V Range		0 to +10V Range	
DAS1152	DAS1153	DAS1152	DAS1153
+4.99969V	+4.99964V	+9.99939V	+9.99964V
+2.50000V	+2.50000V	+5.00000V	+5.00000V
+0.62500V	+0.62500V	+1.25000V	+1.25000V
+0.00031V	+0.00015V	+0.00062V	+0.00031V
+0.00000V	+0.00000V	+0.00000V	+0.00000V

DIGITAL OUTPUT	
Binary Code	
DAS1152	DAS1153
11 111 111 111 111	111 111 111 111 111
10 000 000 000 000	100 000 000 000 000
09 100 000 000 000	091 000 000 000 000
08 000 000 000 001	080 000 000 000 001
07 100 000 000 000	070 000 000 000 000

Table 2. Unipolar Input-Output Relationships

Analog Input		Digital Output	
± 5 V Range	± 10 V Range	Offset Binary Code	Two's Complement Code
+4.99939V	+9.99878V	11 111 111 111 111	01 111 111 111 111
+2.50000V	+5.00000V	11 000 000 000 000	01 000 000 000 000
+0.62500V	+0.00125V	10 000 000 000 001	00 000 000 000 001
+0.00000V	+0.00000V	10 000 000 000 000	00 000 000 000 000
-1.00000V	-10.00000V	09 000 000 000 000	10 000 000 000 000

Table 3. DAS1152 Bipolar Input/Output Relationships

Analog Input		Digital Output	
± 5 V Range	± 10 V Range	Offset Binary Code	Two's Complement Code
+4.99969V	+9.99939V	111 111 111 111 111	011 111 111 111 111
+2.50000V	+5.00000V	110 000 000 000 000	010 000 000 000 000
+0.62500V	+0.000625V	100 000 000 000 001	000 000 000 000 001
+0.00000V	+0.000000V	100 000 000 000 000	000 000 000 000 000
-1.00000V	-10.00000V	000 000 000 000 000	100 000 000 000 000

Table 4. DAS1153 Bipolar Input/Output Relationships

TRI-STATE DIGITAL OUTPUT

The ADC digital outputs are provided in parallel format to the output tri-state buffers. The output information can be applied to a data bus in either a one-byte or a two-byte format by using the HIGH BYTE ENABLE and LOW BYTE ENABLE terminals. If the tri-state feature is not required, normal digital outputs can be obtained by connecting the enable pins to ground.

POWER SUPPLY AND GROUNDING CONNECTIONS

Although the analog power ground and the digital ground are connected in the DAS1152/DAS1153, care must still be taken to provide proper grounding due to the high accuracy nature of these devices. Though only general guidelines can be given, grounding should be arranged in such a manner as to avoid ground loops and to minimize the coupling of voltage drops (on the high current carrying logic supply ground) to the sensitive analog circuit sections. Analog and digital grounds should remain separated on the PC board and terminated at the respective DAS1152/DAS1153 terminals.

No power supply decoupling is required since, the DAS1152/DAS1153, contain high quality tantalum capacitors on each of the power supply inputs to ground.

C872a-20-11/83

PRINTED IN U.S.A.

REFERENCES

1. Palmer, S. E., Garrett, S. L., Wilson, O. B., Yoon, S. W., Autonomous Measurement of Normal Acoustic Modes in STS Cargo Bay, Proceedings, AIAA Shuttle Environment Operations Conference, Houston, Texas, 1985.
2. DATE Report 002, Payload Bay Acoustic and Vibration Data From STS 002, NASA, 1981.
3. Wilby, J. F., Pope, L. D., Prediction of the Acoustic Environment in the Space Shuttle Payload Bay, paper 79-0643 presented at the AIAA 5th Aeroacoustics Conference, Seattle, Washington, 12 March 1979.
4. Heller, H., Bliss, D., Aerodynamically Induced Pressure Oscillations in Cavities - Physical Mechanics and Suppression Concepts, BBN paper AFFDL-TR-74-133, February 1975.
5. Aerospace Technical Memorandum, ATM 83 (3493-37)-7, Mass Flow From Vents and Related Acoustics on STS-5 by C. S. Tanner, 17 August 1983.
6. Stehle, C. D., Vibration Isolation of a Microphone, M.S. Thesis, Naval Postgraduate School, Monterey, California, September 1985.
7. D'Ercole, T. M., A Solid State Data Recorder for Space Based Applications Using Magnetic Bubble Memory, MSEE Thesis, Naval Postgraduate School, Monterey, California, March 1986.
8. Frey, T. J., A 32-Bit Microprocessor Based Solid State Data Recorder for Space Based Applications, MSEE Thesis, Naval Postgraduate School, Monterey, California, March 1986.
9. Jordan, D. W., A Matched Filter Algorithm for Acoustic Signal Detection, MSEE Thesis, Naval Postgraduate School, Monterey, California, March 1986.

10. Boyd, A. W., Kosinski, B. P., Weston, R. L. " Autonomous Measurement of Space Shuttle Payload Bay Acoustics During Launch", Naval Research Reviews, v. 39 pp. 9-17, January 1987.
11. Horowitz, P., Hill, W., The Art of Electronics, Cambridge University Press, 1984.
12. Wilson, O. B., An Introduction to the Theory and Design of Sonar Transducers, p. 55, U. S. Government Printing Office, 1985.
13. Muzzerall, M. L., Investigation of Thermoacoustic Heat Transport Using a Thermoacoustic Couple, M.S. Thesis, Naval Postgraduate School, Monterey, California, September 1987.
14. Ziomek, L. J., Underwater Acoustics, a Linear Systems Approach, Academic Press, Inc., 1985.
15. Kinsler, L. E., Frey, A. R., Coppens, A. B., Sanders, J. V., Fundamentals of Acoustics, John Wiley and Sons, Inc., 1982.
16. Morse, P. M., Vibration and Sound, American Institute of Physics, 1976.
17. Greenspan, M., Simple Derivation of the Boltzmann - Eherenfest Adiabatic Principle, JASA Vol. 27 No. 1, 34-35, January 1955.
18. ILS Command Reference Guide, TWX 910-334-3471, Signal Technology, Inc., 1986.

INITIAL DISTRIBUTION LIST

	No. Copies
1. Defense Technical Information Center Cameron Station Alexandria, Virginia 22304-6145	2
2. Library, Code 0142 Naval Postgraduate School Monterey, California 93943-5002	2
3. Professor S. L. Garrett, Code 61Gx Naval Postgraduate School Monterey, California 93943-5000	6
4. Professor O. B. Wilson, Code 61W1 Naval Postgraduate School Monterey, California 93943-5000	1
5. Professor A. H. Fuhs, Code 67/Fu Naval Postgraduate School Monterey, California 93943-5000	1
6. Professor Rudolf Panholtzer, Code 62Pz Naval Postgraduate School Monterey, California 93943-5000	2
7. Chief of Naval Research ATTN: Dr. L. E. Hargrove Physics Division - Code 1112 800 N. Quincy Street Arlington, Virginia 22217	1
8. LT. Scott Palmer Space and Naval Warfare Systems Command PDW 106/72A Washington, D. C. 20363-5100	1
9. Ms. Carol Tanner Mail Station N4/910 Aerospace Corporation P. O. Box 92957 Los Angeles, California 90009	1

10. Mr. Frank On, Code 731 1
National Aeronautics and Space Administration
Goddard Space Flight Center
Greenbelt, Maryland 20771
11. Mr. Rick Arvesen 1
McDonald Douglas Corp.
Astronautics Division
Group ABDO
Huntington Beach, California 92647
12. Commodore Truly 1
Commander Naval Space Command
Dahlgren, Virginia 22448-5170
13. Mr. Frank Deithrick 1
Space and Naval Warfare Systems Comand
Washington, D. C. 20363-5100
14. Mr. Don Wong 1
Mail Station M5-568
Aerospace Corporation
P. O. Box 92957
Los Angeles, California 90009
15. COMSPAWAR 1
PMW 180-442
ATTN: CDR C. D. Stehle
Washington, D. C. 20363-5100
16. Naval Research Laboratory 1
Code 9110-52
ATTN: LT B. Kosinski
4555 Overlook Avenue-S.W.
Washington, D. C. 20375
17. LCDR Allen Hansen 1
Navy Space Systems Activity
P. O. Box 92960 WWP
Los Angeles, California 90009
18. Dr. Steven F. Watanabe 1
Director, Technology Assessment
McDonnell Douglas Corporation
1550 Wilson Blvd.
Suite 550
Arlington, Virginia 22209

19. LT Mary Cox 1
Dept. of the Air Force
Space Test Program Office (SD/CGTPC)
HQ Space Division (AFSC)
P. O. Box 92960
Los Angeles, California 90009-2960
20. Dr. Bruce C. Edgar 1
Planning and Operations Directorate
Space Test Program
2350 East El Segundo Boulevard
El Segundo, California 90245-4691
21. Julie D. White 1
Project Engineer, Space Test Directorate
Architecture Planning and Technology Division
2350 El Segundo, California 90245-4691